

ABSTRACT

Bone is a unique tissue that serves multiple functions. One of its unique features is the ability to heal by formation of new bone, whereas most other tissues undergo the process of scar formation. When a large amount of bone is lost the only treatment available is the use of bone grafts. Multiple bone graft substitutes are being developed to address the shortage of autologous bone graft. 3-D models are being developed to further our understanding of the cellular processes taking place *in vivo*. In this study I examined the strategy of designing a 3-D model of hard tissue and a potential bone graft substitute using collagen type I and several different porous scaffolds.

Factors influencing collagen gel contraction by human mesenchymal stem cells (hMSC) during the process of osteogenic differentiation were studied and it was shown that collagen type I gels prepared in accordance with our patented technology contract far less than any other collagen gels reported in literature. The validity of MTT assay to track proliferation of hMSC in various 3-D matrices was established and allowed me to show that human mesenchymal stem cells (hMSC) proliferated, differentiated along an osteogenic lineage and mineralized the extracellular matrix (ECM). Higher cell seeding density and greater serum concentration in the culture medium, caused increased collagen type I gel contraction. Late passage cells and osteoblasts caused a greater collagen type I gel contraction than undifferentiated early passage hMSC. hMSC that had been transduced to constitutively express human telomerase reverse transcriptase (hTERT), and which had thereby acquired an extended

in vitro life span (telomerized hMSC or TMSC), contracted the collagen gel lesser than hMSC.

A Collagen type I Gel - Collagen type I foam Scaffold combination (CGCS) was investigated as a 3-D *in vitro* model to allow extrapolation of soft tissue results to those characteristic of hard tissue. Deep penetration of MSC into the CGCS with uniform distribution was achieved by the use of collagen type I gel, as the cell carrier. Collagen type I gel improved seeding efficiency and facilitated retention of cells that penetrated deep into the scaffold. Long-term survival, proliferation, viability and *in situ* osteogenic differentiation within the CGCS were demonstrated. A model that demonstrated migration of cells in and out of CGCS was assembled and tested. A need for the presence of fibrillar collagen gel for mineralization process to take place highlighted the benefit of adding collagen gel to the 3-D models.

Porous Beta-tricalcium phosphate (β -TCP) was used as the scaffold and impregnated with collagen gel to generate Collagen Gel Impregnated Porous Scaffolds (CGIPS). Highly efficient seeding of the cells throughout the porous scaffold was attained with collagen gel. hMSC proliferated in CGIPS without contracting the collagen gel. Cells could migrate into CGIPS and mineralized the ECM when cultured *in vitro* under osteogenic differentiation conditions. CGIPS allowed the application of pressure and hMSC responded to mechanical force by a change in proliferation.

hMSC xenotransplanted into immunocompetent rats survived for a month and expressed markers of osteogenic differentiation. While cells alone improved vascularization of the implants, they did not improve mineralization. Presence of collagen gel alone allowed for faster invasion of cells into the implanted TCP and improved radiodensity but did not affect vascularization. A combination of cell and gel within the TCP (CGIPS) was necessary to

improve all the measured variables (tissue invasion, vascularization, mineralization and radioopacity). Thus biocompatibility, greater vascularization and enhanced mineralization of CGIPS implants established the foundation to proceed with large animal bone defect model studies utilizing CGIPS in the future.

I established that CGIPS could deliver small molecules into the surrounding milieu by a process of simple diffusion. A rapid initial burst followed by a slow sustained release was observed when collagen gel containing EphrinB2-Fc clusters was incorporated into CGIPS. The released EphrinB2-Fc was physiologically functional and increased hMSC proliferation and chemotaxis. CGIPS inhibited the growth of Methicillin resistant *Staphylococcus aureus* when vancomycin was incorporated into the CGIPS. Thus the potential of CGIPS to serve as a drug delivery device was demonstrated.

This work has provided the scientific foundation for use of CGIPS as bone graft substitute and 3-D model of osteogenesis. In this research study, a number of challenges were solved and questions answered, and the applications of the proposed strategy formulated. However, as is frequently the case many more avenues of future research have been exposed and a variety of new questions posed to be pursued and answered in future studies.

STUDY OF OSTEOGENESIS IN 3-D

DISSERTATION

Presented to the Graduate Council of the Graduate School of Biomedical Sciences

University of North Texas Health Science Center at Fort Worth

in Partial Fulfillment of the Requirements

For the Degree of

DOCTOR OF PHILOSOPHY

By

Anupam Ashutosh Sule, M.B.B.S.

Forth Worth, Texas

September 2010

ACKNOWLEDGEMENTS

I wish to acknowledge my major advisor Dr. Dan Dimitrijevic for being a patient mentor who allowed my imagination to run wild but was always present when I needed him to be a beacon to guide me in the right direction. I also acknowledge my Committee members Dr. Robert Mallet, Dr. Arvind Nana, Dr. H. Fred Downey, Dr. Rong Ma and Dr. Porunelloor Mathew for their insightful critique which helped me improve this work.

I wish to acknowledge the staunch support provided by my parents, Mrs. Susmita and Dr. Ashutosh Sule, which allowed me to successfully undertake the rigors involved in graduate research work; my brother, Dr. Ajey Sule who was an inspiration to constantly strive for perfection and last but certainly not the least, my wife, Dr. Arati Kelekar who was a steadying hand in the presence of adverse winds.

I would like to thank all my colleagues, Dr. Jwalitha Shankardas and Hunaid Gurji, I wish to thank the Dean of the Graduate School of Biomedical Sciences, Dr. Jamboor Vishwanatha and Dr. the Chair of the Department of Integrative Physiology, Dr. Steven Mifflin for putting their faith in my work and providing me with a graduate stipend. I will also beg the forgiveness of all the contributors who made this research possible but who could not be acknowledged in this limited space.

TABLE OF CONTENTS

LIST OF TABLES.....	iv
LIST OF ILLUSTRATIONS	v
CHAPTER	
I. INTRODUCTION	1
II. FACTORS AFFECTING COLLAGEN GEL CONTRACTION DURING OSTEOGENIC DIFFERENTIATION OF MESENCHYMAL STEM CELLS	26
III. COLLAGEN GEL AND SCAFFOLD FOR STUDY OF OSTEOGENESIS IN 3-D	51
IV. COLLAGEN IMPREGNATED B-TRI CALCIUM PHOSPHATE– A 3-D MODEL FOR STUDY OF OSTEOGENESIS <i>IN VITRO</i>	84
V. CALCIFICATION OF COLLAGEN IMPREGNATED B-TRICALCIUM PHOSPHATE <i>IN VIVO</i>	113
VI. COLLAGEN GEL IMPREGNATED POROUS SCAFFOLDS CAN SERVE AS DRUG DELIVERY DEVICES	147
VII. DISCUSSION	176
REFERENCES	190

LIST OF TABLES

CHAPTER IV

Table 1. Morphological parameters obtained from microCT scanning of specimen. 103

CHAPTER VI

Table 1. Comparison of various drug release models. 167

LIST OF ILLUSTRATIONS

CHAPTER II

Figure 1. MTT can be used to determine number of cells in a collagen hydrogel.	37
Figure 2. Effect of cell seeding density on collagen hydrogel contraction.	38
Figure 3. Effect of serum on collagen hydrogel contraction.	39
Figure 4. Effect of passage on collagen gel contraction.	40
Figure 5. Effect of telomerase expression on collagen gel contraction.	40
Supplementary figure 1. Osteogenic differentiation at low cell seeding density.	42
Supplementary figure 2. Cell proliferation of hMSC, TMSC and TOST in collagen hydrogel under osteogenic differentiation conditions for two weeks.	43

CHAPTER III

Figure 1. Characterization of collagen foam.	65
Fig. 2. Distribution of human bone marrow derived mesenchymal stem cells (hMSC) in Ultrafoam [®] impregnated with collagen type I gel (CGCS).	66
Figure. 3. Confocal micrograph of CGCS 3-D model assembled with Cy5 labeled collagen type I and GFP expressing telomerized human dermal fibroblasts (GFP-tFbs).	67

Figure 4. Proliferation and viability of GFP-tFbs and hMSC in CGCS.	67
Figure 5. The presence of collagen type I has a significant positive effect on distribution, survival and proliferation of hMSC and hOST cells in CGCS.	69
Figure 6. Our CGCS 3-D model can be used for studies of cell migration in 3-D.	70, 71
Figure 7. The response of cells in CGCS (our 3-D model) to mechanical force.	72
Figure 8. Differentiation of hMSC in CGCS.	73
Figure 9. Immunohistochemical analysis of hMSC differentiation in CGCS.	74
Figure 10. Histochemical analysis (Von Kossa stain) demonstrated the requirement for collagen type I for <i>in vitro</i> mineralization in CGCS model.	75
 CHAPTER IV	
Figure 1. Impregnation and retention by β -TCP of collagen type I gel.	94
Figure 2. Distribution of GFP-tFbs throughout the 5 mm x 5mm x 5mm β -TCP scaffold.	95
Figure 3. Retention and migration of cells in CGIPS.	97
Figure 4. Proliferation of hMSC in CGIPS.	98
Figure 5. Collagen gel does not contract in CGIPS.	99
Figure 6. microCT scanning analysis of CGIPS.	100
Figure 7. Response of hMSC to load (pressure).	101
Supplementary figure 1. Impregnation of collagen gel in porous tantallum.	102

Supplementary Figure 2. MTT assay for CGIPS. 102

CHAPTER V

Figure 1: Surgical implantation of bone graft substitutes. 124, 125

Figure 2. Expression of osteopontin in various study samples. 126, 127

Figure 3. Expression of osterix. 128

Figure 4. Tissue penetration into porous scaffold. 130, 131

Figure 5. Mineralization of scaffolds. 133, 134, 135

Figure 6. X-ray densitometry of implants. 136

Supplementary figure 1. Low magnification view of intramuscular implants. 137

CHAPTER VI

Figure 1. Release of BSA from collagen gels and CGIPS under dynamic conditions. 161

Figure 2. Release of ephrinB2-Fc clusters from collagen gel. 162

Figure 3. EphrinB2-Fc stimulates proliferation of telomerase transfected mesenchymal stem cells (TMSC). 163

Figure 4. EphrinB2-Fc stimulated chemotaxis of TMSC towards it. 164

Figure 5. Release of antibiotic from CGIPS. 165, 166

Supplementary Figure 1. BSA standard curve and release under static conditions. 167

CHAPTER I

INTRODUCTION

Bone - a unique living tissue that regenerates

Anatomy and physiology of bone

The human skeleton is a multifunctional structural tissue that provides form to the human body, acts as a fulcrum for muscles, protects soft internal organs, is a storage of calcium and phosphate and is the main niche of blood and immune system genesis (1), (2). There are two different types of bone: dense cortical (lamellar) bone and porous cancellous (trabecular) bone (1). Bone surfaces consist of lamellar bone, which provides mechanical strength so that this outer layer is thicker in regions that are subjected to higher load. The trabecular bone is composed of a network of spicules, with empty spaces that contain bone marrow. Trabecular bone forms the central core of bones. The porosity and alignment of trabeculae determine the mechanical properties of trabecular bone and these vary widely according to the anatomic site.

During fetal development bone formation can occur by intra-membranous ossification or endochondral ossification (1). Intramembranous ossification involves direct differentiation of mesenchymal stem cells (MSC) into osteoblasts (bone forming cells). Endochondral ossification is a two-step process. Initially MSC differentiate into chondroblasts (cartilage forming cells) and lay down cartilage. The cartilage is then invaded by osteoblasts and converted to bone. The cells that constitute the cellular compartment of mature bone tissue

include osteoblasts, osteoclasts and osteocytes, which are responsible for deposition and resorption and maintenance of bone, respectively. Osteocytes are the most abundant cell type that populates the mineral tissue of bone.

A highly ordered network of collagen type I fibrils strengthened by deposition of sub-microscopic (5–100 nm) inorganic calcium phosphate crystals, by a process called ossification, forms the extracellular matrix (ECM) of the bone and provides hardness and elasticity at a minimal weight (3) (4). The inorganic mineral deposited on collagen fibrils is amorphous tricalcium phosphate [$\text{Ca}_3(\text{PO}_4)_2$], bone apatite (frequently but incorrectly referred to as hydroxyapatite [HA]), with Ca:P ratios of 1.37–1.87 and hydroxyl deficiency. The form and composition of bone apatite is such that the mineral is stable but is easily resorbed or deposited by the cells as necessary. Thus bone is a dynamic tissue that undergoes cycles of resorption-deposition of mineral and realignment of the matrix. This structural remodeling takes place in response to internal - biochemical / physiological (hormonal) as well as external - mechanical signals.

Mechanotransduction

Bone responds to mechanical forces acting on it (in order to optimize its load bearing capacity) by changing its structure and form by a process called remodeling (1). Thus the astronauts in zero gravity (minimal mechanical loading) lose bone mass while athletes as the result of constant training (maximal mechanical loading) have denser bones. The general process by which cells respond to physical forces is called mechanotransduction (5). This process begins with detection of change in mechanical properties of the microenvironment. In response the cells initiate a cascade of events involving, conversion of the stimulus into

biological signal cascade and resulting in physiological response by the cells following activation of appropriate genes. It has been shown that interaction between ECM (collagen) and cell surface receptors - integrins is the basis of this process. The physiological response may vary from resorption or deposition of the bone apatite to collagen synthesis and cell proliferation and differentiation (6), (7).

Fracture Repair

The bone formation process during development is well documented but bone repair and regeneration is not as well understood (8). Bone is unique among tissues in that it heals by regeneration and not by scar formation as is evident in muscle, skin, heart, etc. Bone repair is a complex process directed and modulated by the interplay between cells, extra-cellular matrix and growth factors (9). Fractured bone heals by utilizing both intramembranous as well as endochondral ossification. (10). The blood clot formed at the fracture site is cleared by an inflammatory process (macrophages) (11). The hematoma formation is followed by proliferation of surrounding tissue to form a fracture callus. The proliferation of cells that are involved in wound repair is directed not only by biochemical signals but also by mechanical signals (1), (10), (11). At the fracture site near the marrow the cells differentiate to osteoblasts while at sites away from the marrow differentiation into chondroblasts takes place. Following angiogenesis within the fracture callus osteoblasts invade the cartilage, mineralize it, become embedded in lacunae (spaces within the porous collagen scaffold) and differentiate into osteocytes to complete conversion of the fracture callus to bone (8). Once the inner - trabecular bone has been formed the bone marrow is populated by hematopoietic and mesenchymal cells, while the outer bone layers are remodeled into lamellar bone.

Need for study of osteogenesis in 3-D

Need for a 3-D model

While differentiation of MSC to osteoblasts has been demonstrated in 2-D (12), (13) and 3-D cultures (14), (15), the expression levels of osteogenic biomarkers are significantly higher in 3-D cultures (16), (17). 3-D morphology is essential for initiation of mineralization of ECM (14), (18). In contrast 2-D osteoblast cultures have to form “nodules” (3-D like structures) prior to calcification (14), (18). Mineralization begins earlier and proceeds faster in a 3-D environment (15), (16), (17). *In vivo*, osteoblasts repair a fracture by invading and mineralizing the collagenous matrix (a 3-D environment) (19). Therefore, the process of differentiation and mineralization in an *in vitro* 3-D environment represents an *in vivo* relevant ossification and validates the superiority of 3-D models as tools for bone biology research.

An important aspect of the 3-D structure is that it allows the bone to respond to mechanical forces by undergoing deformation to optimize its load bearing capacity (5). This mechanosensing capability and the ensuing remodeling process is an integral component of the bone function *in vivo*. Thus *in vitro* studies of bone tissue biology would be incomplete without a 3-D model that is capable of mechanotransduction and subsequent remodelling response. Majority of the current 3-D models used as research tools lack mechanical integrity (stiffness) and stability because they are soft hydrogels (7). Cellular contraction of the matrix in these models, compacts the matrix followed by expulsion of water, which invariably results in cell death. Studies that examine the responses to applied forces use cells cultured as monolayers on elastic membranes that can generate continuous or cyclic stretching. This approach may be appropriate for studying the effects of *in vivo* to tensile forces (vascular, tendon and skeletal

muscle cells) but it is inappropriate for studying responses to compressive and torsional forces acting on bone. Thus there is a great need for a stable 3-D bone model that is populated with the appropriate osteogenic cells and is responsive to factors that regulate bone functions *in vivo*. The model should also be responsive to controllable biochemical and physical stimuli that reflect physiological and pathological behavior of cells in the *in vivo* environment (20).

In the last decade 291 studies related to fracture healing were carried out in animals. These studies included not only small animals (mice, rats and rabbits) but also larger animal models (dogs, sheep, pigs and goats) (10). A useful 3-D model would allow a variety of studies to be undertaken *in vitro* sparing the cost and ethical issues involved in animal experimentation.

Need for grafts

Similarly to a number of other tissues there are limitations to the capacity for bone to regenerate (1). In pathological situations involving considerable loss of bone tissue such as complicated fractures, treatment of bone tumors, osteoradionecrosis, joint replacement, congenital defect repair or spinal fusion surgeries, the bone defects cannot heal unassisted. In such cases surgical reconstruction becomes a necessity so that the damaged or missing tissue can be replaced and the functional state of the bone restored quickly and with minimal patient discomfort. The mainstay of surgical “tissue replacement therapy” in such cases is bone grafting, wherein the bone defect is filled in using bone from another site of the patient’s bone system (**autograft**) or from a suitable donor (**allograft**). Autologous bone grafts are thus considered as the gold standard of therapy but harvesting the bone graft material can cause pain, infection and bleeding at the donor site and the amount of bone that can be obtained is limited (21).

Allografting overcomes these problems but the supply of human tissue from bone banks fails to meet the demand. The possibility of transmission of pathogens and biological variability leading to inconsistent results further hamper this modality of treatment.

Metallic prostheses and implants are commonly used to replace parts of bones that are damaged beyond the regenerative efforts (1). However, metal implants can generate, due to wear and tear, small submicrometer particles which and can trigger an immune response leading to loosening and implant failure. Although the life of the implant may be increased by surface coating with biocompatible material, the problem is not solved. In case of younger patients it may be necessary to remove the implant as the normal growth creates size disparity. In such cases a “second injury” at the initial site can cause tissue loss due to a phenomenon called “stress shielding”. Bone cement is a commonly used grafting material but it is not biodegradable, does not allow bone growth, is not replaced by native bone (22), and it increases the chances of infection at the site of injury. Thus one of the main attributes for a good graft would be “bioresorbability” - ability to remodel. Bioresorbability implies the ability of the graft to be degraded by cells and to be replaced by the native tissue, in this case by bone.

An “ideal graft” should be comprised of a supporting structure - a scaffold that provides physical properties mimicking the target tissue, a cytocompatible environment (which will be referred to as the matrix throughout this Dissertation), component cells of the target tissue and growth factors (chemokines) that complete biochemical modifications which will facilitate a better graft integration.

Tissue engineering is a new science / biotechnology that attempts to utilize various artificial and natural materials to help repair tissues and organs in the body (2). To meet

FDA approval and be a successful bone graft substitute, a tissue engineered graft has to be cost effective, sterile, radiographically distinguishable, totally biodegradable to non-toxic degradation byproducts, mechanically strong, and finally amenable to being remodeled into native bone (23).

Cell based tissue engineering

Osteogenesis with MSC

Mesenchymal stem cells present in the bone marrow are a continuous source of osteoprogenitor cells for bone growth, remodeling and repair. (12). When grafts were implanted into rabbit bone defects, bone deposition progressed from the deeper end of the graft outwards i.e. progression from a richer source of stem cells (24). The role and utility of MSC was also demonstrated when segmental bone defects in rats were healed by injection of rat bone marrow and the healing took place faster with a stronger graft-host interface when more quantity of marrow was used (25).

In vitro (18) and *in vivo* (26) studies failed to demonstrate difference in the osteogenic potential of primary rabbit osteoblasts and rabbit MSC. In a study by Peters et al when osteogenically differentiated rat cells were injected precutaneously into fracture hematoma, they produced more bone than MSC (27). Thus it is not clear whether MSC should be differentiated *in vitro* prior to implantation *in vivo*.

Ceramic (mineral) scaffolds alone can not heal long bone defects as adequate number of osteogenic cells is not available for the wound healing process (28). Calcium phosphate ceramic scaffolds combined with bone marrow healed long bone defect in dogs earlier than bone marrow alone (28), (29). A combination of bone marrow and β -TCP implanted subcutaneously formed bone in mice whereas β -TCP alone did not (30). Following implantation

in rats and an eight week experimental time, β -TCP combined with rat MSC had greater osteocalcin expression, alkaline phosphatase activity, blood vessel invasion (angiogenesis) and bone formation than cell free β -TCP (31). HA with β -TCP and human MSC (hMSC) bound strongly to mouse bone while cell free HA and β -TCP was encapsulated with fibrous tissue without bone formation (32). When implanted into nude mice, HA and β -TCP with hMSC formed more bone as compared to HA alone or cell free hydroxyapatite combined with β -TCP (33). Hydroxyapatite+ β -TCP with hMSC led to better facial bone healing in human patients as assessed by the speed of host tissue invasion and integration as shown by radiography (34). All these studies demonstrate the improvement in osteogenic performance due to the presence of hMSC as a component of bone graft substitutes.

Telomerase and MSC

Long term *in vitro* expansion of MSC induces replicative senescence (23), (35), indicating a loss of stem cell status and reducing their therapeutic utility. This can be overcome by ectopic expression of telomerase in MSC, which improves their proliferation *in vitro* and bone forming potential *in vivo* indicating that response to the differentiation signals is still operational (23). Telomerase transfected human mesenchymal stem cells (TMSC) and primary human MSC (hMSC) undergo similar changes in gene expression when exposed to differentiation inducing stimuli (our unpublished data and (35). Thus TMSC are a good substitute for hMSC in studies concerned with design and evaluation of engineered bone grafts.

Immunomodulation by MSC

Human MSC survive after implantation into rat intervertebral discs whereas hematopoietic stem cells do not (36). This apparent immunoprivileged status of MSC is due to the lack of expression of MHC-2 and lymphocyte costimulatory antigens (37). Although MHC-1

is expressed by MSC they are not recognized by immune system and allogenic transplantation of MSC does not cause rejection. MSC are also immunomodulatory since they reduce rejection of other cell types (e.g. like hematopoietic stem cells) when they are simultaneously transplanted. Xenogenic implantation of 20 million hMSC into sheep bone defect did not cause fever, weight loss, rise in inflammatory markers, leukocytosis or expression of acute phase reactants in the experimental animals. Viable hMSC were detected as long as six weeks after the transplantation. Furthermore hMSC could form bone when transplanted into not only immunodeficient mice (38) but also immunocompetent mice (32). These data form the basis for the use of hMSC in our experiments with immunocompetent rats.

Selection of matrix

Collagen type I ECM

Collagen is the most abundant protein in the human body and is involved in formation of the ECM of most tissues (4). Collagen fibrils are formed from 300 nm long and 1.5 nm wide parallel tropocollagen arrays. Tropocollagen itself is a right-handed helical trimer of monomeric collagen peptide (left handed helices) also known as the α -chains: one $\alpha 1$ -chain (1056 amino acids) and two $\alpha 2$ -chains (1038 amino acids). Each type of α -chains is the product of a separate gene. The α -chain peptides are a repeating sequence of Gly-X-Y with hydroxyproline and hydroxylysine being the main amino acids at X and Y. Type 1 collagen comprises 70 to 90% of the extracellular matrix of bone (3). The fibrils are held together as bundles by intra and inter chain cross-links to form 0.2 to 12 micron diameter collagen fibers. Bone apatite crystals are deposited on the scaffold formed by type I collagen fibers.

Role of ECM in function of bone tissue

The involvement of ECM in regulation of cellular function is receiving increasing attention (4), (39). Signal transduction following interaction of cell surface receptors with ECM, transmission of mechanical forces, regulation of diffusion of growth factors, and influence on cell adhesion, migration proliferation and differentiation are some of the functions that are orchestrated by the extra-cellular matrices.

The bone forming osteoblasts can interact with the extracellular matrix using two classes of receptors: integrins (e.g. $\alpha1\beta1$ and $\alpha2\beta1$) and discoidin domain receptors (DDR2), which can trigger outside-in mechanosignaling (transduction) important for differentiation (5) (19). Cell lineages that are involved in the formation and maintenance of musculoskeletal tissues have been shown to be sensitive to the stiffness and elasticity of their microenvironment. Thus mechanical stimulation is a pivotal factor in determining the differentiation pathway of MSC with stiffer matrix favoring osteogenic differentiation (40). The osteoblasts in turn upregulate matrix metalloproteinases (MMP) to degrade and remodel their surrounding matrix. This not only releases latent collagen bound growth factors but also releases collagen peptides that can trigger further outside-in signaling.

Collagen Gel

The use of collagen gels as the matrix for 3-D tissue models was first reported by Elsdale in 1972 (41), who described a method of preparation of type I collagen gels to accommodate and culture dermal fibroblasts. Following neutralization of acid solubilized collagen type I, hydrogel formation is the consequence of spontaneous fibrillogenesis (4).

hMSC could migrate on the surface and enter into collagen type I gel (42). MSC (6) and osteoblasts (14), (19) deposited calcium phosphate on collagen type I fibers during differentiation in or on collagen gel. When comparing various ECM gels as *in vitro* models for osteogenesis, Weinand et al found collagen type I gel to be superior to fibrin glue, alginate gel, hyaluronate gel, agarose gel, matrigel, laminin gel or pluronic F127 gels (43),(44), (45). These studies also demonstrated that the presence of collagen type I is essential for *in vitro* ossification.

Greater numbers of hMSC adhere to native collagen type I as compared to denatured collagen (46). MMP activity in collagen type I gel is important not only for terminal differentiation of osteoblasts into osteocytes but also for creating tracks for cell migration, production of signaling fragments of the matrix, release of matrix bound latent growth factors and cell survival (19), (40). Cross-linking collagen and/or altering its native conformation to create a biomaterial with more favorable mechanical properties is an approach adopted by increasing number of tissue engineering groups. This approach suffers serious drawbacks such as decline in biocompatibility since the cross-linking often creates collagen that can trigger inflammation and degeneration of implant (47). When the cells are unable to degrade the matrix (e.g. the presence of uncleavable cross-links) the differentiation is suppressed. (48). Osteogenic differentiation of hMSC on native collagen is superior to that on denatured collagen substrata (48), (49). All these observations highlight the use of native collagen as a requirement in developing tissue engineered grafts.

Collagen type I gel alone can trigger an inflammatory response when implanted in animals (50), (51) but when combined with rabbit MSC no inflammatory response after implantation into rabbits was observed (51). In human trials with Collagraft[®] (a collagen derived bone graft substitute) small percentage of patients developed antibodies to collagen but these did

not react with human collagen or cause any adverse immunologic reaction (52). Even if a potential recipient is allergic to collagen, as discussed earlier, the use of collagen based bone marrow implants may not cause adverse clinical reactions (53).

Collagen Gel Contraction

An important factor that needs to be considered when engineering tissue grafts or 3-D models based on collagen type I gel is the contraction of the gel by the resident cells. In 1979 Bell et al observed that contraction of collagen type I gel by fibroblasts caused expulsion of water (54) and occurred spontaneously. They concluded that the presence of fibroblasts in the collagen gels was responsible for contraction since acellular collagen gels, cultured under similar conditions did not contract. Gel contraction produces a denser matrix which *in vitro* may decrease the availability of nutrients to the cells (55). The availability of nutrients is influenced by gel porosity, cell density and metabolism, all of which are negatively affected by collagen gel contraction. ECM contraction *in vivo* may interfere with invasion of host cells into the provisional wound matrix and with vascularization, leading to scar formation.

Human MSC (56), (57), rat MSC (55), rat osteoblasts (58), and human osteoblasts (14) contract collagen gel by 60 to 70% in one week with a consequent decrease in cell viability. Thus collagen gel contraction is a major impediment in the use of collagen type I gels in tissue engineering.

Collagen Based Models

In order to generate consistent and uniform osseous structure and facilitate proper function a 3-D model requires homogeneous cell distribution. Penetration of cells into the interior of a scaffold at depths greater than 500 μ m has been a challenge (17), and has been

approached by utilizing very high seeding density (59) even though it has been shown that lower seeding density does not affect tissue formation (60) resulting in wastage of cultured cells. Very poor cell proliferation has been observed within collagen scaffolds (17), (59). A very poor seeding efficiency (40%) has been reported when collagen diluted with culture medium was used as the cell delivery vehicle (61). Previous *in vitro* studies with cross-linked collagen scaffolds did not differentiate between physiological (cell-mediated) calcification and the crystallization due to spontaneous degradation of β -glycerol phosphate (62) in the monolayer culture controls. A good *in vitro* 3-D model should accommodate high and low seeding density, allow cell migration, differentiation and matrix mineralization.

Study Proposal

Grinnell compared two models of collagen type I gel contraction: free floating gels and anchored gels (63). The cells in anchored gels were shown to align along lines of tension and the anisotropic contraction resembles that observed in granulation tissue. In contrast, the cellular function in contraction of free-floating gels resembles cell behavior within scar tissue. As all body tissues and cells are in a 3-D environment and in contact with each other (and hence under tension), free-floating gels seem to be a model with little relevance to the *in vivo* conditions. As bone heals by regeneration, the use of anchored gels to study contraction during osteogenic differentiation is more appropriate.

Previous research in our laboratory led to the development of a non-contracting dermal equivalent generated using native fibrillar collagen type I gel (64). When fibroblasts are cultured in this 3-D construct under appropriate culture conditions, they remain quiescent and do not contract the collagen gel. As collagen gel contraction is a major impediment to cell viability,

we have studied various factors that may affect collagen gel contraction that may occur during the process of osteogenic differentiation of hMSC (**Chapter I**).

Although the course of osteoblast differentiation in 2-D is relatively uniform, the differentiation in various 3-D systems is dependent on the model used since not all the models are truly three-dimensional. Cells seeded on various porous scaffolds form a monolayer on the pore surfaces, and although these surfaces are tortuous and convoluted, the monolayers of cells stack into multilayers that synthesize collagen and form nodules of mineralization, a progression that is typical of 2-D cultures (51) but not analogous to 3-D or *in vivo* behavior.

Our efforts in engineering human tissue have led to the development of three - dimensional (3-D) models (also known as tissue equivalents or organotypic cultures) of the skin, cornea and conjunctiva (64). In these 3-D models of living human tissue, appropriate connective tissue cells (usually fibroblasts) populate the acid solubilized non-denatured collagen type I gels (the extracellular matrix, ECM). In contrast to similar tissue constructs that contract spontaneously (65), our patented connective tissue models are dimensionally stable. A benefit of non-contractile matrix is the translucency of my 3-D models that allows morphological observation of the cellular behavior by non-intrusive microscopic methods. Furthermore, our gel allows free exchange of nutrients and waste products, resulting in long-term (months) stability and cell viability, and supports cell migration (64). I have examined the suitability of porous non-denatured commercially available collagen type I foam (Ultrafoam[®]), a scaffold stiffer than the collagen gel alone, yet cytocompatible, easy to handle and amenable to physical deformation (**Chapter II**) In order to prevent compaction and allow long-term cell viability I selected collagen foam (Ultrafoam[®]) as a stiff scaffold that will reinforce our patented collagen hydrogel (64) during development of a 3-D model for bone.

Selection of scaffold

β -Tricalcium phosphate- the scaffold

Calcium phosphate based ceramics are commonly utilized in bone tissue engineering. Calcium sulfate and calcium carbonate dissolve too rapidly to be of clinical use while hydroxyapatite is very resistant to cellular degradation (66). Beta-tricalcium phosphate (β -TCP) is a “sintered” version of hydroxyapatite (hydroxyl deficient calcium phosphate apatite) which has mechanical properties similar to bone, can bond directly with bone (67) and is almost completely resorbed in the human body in 6 to 9 months with no adverse reactions (66). β -TCP is prepared by heating hydroxyapatite at 1300°C, a process known as “sintering” (67). The porosity of β -TCP can be modulated by inclusion of polyurethane foam or paraffin beads in the ceramic slurry prior to baking. The foam / beads melt leaving a porous structure.

Bioresorbability

Bioresorbable scaffolds like polyurethane, poly lactic acid, etc. take advantage of the ability of the bone to remodel and degrade the device as native bone tissue fills the site of injury/ deficiency (1). However, all these polymeric scaffolds suffer from reduced strength and questionable safety of the degradation products released. We elected to use in our studies β -tricalcium phosphate (β -TCP, $\text{Ca}_3(\text{PO}_4)_2$) which can be completely resorbed by cells in six months releasing calcium and phosphate ions (68). The high local concentration of calcium and phosphate ions released during degradation of β -TCP stimulates crystalline re-precipitation of calcium phosphate and active cellular mineralization of ECM by osteoblasts (69). It also stimulates osteoclast activity which in turn stimulates osteoblast activity, most likely through

ephrin signaling (70). This local mineralization is expected to enhance the bone-graft apposition and interface strength.

Porosity

The geometry of the scaffold can also influence its ability to integrate with the native tissue. Porous scaffolds are more advantageous than non-porous scaffolds as pores allow rapid cell migration deeper into the inner scaffold, provide space for cell proliferation, and allow diffusion of nutrients to the cellularized regions. The larger surface area provided by the porous scaffolds encourages faster and more extensive invasion of the graft by host tissue and graft angiogenesis, and leads to a more seamless bone-graft interface (1), (7), (71), (72).

Pore diameter of more than 100 μm in hydroxyapatite leads to better osteogenesis than smaller pore sizes. (73) β -TCP with pore size greater than 100 μm led to rapid bone deposition while smaller pore sizes do not show bone tissue formation. (74). “Porosity” is also an indicator of the volume of the graft occupied by the pores and reflects how well the pores are interconnected by a network of channels. Because the connectivity of pores is a feature that resembles bone structure it is as important as pore size in determining graft-host integration (24), (1), (7). β -TCP scaffold used in our studies contains pores ranging in size from 100 to 500 μm with 90% porosity and is FDA approved for clinical use.

Osteoinductivity

Any device that assists in bone regeneration and repair may be osteoconductive or osteoinductive. Osteoinductive scaffolds that can induce differentiation of stem cells along osteogenic lineage and enhance the mineralization potential of osteoblasts are highly desirable

(1). The interaction between the scaffold biomaterial, cells and proteins can be attributed to the aspects of material science dealing with micro-topography. Osteoinductivity encompasses the ability of the scaffold to not only support cell growth and mineralization to produce the native tissue but also recruit the appropriate cell population, stimulate their growth and differentiation i.e. actively participate in all stages of the regeneration process. In contrast “Osteoconductivity” refers to the passive ability of the scaffold to allow deposition of native tissue.

MSC can attach to and migrate within β -TCP, differentiate into osteoblasts, deposit ECM and mineralize the ECM (67). MSC cultured on β -TCP expressed markers of osteogenic differentiation: Runx2, osteocalcin, osteopontin, alkaline phosphatase and collagen type I at higher levels than cells cultured on plastic (75). Osteogenic cells proliferate more and apoptose less on β -TCP than when cultured on HA (76). Thus a scaffold should provide an environment into which the host bone and vasculature can invade. It should also provide some degree of mechanical stability to the fracture site while interacting with the host bone to integrate the load stimulated induction of osteogenesis. Over time the scaffold should be remodeled by the body and completely replaced by native tissue.

Need for a matrix

When MSC (various species) were seeded directly on β -TCP scaffold they stayed on and close to the surface of the 3-D form (17), (67). Movement deeper into the 3-D form is dependent on cell migration from the periphery which is a slow process. Nutrient supply to the inner portions of the 3-D form is poor and hence proliferation is reduced

Differentiation of SV40 immortalized osteoblasts (a cell line) on hydrophobic surfaces was compromised when compared to their response on hydrophilic surfaces (77). Seeding

efficiency of MSC (various species) was higher, the cell proliferation was greater and expression level of differentiation markers was higher on collagen scaffolds than any other including those that are calcium phosphate based or formed using de-mineralized bone (6), (17), (46), (78). These results demonstrate that collagen type I supports MSC proliferation and differentiation better than β -TCP. Similarly terminal differentiation to osteocytes has been demonstrated on collagen but not on β -TCP (19). Osteoblasts cultured in collagen gels deposited calcium phosphate on collagen fibrils (6), (14), (19). Thus the presence of collagen type I matrix would lead to faster deposition of calcium phosphate and better osseointegration. Human osteosarcoma cells cultured on mineralized collagen composites expressed higher levels of differentiation markers than on either β -TCP or collagen alone (79). The above findings form the basis of my proposal that a combination of collagen as matrix with β -TCP as scaffold would be more advantageous than either material alone.

Previously Reported Collagen - β -TCP composites

Hydrogels lack mechanical strength to physically survive experiments involving application of pressure without compromising cell viability of the populating cells. I propose that a combination of β -TCP and collagen type I would be superior to either material alone in terms of cytocompatibility and mechanical strength. Various combinations as well as stand alone products of animal collagen and calcium phosphate have been approved by FDA for clinical use (51).

When the pores in β -TCP were filled with collagen gel before seeding with the cells the penetration of cells deep into the scaffold was prevented (46), (51). When collagen was added to the cell suspension in the medium, seeding efficiency of alginate-gelatin- β -TCP with mouse MSC improved from 30% to 40% but most of the cells still did not attach or

migrated out of the scaffold within one day of seeding (61). On the other hand, rabbit adipose derived stem cells (ASC) were suspended and seeded with collagen gel into PLGA- β -TCP scaffolds with 100% efficiency and the cells were distributed in the pore spaces (51). These cells deposited more mineral when compared to cells seeded directly on PLGA-TCP scaffold. Collagen type I gel containing porcine MSC when introduced into β -TCP was shown to undergo significant contraction during the experiment which impacted negatively on long term survival of the cells in the inner scaffold with calcification being observed only on the surface, under static culture conditions (44). Human MSC proliferated to a greater extent and formed more bone on porous β -TCP-HA with collagen gel as compared to uncoated β -TCP-HA, or porous β -TCP-HA containing alginate gel, fibrin gel, hyaluronate gel, pluronic gel or agarose gel (43).

Collagen gel with porcine MSC formed bone after subcutaneous implantation of polycapronolactone with β -TCP scaffold in nude mice (80), (81). Rabbit ASC suspended in collagen gel impregnated within porous polylactate-glycolate scaffold showed more bone formation and higher incidence of non-union healing as compared to scaffolds with cells without collagen gel (82).

HA impregnated with collagen and canine MSC showed greater healing rates for canine radius bone defect than canine MSC seeded HA without collagen gel (28). HA impregnated with collagen type I gel showed similar results with and without canine MSC. This data suggests that transplanted MSC did not improve graft performance above that observed when collagen gel was incorporated in the graft. It was also observed that transplanted rodent MSC in collagen gel did not contribute to bone formation as much as the locally recruited MSC (2) implying that recruitment of endogenous MSC into the gel was important for bone formation.

On the other hand when porcine MSC suspended in collagen gel impregnated β -TCP and implanted in nude mice, samples with cells had higher density and stiffness than those without cells (81). In this case the bone was formed by exogenous - transplanted cells.

Study Proposal

Tissue engineering is a branch of science that aims to utilize various artificial and natural materials to help repair tissues and organs in the body (2). For a tissue engineered product to meet FDA approval and be a successful bone graft substitute, it has to be cost effective, easy to sterilize, radiographically distinguishable, totally biodegradable with non-toxic degradation byproducts, mechanically strong, and amenable to remodeling into native bone tissue (23). Bone cement and other non-biodegradable graft substitutes that were previously developed to repair bone voids are not resorbed and replaced by bone tissue (44). Gels and other soft scaffolds lack mechanical strength and are inappropriate for use in a mechanically active environment.

I have studied the *in vitro* and *in vivo* osteogenic potential, capacity and biocompatibility of a bone graft substitute formed from β -TCP, collagen type I gel and MSC. (Chapters III and IV).

Delivery of cytokines

Recruitment of cells

The present paradigm is that circulating adult stem cells can gravitate to the site of injury (fracture) and participate not only in the homeostasis of the tissue but also in the repair process. Thus MSC and osteoblasts from the bone marrow can enter the circulation (83).

Examination of the site of new bone formation shows that osteoblasts are found at the locations where endothelial cells have formed new blood vessels. (84) The recruitment of MSC and osteoblasts to the site of injury is a vital component of the wound healing process and the invading vasculature provides a route for the recruitment of circulating MSC and osteoblasts. (85) (86). This process appears somewhat analogous to extravasation of inflammatory cells to the site of inflammation or perhaps the release of metastatic cells at distal metastasis.

Addition of BMP to autologous bone graft improves the bone formation in spinal fusion surgeries in dogs (21). This supports the utility of biocompatible matrices which can serve as carriers and targeted delivery vehicles of growth factors as well as being substrates for cell attachment/migration and vascularization (87). Biodegradable bone graft substitutes can release appropriate cytokines to stimulate bone repair as they remodel (1) but controlling the target zone and the rate of delivery remain a challenge.

Ephrins

At the site of injury, bone resorption takes place by osteoclasts and is followed by influx of osteoblasts that lay down new bone matrix (70). It has been proposed that osteoblasts are recruited to the site of injury and their function stimulated and orchestrated by matrix bound growth factors released during bone resorption (70). VEGF-A, BMP-2, PDGF, IGF-1, have been proposed as mitogens and chemo-attractants for MSC. (88), (89), (90), (91), (92), (93) A myriad of growth factors have been used in attempts to accelerate bone healing e.g. BMPs, TGF- β , FGF, PDGF, VEGF and IGF (9).

The ability to recruit cells to the site of injury is an important facet of tissue-engineered grafts and the principle of stem cell therapy. Growth factors are the most commonly

used chemoattractants. One of the areas of research that can provide valuable information about cell recruitment to the site of injury is osteoblast-osteoclast “coupling” (70). When osteoclasts resorb bone at the site of injury, osteoblasts are recruited to start depositing new bone at the time when osteoclasts finish removing the dead or damaged tissue. One of the proposed mechanisms of osteoblast-osteoclast coupling is release of matrix bound growth factors by osteoclasts, the other is ephrin-ephrin interaction. Erythropoietin-Producing Hepatocellular Carcinoma (Eph) was the cell type from which Eph receptors were first cloned (94). Eph receptors are subdivided into classes A (EphA1–EphA9) and B (EphB1 to EphB6, no EphB5) and the ligands for Eph receptors are ephrins (Eph family receptor interacting proteins). The ephrin A ligands (ephrinA1–A5) interact with Eph A receptors while ephrin B ligands (ephrinB1–B3) interact with Eph B receptors. Ephrin-ephrin signaling is bidirectional (70). When cell expressing eph comes in contact with cell expressing ephrin both cells participate in signal transduction. The signal transduction in the cell bearing the Eph receptor is termed "forward signaling" while for the cell with ephrin the signal transduction is considered "reverse signaling".

Mesenchymal stem cells and osteoblasts both express ephrin B 2 as well as eph B 4 (95). Eph-ephrin interactions are involved in bone patterning during development (70) and have also been implicated in osteoarthritis and cancer induced bone pathology (94), (95). Eph B 4 is constitutively expressed tyrosine kinase receptor on osteoblasts and its stimulation leads to osteoblast differentiation (96) Ephrin B2-ephrin B4 interaction can occur between osteoblasts as they can express both molecules (94). Parathyroid hormone increases ephrin B2 expression on osteoblasts and increases bone formation and its expression is induced via RANKL-NFAT signaling cascade. Ephrin B2 inhibits osteoclast function (96). Ephrin B2-fc chimeric protein can stimulate eph B4 phosphorylation and osteocalcin expression and calcium deposition by human

MSC (95). Ephrin B2- fc was shown to increase angiogenesis at site of injection in mouse bone, and also improved bone density parameters and number of trabeculae. This indicates the potential for use of ephrin B2-Fc clusters as a molecule to accelerate bone healing.

Implant site infection

A serious complication during repair of significant bone loss is infection (97). The infecting organism may be autogenous - existing infection or may be introduced into the wound during injury and/or surgery. Prolonged intravenous antibiotic therapy is required to manage foci of bone infection like open fractures or osteomyelitis, and serum levels have to be continuously monitored for toxicity. Compromised blood supply at the site of injury may lead to suboptimal delivery of antibiotics at site of infection. Locally applied vancomycin has been shown to achieve very high local concentrations without exceeding safe levels systemically and powdered antibiotics can be released from hand mixed bone cement mixtures. FDA has approved clinical use of antibiotic containing bone cements at sites of infection after eradication of prior infections (98)

Local antibiotic therapy has definite advantages over systemic therapy for the treatment of bone infections. Small molecules and drugs have been shown to be released rapidly from collagen gels. (99). Vancomycin is an antibiotic with a spectrum of activity against most gram positive organisms including Methicillin Resistant Staphylococcus Aureus (98). Gentamicin can be added to Vancomycin to broaden the spectrum of activity. Vancomycin suppressed osteoblast cell line proliferation only at doses of 10,000 µg/ml (97) and has the advantage of high water solubility, heat stability and low allergy and resistance rates.

Study proposal

Tissue engineering strategies either deliver cells preloaded into a scaffold and/or recruit host cells to the site of scaffold implantation (38). I have studied the ability of collagen gel impregnated porous scaffolds to deliver Ephrin B2-Fc clusters and the effect of Ephrin B2-Fc clusters on MSC proliferation and migration (**Chapter V**).

Economic impact of musculoskeletal disease

According to WHO musculoskeletal diseases are responsible for not only mortality but also considerable morbidity (100). They result in a significant burden of disease in terms of disability and are growing in both developed and developing countries. Most of the non-traumatic and osteoporotic musculoskeletal diseases are associated with increasing age. Data from the WHO website show that the population over 65 years of age is increasing at 2-3% per year and that by 2100 will reach 10 billion. This highlights the enormity of the health care challenges that will be faced by future generations.

Another important sequel associated with musculoskeletal diseases is pain (100). There is a strong correlation of pain due to musculoskeletal diseases with increasing age as well as obesity. Almost 20% of the population in some developed countries was reported to be suffering from chronic pain.

In the USA the estimated financial burden of musculoskeletal conditions is approximately \$ 250 billion per year (101). Traumatic injuries account for 1 million deaths and 30 million cases of severe disability per year costing another \$500 billion annually. In 2001 worldwide sales of orthopedic products were nearly \$15 billion, with an increase in the cost at a rate of 13% per annum. The bone grafting segment is estimated to account for \$1 billion worldwide (1). Bone grafting accounted for 408,000 procedures in Europe and 605,000

procedures in US. The fact that the WHO has declared the current decade as the “Bone and Joint Decade” highlights the significance of musculoskeletal health care issues (101).

Therefore a composite that would be a suitable 3-D model for studies of cell biology in mechanoresponsive manner as well as serve as a potential graft for wound healing would be of great benefit. It would aid basic research by allowing studies to be conducted in a *in vivo* relevant fashion as well as greatly reduce the cost and ethical dilemma arising from the use of animal models. Concurrently, the availability of such a composite as a graft will accelerate healing, reduce the immunorejection and infections, alleviate pain and disability associated with segmental bone defects and diminish the financial burden in terms of not only the actual healthcare associated cost but also the cost to society in terms of physical impairment.

CHAPTER II

FACTORS AFFECTING COLLAGEN GEL CONTRACTION DURING OSTEOGENIC DIFFERENTIATION OF MESENCHYMAL STEM CELLS

Introduction

Collagen is the most abundant protein of the human body that forms the basis of the extracellular matrix (ECM) in most tissues and is a key component of healing wounds (4), (39). Type I collagen, comprising 70-90% of the bone ECM, in combination with the deposited calcium phosphate crystals impart the characteristic hardness to bone while allowing it to retain some degree of flexibility thus being responsible for the mechanical properties of the bone (3). The regulatory role of the ECM in cellular function has been receiving increasing attention in the recent years (4), (39). Signal transduction following interaction of cell surface receptors with ECM, transmission of mechanical forces, regulation of diffusion of growth factors, and influence on cell adhesion, migration and invasion are some of the functions that are orchestrated by the macromolecular components of the ECM. Osteoblasts can bind to collagen type I using two types of receptors, integrins ($\alpha1\beta1$ and $\alpha2\beta1$) and discoidin domain receptors (DDR2) (5), (19). Receptor-ECM interaction can transduce mechanical stimuli and initiate outside-in-signaling cascades that are important for osteogenic differentiation (mechanotransduction). These facts highlight and support the central role of collagen type I in the tissue functions of bone.

Comparing various hydrogels as *in vitro* models for osteogenesis, it was found that collagen type I gel is superior to fibrin glue, alginate or pluronic F127 gels (44). Seeding efficiency of hMSC is higher and hMSC proliferate faster on collagen scaffolds than on any other, including those that are calcium phosphate based or are formed using demineralized bone matrix (17), (78). hMSC cultured on collagen scaffolds expressed higher levels of differentiation markers than hMSC differentiating on calcium phosphate ceramics (17).

Cross-linking collagen type I and/or altering its native conformation to create a biomaterial with more favorable mechanical properties is an approach proposed and adopted by increasing number of tissue engineering groups. However, this is implemented at the expense of decline in biocompatibility since the cross-linking renders collagen susceptible to pathologic calcification and degeneration (47). Degradation of collagen by matrix metalloproteinases (collagenases) is important not only for remodeling of ECM and cell migration but also for osteogenic differentiation of hMSC (19), (40). The cleavage of collagen produces peptides that themselves serve as signaling molecules and release ECM bound latent growth factors like TGF- β . Cells do not migrate into and remodel modified non-native collagen matrix as effectively as they interact with native fibrillar collagen. The inability of cells to degrade collagen that contains inert cross-links or has been forced into non-native conformation, interferes with the process of osteogenic differentiation of hMSC (48). hMSC on native collagen tend to differentiate along osteogenic lineages while those on denatured collagen substrata differentiate along adipogenic lineage (49). The above observations strongly emphasize the need for the use of native collagen type I in developing tissue engineered grafts.

In addition to the native status of collagen, contraction of the collagen gel by the resident cells also needs to be considered when engineering tissue grafts or 3-D models based on

collagen type I. The contraction process reduces the overall size of the construct by expulsion of water from the gel and increase in the matrix density (55). *In vitro* the reduced porosity of the contracted matrix (gel) may restrict the availability of nutrients to the components cells and significantly reduce the number of viable cells. *In vivo* ECM contraction assists wound closure but when it is excessive it is responsible for scar formation (64). Because of the poor cell supporting environment dense scars are impermeable to cell invasion and cannot vascularise and remodel to more viable tissue. Previous research in our laboratory led to the development of a non-contracting connective tissue equivalent generated using native collagen type I gel (64). When fibroblasts are cultured in this 3-D construct under appropriate culture conditions, they remain quiescent and do not contract the collagen gel. In the present study we examined and report on various factors that affect native collagen type I gel contraction that may occur during the process of osteogenic differentiation of hMSC.

Materials and Methods

Collagen Type I Gel

Cold (4°C) porcine collagen type I solution (3mg/ml, Cellmatrix[®], Wako Chemicals, Richmond, VA,) (8 parts v/v) was mixed thoroughly with cold (4°C) solution of MEM- α (10X, non-buffered, serum free) (1 part, v/v) and then neutralized (pH 7.4) with cold (4°C) reconstitution buffer (sodium hydroxide 0.5N, sodium bicarbonate 22g / L, HEPES free acid 47.7 g / L) (1 part v/v). After each addition careful and thorough mixing was required to prevent air bubble formation in the viscous solution. All mixing steps were conducted under

sterile conditions at 4°C (on ice). When incubated at 37°C and at 5% CO₂ the solution gelled within 30 min. All experiments were performed using this collagen type I gel forming process.

Cells

Human bone marrow derived mesenchymal stem cells (hMSC) (Lonza, Switzerland) from a male donor were cultured in MEM α (GIBCO, Invitrogen, Carlsbad, CA) containing fetal bovine serum (FBS, 10%, Atlanta Biologicals, Lawrenceville, GA) and FGF (10 nM, R&D Systems, Minneapolis, MN), with medium changes every second day. When 80-90% confluent hMSC were sub-cultured by harvesting with trypsin (0.05%) with 0.53 mM EDTA in HBSS (GIBCO, Invitrogen, Carlsbad, CA), and neutralization of the enzymatic activity with trypsin inhibitor (Soy protein, GIBCO, Invitrogen, Carlsbad, CA). Cells were counted using hemocytometer and Trypan blue (Sigma-Aldrich, St. Louis, MO) dye exclusion viability stain and then plated at 3000 cells/cm². Cells were used in either passage 4 (early passage is passage less than 5) or passage 10 (late passage is more than 10).

Osteogenic differentiation to produce human osteoblasts (hOST) was conducted by culturing hMSC in osteogenic differentiation medium (ODM). Medium was prepared using MEM α (GIBCO, Invitrogen, Carlsbad, CA) containing FBS (10%, Atlanta Biologicals), ascorbate-2-phosphate (200 mM, Sigma-Aldrich, St. Louis, MO), dexamethasone (10nM, Sigma-Aldrich), and β -glycerol phosphate (10mM, Sigma-Aldrich). Medium was changed every second day. When nearly confluent cells were harvested and counted as described above for hMSC.

Telomerase transduced human mesenchymal stem cells (TMSC) (a kind gift from Dr. Dario Campana, St. Jude Children's Research Hospital, Memphis, TN) (35) were cultured as

described for hMSC. Osteogenically differentiated TMSC (TOST) were obtained by culturing TMSC in ODM for 10 weeks as described above for hMSC.

Collagen gel contraction

Collagen solution was prepared as described above. Appropriate number of cells (150,000 to 2,400,000) were pelleted (15 ml centrifuge tube) and the pellet suspended in cold (4°C) neutralized collagen type I solution (3 mL) by passing the suspension through a syringe (5 mL) and needle (21 G, 1.5 inches). The resulting suspension of cells (250 µL) was dispensed in each well of a 48-well plate. After gelling (incubation at 37° C and 5% CO₂ for 30 min) the appropriate medium (MEM α or ODM) was added to each well (1 ml/well). At specific time points (day 1, 7, 14 and 28) the medium was carefully aspirated from the wells, the gels were transferred from the wells to plastic weighing boats and weighed (OHAUS GA110 analytical balance, Pine Brook, NJ). The fluid released from the gel during this handling was also weighed.

MTT Assay

TMSC and TOST were plated in 12-well plates at densities of 2500, 5,000, 10,000, 20,000, 40,000, 80,000, 100,000 cells per well, using biological triplicates for each seeding density value. After allowing the cells to attach, medium was removed, cells washed with phosphate buffered saline (0.256g/L NaH₂PO₄ H₂O, 1.19g/L Na₂HPO₄, 8.76g/L NaCl, pH 7.4, in distilled water) (PBS) and incubated with MTT [500 µL per well of a 0.2 mg per ml solution of 3-(4,5-Dimethylthiazol-2-yl)-2,5-diphenyltetrazolium bromide, Sigma-Aldrich in PBS] for two hours at 37°C. MTT solution was aspirated and the formazan formed in the cells recovered using formazan solubilization solution (250 µl, Sigma-Aldrich), with rocking for 90 minutes. Aliquots of dissolved formazan (100 µL) were transferred to wells of a 96-well plate, as

two statistical replicates for each cell density. The 96-well plate was scanned at 570 nm using a plate reader (Molecular Devices Spectramax 340 PC, MDS Analyticals, Toronto, Canada) and the results recorded.

Collagen gels were populated with cell densities from 3×10^4 cells per ml (60K, 125K, 250K, 500K) to 1×10^6 cells per ml. Following overnight incubation the gels were transferred from their original wells to wells of a 24-well plate, washed with PBS, (1 mL per well), and analyzed using the MTT assay described above. The same assay technique was used to assess the cell number at various time points.

Tissue processing for Immunocytochemistry

Collagen gels were fixed in 10% buffered formalin (formaldehyde 10mL, Na_2HPO_4 1.6g and $\text{NaH}_2\text{PO}_4 \cdot \text{H}_2\text{O}$ 0.4g in 100 mls of distilled water, all from Fisher Scientific, Pittsburg, PA, USA), at 4°C for 24 h, dehydrated through a series of ethanols and xylenes and embedded in paraffin. Embedded tissues were sectioned and the sections (~30 μ) were deparaffinized by incubations in xylenes and ethanols. After rehydration for 30 min in PBS and distilled water washes (3x10 min), the tissue sections were subjected to immunohistochemistry (by indirect immunofluorescence). Mounted specimens were examined on Olympus AX70 fluorescent microscope (Olympus, Center Valley, PA) using SPOT[®] TWAIN software (Microsoft, Issaquah, WA).

Immunohistochemistry

Slides were stained according to recommendations of IHC kit manufacturer (Prohisto, Columbia, SC, USA). Rehydrated tissue sections were washed in Amplifying IHC wash buffer (1x, IHC Kit, Prohisto, Columbia, SC), 3 mL per slide for 5 minutes, rocking at

room temperature (RT), in the amplifying chamber (IHC, Prohisto). Slides were then placed in epitope unmasking solution (1x, IHC Kit, Prohisto), using sufficient volume to cover all slides in the slide rack, and the slide rack was placed in boiling water for 20 minutes. After cooling to room temperature, slides were transferred to amplifying chamber (IHC Prohisto) in which all the subsequent steps were performed. Slides were washed with amplifying wash buffer (1x, 3mls/slide, IHC Kit, Prohisto), rocking for 5 minutes at RT and then blocked with 1% BSA (3ml per slide, EMD Chemicals, Gibbstown, NJ, USA) in PBS, rocking for 30 minutes at RT. Primary antibodies were diluted in amplifying antibody dilution buffer (1x, 3 ml per slide IHC Kit, Prohisto) as follows: mouse anti-osterix antibody (Novus biologicals, Littleton, CO, USA), to 1:500 and rabbit anti-osteopontin (Abcam Inc., Cambridge, MA, USA) to 1:800. The slides were incubated with rocking for 24 hours at 4°C. The slides were then washed 3 times in amplifying wash buffer (1x, 3 ml per slide, IHC Kit, Prohisto), rocking for 5 minutes at RT. Alexa Fluor 594 labelled goat anti mouse and Alexa Fluor 488 labelled goat anti rabbit (both from, Invitrogen, Eugene, OR, USA) secondary antibodies were diluted in PBS to 1:4000 and slides were incubated with 3 ml antibody solution per slide for 24 hours at 4°C on a rocker. Slides were then washed 3 times in amplifying wash buffer (1x, 3 ml per slide, IHC Kit, Prohisto), rocking for 5 minutes, at RT, followed by distilled 3 water washes, 3 ml per slide rocking for 5 minutes at RT. Coverslips were mounted on the slides using Prolong Gold antifade reagent with DAPI (Invitrogen, Eugene, OR, USA). After allowing the slides and coverslips to dry overnight the slides were examined by fluorescent microscopy as described earlier.

Statistical analysis

GraphPad Prism 4 (GraphPad Software, LaJolla, CA) was used to graphically represent and statistically analyze the results. Two-way ANOVA was used for analysis of gel

contraction and was followed by Bonferroni post comparison tests to compare individual groups. In all the experiments the “*n*” indicates biological replicates. Area under the curve (AUC) was calculated using trapezoid formula in order to compare the effect of cell density (for early and late passage cells) on collagen contraction. It served as a representation of the total contraction over 28 days. $AUC = \frac{1}{2} [\text{Weight on day 1} + 2 * \text{Weight on day 14} + \text{Weight on day 28}] * 4$

One-way ANOVA was applied for AUC analysis and this was followed by Bonferroni post comparison tests, which were utilized to compare individual groups.

Results

Determination of cell number in 3-D

Absorbance of light by formazan plotted against cell number is a linear relation with r^2 values above 0.99 for both telomerase transfected mesenchymal stem cells (TMSC) and their differentiated progeny, telomerized osteoblasts (TOST) ($n=3$ for both) when cells are cultured as a monolayer (Figure 1A).

When light absorbance by formazan is plotted against number of hMSC in collagen gel a linear relationship (with spearman's correlation statistic of 1.000) is observed for cell numbers ranging from 0.75×10^4 cells to 25×10^4 cells (corresponding to cell densities of 3×10^4 cells/ml to 100×10^4 cells/ml collagen gel) (Figure 1B).

Effect of cell number on collagen gel contraction

A rapid contraction phase during the first 24 hours was observed for all seeding densities of hMSC (passage 4), with the gels contracting by approximately 20% (Figure 2A).

After this initial period gels with 10×10^4 hMSC per mL did not contract further while gels with 20×10^4 and 40×10^4 hMSC per mL continued to contract ($40 \times 10^4 > 20 \times 10^4 > 10 \times 10^4$) over the first fourteen days in culture. Thereafter the contraction stopped even in high cell density gels. This relationship between initial seeding density and contraction remained even though the cell proliferation in the gels continued (Figure 2B). When average contraction over a period of one month is considered (area under the curve) cell density is a significant determinant in the collagen gel contraction process by early as well as late passage cells (Figure 2C).

In collagen gels containing a low cell density there was a change in morphology of the cells from bipolar to rounded / dendritic (osteoblast like) (Supplementary Figure 1A and 1B) along with expression of osterix at day 28 (Supplementary Figure 1C and 1D).

Effect of serum on collagen gel contraction

With early passage hMSCs (passage < 5) are used, gel contraction in the presence of high (10%) and low (4%) serum culture medium was not significantly different for 10×10^4 hMSC per mL (Figure 3A). Similar “contractile insensitivity” to differences in serum content were observed with collagen gels containing 40×10^4 hMSC per mL. But significant difference in collagen gel contraction was observed when comparing 10×10^4 cells per ml to 40×10^4 cells per ml regardless of serum concentrations.

Effect of Serum on Cell Proliferation

hMSC populating collagen gels and cultured under high serum conditions show proliferation of cells over a period of one month irrespective of initial seeding density (Figure 2B). On the other hand when hMSC populating collagen gels are cultured under low serum conditions, gels seeded initially at 40×10^4 and 20×10^4 cells per mL show proliferation for 14

days but a decrease in the cell number from 14 to 28 days (Figure 3B). Collagen gels initially populated with 10×10^4 hMSC per mL showed cell proliferation over 28 days when cultured in low serum medium

Effect of cell passage on collagen gel contraction

Late passage (>10) and early passage (<5) hMSC contracted the collagen gels similarly (20%) during the first 24 in culture in the presence of 10% serum (Figure 4A). However over a period of 28 days in culture late passage hMSC caused significantly higher collagen gel contraction than early passage cells. Approximately 6% higher contraction was observed irrespective of the initial cell seeding density (10×10^4 - 40×10^4 cells per mL) with late passage hMSC. Early passage hMSC proliferated over a culture period of 28 days (Figure 2B) but late passage hMSC did not proliferate over the same period (data not shown).

Late passage hMSC in low (4%) serum conditions (Figure 4B) differed from early passage hMSC (Figure 3A). When serum concentration was reduced to 4% there was no significant contraction of the collagen gels over a one-month culture period in case of late passage MSC whereas early passage hMSC had contracted the collagen gel under low serum concentrations.

Effect of constitutive expression of telomerase on collagen gel contraction

During the first 24 hours of culture in 10% serum containing ODM telomerised MSCs, (TMSC, 10×10^4 cells/ml) contracted collagen gels by 10% (Figure 5A). Cultured under the same conditions collagen gels populated with hMSC a significantly greater contraction (20%) was observed. At the end of 14 days TMSC were significantly less (13%) contractile than hMSC cultured under identical conditions (FIG 5A).

Telomerised human osteoblasts (TOST) were derived by osteogenic differentiation of TMSC over a period of 12 weeks. When populating collagen gels (10×10^4 cells/ml) at the end of 24 hours culture period in 10% serum containing ODM, TOSTs caused a significantly higher collagen gel contraction (20%) than TMSC (10%) (Figure 5B). Over a period of 14 days in culture TOST populated collagen gel contraction was significantly higher (by 8%) than that caused by TMSC. The proliferation of hMSC, TMSC and TOST in the collagen gel were similar and conform to the same equation (supplementary figure 2)

Figures and Legends

Figure 1. MTT can be used to determine number of cells in a collagen hydrogel. Figure 1A.

The formazan formed is linearly related to the number of cells ranging from 0.25×10^4 to 10×10^4 cells. The formazan formation is similar for TMSC and TOST. Runs test indicates that both lines are not significantly different from one another confirming that MTT assay can be used to determine cell numbers during osteogenic differentiation (Mean and SEM, $n = 3$) **Figure 1B.**

Formazan formation is linearly related to the number of cells in collagen hydrogel over a range of 3×10^4 cells per ml to 100×10^4 cells per ml. A spearmans correlation statistic of 1 indicates a strong correlation between formazan formation and number of cells in collagen hydrogel. Thus MTT absorbance can be used to quantify the number of cells in a collagen hydrogel. (Mean and SEM, $n = 3$)

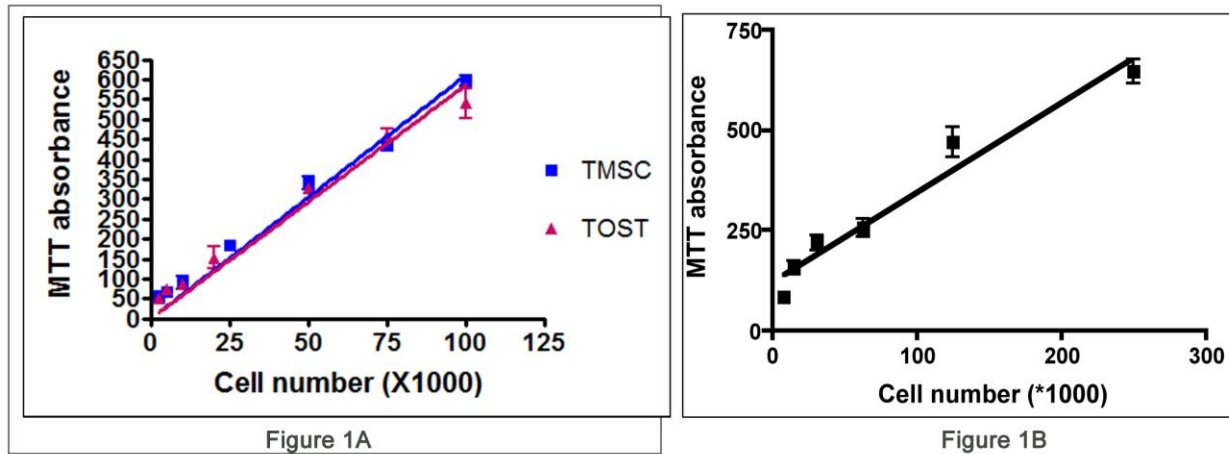


Figure 2. Effect of cell seeding density on collagen hydrogel contraction. Figure 2A. Collagen hydrogels contract to about 80% of their original weight within 24 hours, regardless of the cell seeding density with 10% serum. Over the next 14 days collagen gel with higher seeding density contract significantly more than those with lower seeding density. The gels do not contract significantly after 14 days. (Mean and SEM, $n = 3$, $p < 0.05$) **Figure 2B.** hMSC continue to proliferate over a period of 28 days under osteogenic differentiation conditions with 10% serum at all seeding densities. (Mean and SEM, $n = 3$, $p < 0.05$) **Figure 2C.** Early as well as late passage cells contract the collagen gel significantly more at higher cell seeding densities under osteogenic differentiation conditions with 10% serum. A lower area under the contraction curve indicates greater contraction. 10×10^4 cells per ml have a significantly greater area under the curve than 40×10^4 cells per ml regardless of whether early or late passage cells are used. (Mean and SEM, $n = 3$, $p < 0.05$)

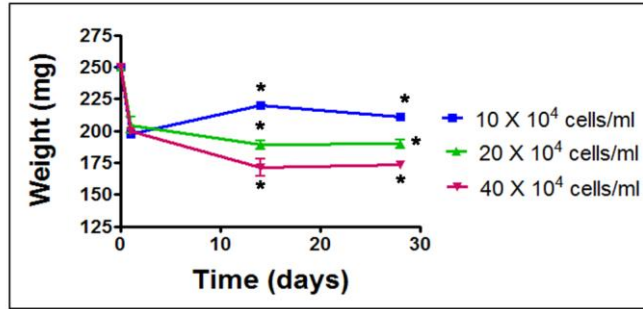


Figure 2A

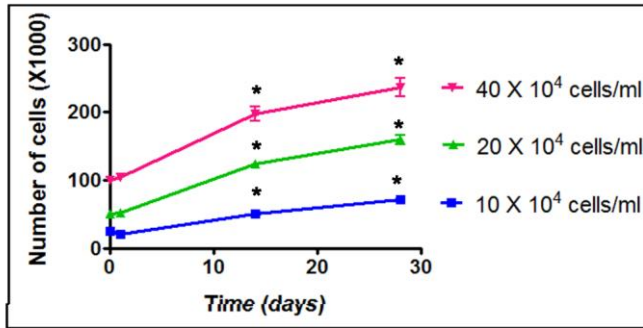


Figure 2B

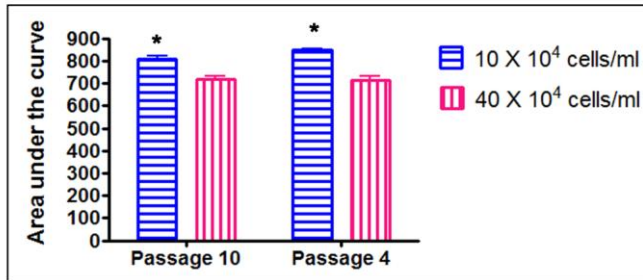


Figure 2C

Figure 3. Effect of serum on collagen hydrogel contraction. Figure 3A. Collagen hydrogels contract in a similar fashion at 10×10^4 cells per ml and at 40×10^4 cells per ml when cultured under either 10% or 4% serum supplementation. This indicates that lowering the serum contraction does not prevent collagen hydrogel contraction. (Mean and SEM, $n = 3$, $p < 0.05$)

Figure 3B. At low serum concentration in the medium cells at 20×10^4 cells per ml and 40×10^4 cells per ml proliferated for 14 days after which the cell number decreased. At 10×10^4 cells

per ml proliferation continues to occur over 28 days. Thus low serum culture conditions do not support cell survival or proliferation in early passage cells over a long culture period. (Mean and SEM, $n = 3, p < 0.05$)

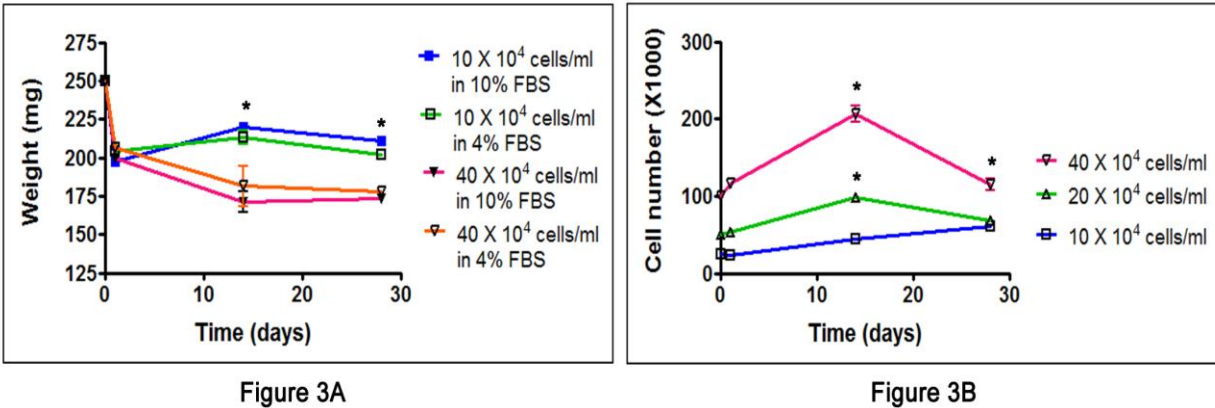


Figure 4. Effect of cell passage on collagen gel contraction. Figure 4A. Early and late passage cells contract the collagen gel in a similar fashion over the first 24 hours. At the end of 28 days late passage cells contracted collagen gel significantly more than early passage cells at 10 X 10⁴ cells/ml and 40 X 10⁴ cells/ml seeding densities. Late passage cells did not proliferate over the duration of the experiment (data not shown) (Mean and SEM, $n = 3, p < 0.05$) **Figure 4B.** Decreasing serum concentration in the culture medium (4%) for late passage cells prevented collagen gel contraction at all seeding densities. This is different from early passage cells where serum did not have any effect on collagen gel contraction. (Mean and SEM, $n = 3, p > 0.05$)

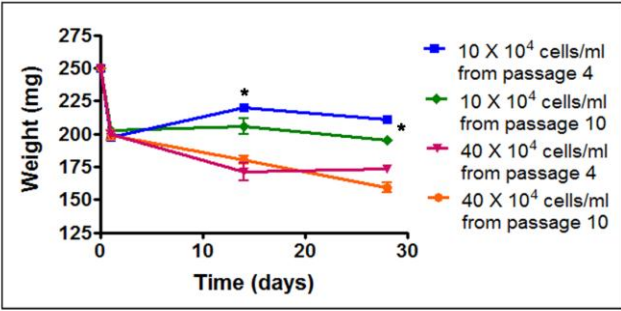


Figure 4A

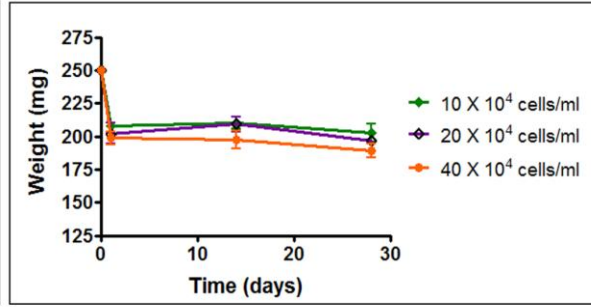


Figure 4B

Figure 5. Effect of telomerase expression on collagen gel contraction. Figure 5A. Telomerase transformed mesenchymal stem cells (TMSC) contracted the gel significantly less as compared to primary mesenchymal stem cells (hMSC) at 24 hours as well as at the end of 14 days. (10×10^4 cells/ml, Mean and SEM, $n = 3$, $p < 0.05$) **Figure 5B.** Effect of differentiation on collagen gel contraction. Telomerase transformed human osteoblasts (TOST) contracted the gel significantly more at 24 hours and 14 days as compared to TMSC. (10×10^4 cells/ml, Mean and SEM, $n = 3$, $p < 0.05$)

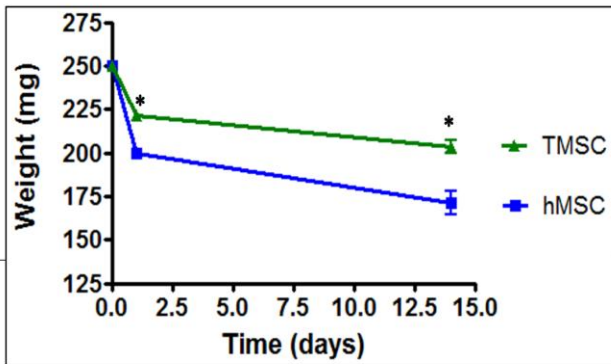


Figure 5A

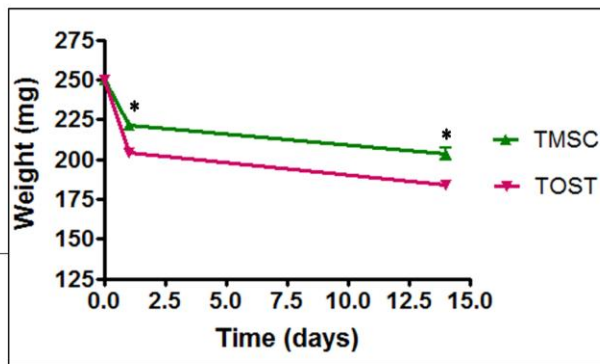
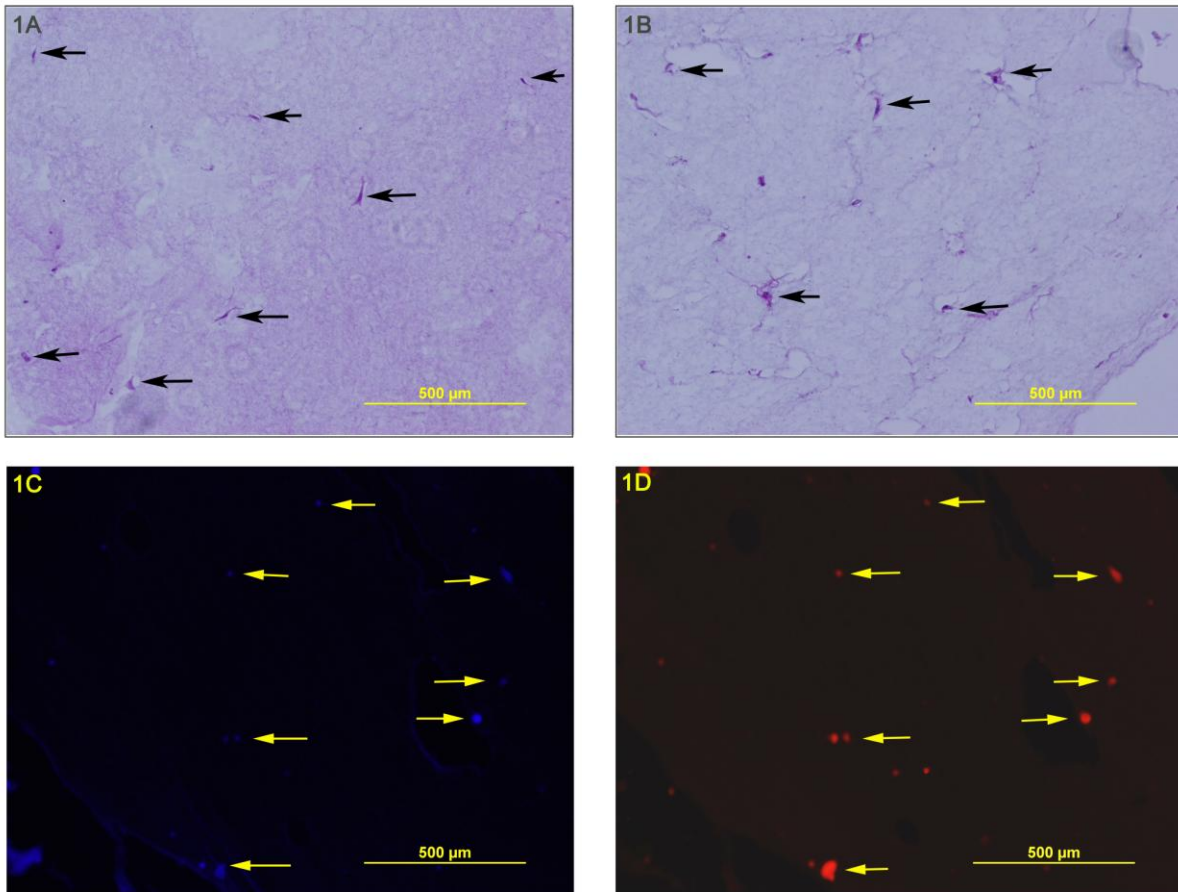


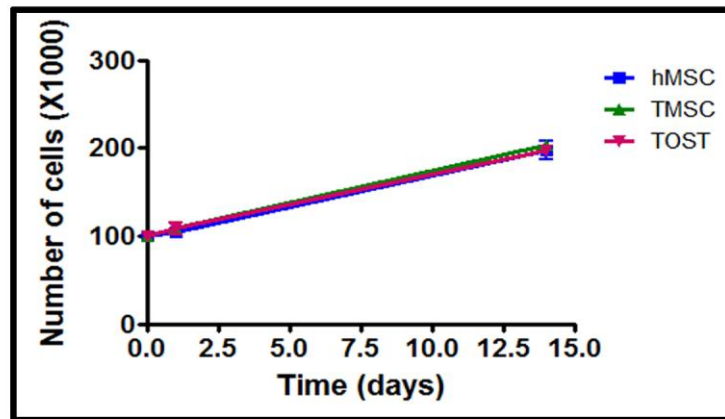
Figure 5B

Supplementary figure 1. Osteogenic differentiation at low cell seeding density (100,000 early passage hMSC per ml collagen gel maintained under osteogenic differentiation conditions with 10% serum). **Supplementary figure 1A.** Hematoxylin and eosin stained paraffin embedded section of collagen gel showing bipolar hMSC in the gel on day 1. **Supplementary figure 1B.** Hematoxylin and eosin stained paraffin embedded section of collagen gel on day 28 demonstrates change in morphology of the cells to a multipolar, more osteoblast like phenotype. **Supplementary figure 1C.** Collagen gel stained with DAPI to identify positions of nuclei. Nuclei are marked with yellow arrows which are copied in the same position in panel 1D. Image was enhanced to see the nuclei more clearly. **Supplementary figure 1D.** Immunohistochemistry with osterix, a differentiation marker, on collagen gel on day 28 demonstrated nuclear expression of osterix a differentiation marker. Gels on day 1 did not express any differentiation markers (data not shown)



Supplementary Figure 1

Supplementary figure 2. Cell proliferation of hMSC, TMSC and TOST in collagen hydrogel under osteogenic differentiation conditions for two weeks. All three cells were seeded at a density of 40×10^4 cells per ml of collagen gel and the cell number doubled over a period of 14 days. The rate of proliferation was the same for all three cell types.(Mean and SEM, $n=3$, $p>0.05$).



Supplementary figure 2

Discussion

Collagen is the most important structural protein in the body and is therefore a natural choice for tissue engineering applications (4). Fibrillar collagens, types I, II and III are basic components of connective tissues, in which collagen is synthesized by resident cells. Collagen fibrils are formed from 300 nm long and 1.5 nm wide parallel tropocollagen arrays. The use of collagen gels as matrices for the construction of 3-D tissue models was first reported by Elsdale in 1972 (41), who described a method of preparation of type I collagen gels as an environment in which fibroblast can be cultured. In 1979 Bell et al observed that contraction of collagen gel by fibroblasts caused extrusion of water that could be detected as a decrease weight (54). It was concluded that the presence of fibroblasts in the collagen gels was responsible for contraction since acellular collagen gels, cultured under similar conditions did not contract. In our study a 10% loss in weight was observed when acellular collagen gels extruded water during physical handling (e.g. transfer from the casting wells to the weighing boats). If the extruded water is taken into consideration there was no change in weight. Thus in all our experiments

involving collagen gels the loss in weight was compensated to account for mechanical perturbation during handling and were compared with the weight of collagen gel that was initially dispensed.

Grinnell compared collagen gel contraction, in two gel formats, “free floating” gels and “anchored” gels (63) that were similar with respect to tractional remodeling, integrin expression and extracellular forces. In anchored gels tension develops anisotropically and contracted gel is under tension as long as it remains anchored. The free-floating gels were proposed to be more *in vivo* like because they were not constrained and responded freely to mechanical perturbation. However, *in vivo* all tissues are under homeostatic tension and *in vitro* cells can proliferate in anchored gels but do not proliferate, are not as responsive to growth factors and show reduced collagen synthesis in free-floating gels. The cells in anchored gels align with lines of tension and the anisotropic contraction resembles that observed in granulation tissue *in vivo* while the cellular functions within free-floating gels resembles cell behavior within scar tissue. Therefore use of anchored collagen gels to study contraction during osteogenic differentiation is appropriate.

Use of MTT to track cell number

Resident cell viability is clearly an issue in 3-D matrices including collagen gels. Following cell viability using live-dead assays Sumanasinghe et al (57) acknowledged the limitations of this protocol and the difficulties in accurate determination of the cell number in a 3-D collagen gel. The use of collagenase digestion of the collagen gels was proposed to lead to cell death and was the contributing factor to the low cell numbers. In the present study we showed that MTT conversion to formazan is a simple and effective assay to determine the cell

number in collagen gels and other 3-D matrices (collagen based scaffolds, unpublished data). For example the response of the assay, graphical plot of absorbance against cell number, when applied to gels populated with freely proliferating TMSC is not significantly different from the response of TOST, and the same equation can be used to describe both responses (Figure 1A). This indicated that osteogenic differentiation (differentiation of TMSC into TOST) did not affect the performance of the MTT assay. This indicated that the MTT assay was appropriate protocol for studies of cell proliferation during osteogenic differentiation of hMSC in 3-D collagen matrix. A Spearmans correlation statistic of 1.000 indicates a strong corelation between formazan formation (light absorbance by dissolved formazan) and cell number (Figure 1B) in collagen gel. This standard curve can be used to calculate the number of cells from the observed absorbance. The correlation between number of cells in a collagen gel and the absorbance was statistically significant and linear over the range 30k - 1 million hMSC per mL, an appropriate range for our studies.

Effect of cell density

Bell et al observed that collagen gel contraction by fibroblasts was initially dependent on the number of cells populating the gel matrix. After extended culture time and after a certain cell density threshold is exceeded, the contractions were independent of starting cell density (54). Below this poorly defined contractile sensitivity threshold, collagen gel contraction was linearly dependent on cell density. Nishiyama also observed similar cell density dependence of collagen gel contraction by fibroblasts (65).

During the first 16 hours of culture, Awad et. al. observed that the rate of contraction for collagen gels populated by 1 million rabbit MSC cells / mL was slower than for

gels with 4 and 8 million cells (102). By measuring the initial and final diameter of the constructs they determined that after 72 hours in culture the collagen gel contracted by 60-77% but thereafter the contractions rate was independent of cell number. Using rabbit MSC and extending the study period, Nirmalanandhan (103) showed that the threshold of dependence of collagen gel contractions on cell number was ~ 500k cells per mL, 100k rMSC per ml collagen contracted the collagen gel by 70% determined by measuring the initial area of the construct and comparing with the area at 7 days, while 1 million cells resulted in 95% contraction. In our present study using human primary cells we observed collagen gel contraction of 20% after the first 24 hours in culture independent of initial seeding density (Figure 2A). Collagen gels prepared in accordance with our patented technology (64) and seeded with 400,000 cells per ml contracted by 30% which is far less than that previously reported by other groups (55), (57), (102), (103).

Rat calvarial osteoblasts proliferation was reduced when in 3-D (collagen gels) when compared with that in monolayers cultures (58). Unfortunately the low amount of collagen used makes this and a number of other studies an example of cell behavior in thin collagen films and not 3-D matrices. Primary human osteoblasts in collagen gels did not proliferate and a significant decrease in cell viability was reported after day 16 (14). The diameter of gel containing the osteoblasts decreased by 50% in 24 hours (a decrease in volume of 87.5%) and the diameter of the construct stabilized at one-third the original for the remaining 10 days of the experiment. Although it was proposed that the cells became quiescent (arrest in proliferation) it is more likely that there was a loss in cell viability and cell death subsequent to inadequate nutrient supply due to severe increase in matrix density. In our study, minimized contraction allowed continued cell proliferation over 28 days at all seeding densities in the presence of 10%

FBS supplementation (Figure 2B) and proved to be a suitable environment for osteogenic differentiation.

In our experiment with hMSC and TMSC the gel contraction at the end of 24 hours was similar for all gels regardless of the initial seeding density (Figure 2A) and the contraction over one month (Figure 2A and 2C) was only marginally increased (9% difference, $p < 0.05$) for high initial seeding density when early and late passage cells were used. Holy et al demonstrated that bone tissue formation in polymeric scaffolds does not depend on initial cell seeding density (60). Morphological changes (H&E staining) and expression of osterix showed that in our experiments the cells populating collagen gels at low seeding density (efficient use of therapeutically important cells) were able to differentiate (Supplementary figure 1). The use of a low cell seeding density to prevent collagen gel contraction during generation of tissue engineered grafts may be a viable option to overcome the problems associated with gel contraction.

Effect of serum

The supply and free access of nutrients is critical in all phases of the wound healing in all tissues and is equally important in bone regeneration. *In vitro* increasing the serum concentration (10% to 20%) increased collagen gel contraction by rat MSC (55) a similar response to that exhibited by fibroblast populating collagen type I gels (65), (104). The diameter of native gels with rat MSC contracted by 20% in 24 hours and by 76% in 14 days at 10% serum concentration (55). Gels modified by addition of polymerized dehydrated collagen fibers contracted by 45% in 14 days. Comparing contractions of collagen gels is challenging because of the variety of measurement methods used. Thus although in Lewus study a plateau in

contraction was noted at 7 days, the reduction of 30% in diameter translates to a 66% decrease in volume. Furthermore addition of polymerized dehydrated collagen fibers would lead to previously discussed (Introduction) drawbacks associated with cross-linked, non-native collagen. Since in our gels acid solubilized native collagen is used we have shown a complete resorption without adverse reactions after implantation *in vivo* (105). We observed that decreasing serum concentration to 4% did not have any effect on the overall collagen contraction (Figure 3A) but inhibited proliferation after 14 days in culture (Figure 3B). This supports the observation that overall collagen contraction is dependent on the initial seeding density for hMSC as both the gels in which cells proliferated (high serum, Figure 2B) and in which the cells could not (low serum, Figure 3B) contracted to the same extent. Thus decreasing serum in culture medium may be a feasible strategy to decrease collagen gel contraction for fibroblasts (105) but is not applicable for hMSC.

Cytoskeletal changes, particularly the expression of alpha smooth muscle actin (α SMA), in a substantial population of the contractile fibroblast phenotype – the myofibroblasts, has been the hall-mark of collagen gel contraction. Since contraction of collagen gels by MSC was linearly related to α SMA content of the cells, the α SMA content of cells has been proposed as an important determinant of gel contraction (56). Human mesenchymal stem cells and osteoblasts both express α SMA and its expression in MSC was not affected when cells were cultured under different serum concentrations for five days (56). This may explain why we did not observe any effect of the serum concentration on collagen gel contraction by early passage cells (Figure 3A).

Effect of Passage

Late passage fibroblasts were more contractile compared to early passage cells (54). We observed similar results with late passage hMSC contracting the gel significantly more than early passage hMSC over a culture period of 28 days (Figure 4A). The late passage cell population probably contains a larger number of osteoblasts that are more contractile by virtue of greater SMA content (56).

The response of late passage cells to a decrease in serum was different from that of early passage cells. Lowering the serum concentration to 4% prevented contraction of collagen gels after day one, at all initial seeding densities of hMSC (Figure 4B). Thus use of late passage cells under low serum conditions may provide an alternative method of preventing collagen gel contraction when a high number of cells is required in a potential engineered graft.

Effect of telomerase

It was reported that transformed fibroblasts contract the collagen gels less than normal cells (104). We found that telomerase transformed MSC (TMSC) contracted the gel significantly less after 24 hours as well as after 14 days when compared to normal hMSC (Figure 5A). We hypothesize that fewer transformed cells adopt a contractile phenotype and develop a contractile phenotype later than normal cells.

It has been reported that culture of hMSC in ODM caused greater contraction when compared to MSCGM (57), indicating greater contraction by osteoblasts. We observed that TOST contracted the collagen gel significantly more than TMSC during the first 24 hours (10% difference) and over a period of 14 days (8% difference) (Figure 5B). The cell numbers for hMSC, TMSC and TOST doubled after two weeks of culture in collagen hydrogel under osteogenic differentiation conditions (supplementary figure 2). Thus the difference in contraction

observed is likely due to increase in the population of the contractile phenotype of the cells. A greater contraction by TOST than TMSC is likely to be due to difference in expression of α -SMA, a contractile phenotype marker, which is upregulated during osteogenic differentiation (56).

In summary we have demonstrated that high initial cell seeding density, late passage cells, non-transformed cells, and differentiated hMSCs cells all increase collagen gel contraction. In contrast a low initial cell seeding density, early passage hMSC (non-differentiated) low serum culture medium, late passage cells, all minimize collagen contraction. Also allowing non-differentiated early passage hMSC to differentiate *in situ* could be an additional strategy to prevent collagen gel contraction of collagen type I hydrogels used as 3-D tissue culture models or tissue engineering grafts. A non-contracted matrix will provide a permeable matrix composed of loosely spaced native fibrils. These features would facilitate faster cell invasion (early vascularization), extensive remodelling and greater survival of implanted grafts leading to better host-graft integration and superior graft performance.

CHAPTER III

COLLAGEN BASED 3-D MODEL FOR *IN VITRO* STUDIES OF OSTEOGENESIS

Introduction

Musculoskeletal diseases and trauma are responsible for mortality (1 million annually in the US (101) and considerable morbidity (30 million / severe disabilities annually, WHO) and can seriously impact the quality of life. The cost of health care in this arena is over \$700 billion annually in the US, and is a significant national economic burden. Most of the non-traumatic, chronic musculoskeletal diseases are age related (100) and the increasing population over 65 years of age is projected to reach over 2.8 billion by 2100 (UN statistics). All these factors have contributed to the designation of 2001-2011 as the “Bone and Joint Decade” by the WHO, highlighting the importance and the need for musculoskeletal research.

The human skeleton is a multifunctional system that provides mechanical support and protects soft internal tissues, stores physiologically essential calcium and phosphate ions and is the hematopoietic and immune system stem cell niche (1). Bone is a dynamic tissue in which three cell types, osteoclasts, osteoblasts and osteocytes, regulate its homeostasis by constant resorption and deposition of the mineral components and structural realignment and remodeling of its matrix in response to biochemical and mechanical signals. The primary component of bone matrix is collagen type I, which is converted to a hard porous scaffold by the process of

ossification – deposition of hydroxyapatite (HA, a complex calcium phosphate salt) (3), (4). A 3-D morphology is required for the initiation and completion of ossification (14), (18). When cultured as a monolayer, osteoblasts initiate mineralization only after formation of nodules, a 2-D approximation of a 3-D scaffold. The expression of proteins characteristic of osteogenic differentiation is much more pronounced in 3-D cultures than in cultured cell monolayers (16), (17). Thus *in vitro*, when the cells populate a 3-D matrix, the mineralization process begins earlier and proceeds faster. *In vivo*, osteoblasts repair a fracture by invading and mineralizing the collagenous matrix in a random manner (19), and as the mineral content increases, osteoblasts terminally differentiate into osteocytes, the most abundant cell type in bone. Thus the course of ossification in 2-D cultures differs markedly from that which takes place in 3-D, and supports superiority of 3-D models as *in vivo* like tools for bone biology research.

An important aspect of the 3-D structure is that it allows the bone to respond to mechanical forces by undergoing deformation to optimize its load bearing capacity (5). This mechanosensing capability and the ensuing remodeling process is an integral component of the bone function *in vivo*. Thus studies of bone tissue biology would be incomplete without the 3-D environment that facilitates studies involving mechanotransduction and remodeling. Majority of the current 3-D models used as research tools lack mechanical integrity and stability because they are soft hydrogels (7). Application of compression or tension forces to these models, causes compaction of the matrix followed by expulsion of water, and invariably results in cell death. Studies that examine the responses to applied forces use cells cultured as monolayers on elastic membranes that can be stretched continuously or cyclically. This approach may be appropriate for studying the effects of tensile forces (vascular, tendon and skeletal muscle cells) but is inappropriate for studying responses to forces acting on bone (compressive and torsional forces).

Thus there is a great need for a stable 3-D bone model that is populated with the appropriate osteogenic cells and is responsive to factors that regulate bone functions *in vivo*.

In the last decade 291 studies related to fracture healing were carried out in animal models (10). These studies included the use of small animals (mice, rats and rabbits) and large animals (dogs, sheep, pigs and goats). An appropriate 3-D *in vitro* model would allow execution of a variety of preliminary (proof of concept) studies at a greatly reduced cost and minimize ethical considerations that regulate the use of experimental animals.

A composite that best serves as a model for hard tissue biology research in 3-D relevant mechanoresponsive fashion, would also be of great benefit in tissue engineering of bone grafts. It will assist performance of fundamental studies in an *in vivo* relevant fashion and bridge the gap between the cell monolayer and animal models. Such a 3-D model should be easy to assemble, versatile, convenient to handle, and simple to evaluate using traditional and novel analytical approaches. We here present initial studies that are directed towards the design and assembly of such a 3 –D model.

Materials and methods

Collagen scaffold

Porous collagen scaffold - Avitene Ultrafoam[®] was a kind gift from Davol Inc. (Warwick, RI, USA). Ultrafoam[®] is a native collagen type I sponge (US Patent 6454787, Davol Inc), which is completely bioabsorbed within six months of implantation without any residue

(information from Davol). In all experiments the Ultrafoam[®] scaffold was divided into cubes (5mm x 5mm x 5mm).

Collagen Type I Gel.

Cold (4°C) porcine collagen type I-A solution (Cellmatrix[®], Nitta Gelatin, Wako Chemicals, Richmond, VA, USA, 3mg/ml) (8 parts v/v) was mixed with cold (4°C) solution of MEM- α (serum free, 10X, non-buffered) (1 part, v/v) and then with cold (4°C) neutralization buffer (1 part v/v, sodium hydroxide 0.5N, sodium bicarbonate 22g / l, HEPES free acid 47.7 g / l, to pH 7.4)) with thorough and careful mixing after each addition to obtain an homogeneous air bubble free viscous solution (CS). When incubated at 37°C under 5% CO₂ the CS gelled within 30 min. and this impregnation method was used in all experiments.

Characterization of Collagen Type I Scaffold

Cubical pieces (5mm x 5mm x 5mm) of dry Ultrafoam[®] were weighed and then immersed in water or CS (from above) for 24 hours in a humidified incubator (37°C, 5% CO₂). Once the uptake of fluids was complete the Ultrafoam[®] pieces were weighed and the ratio of (wet weight – dry weight) / dry weight was determined. The time taken for the collagen scaffold to become saturated after immersion in water was noted and used to estimate the amount of cross-linking in Ultrafoam[®] (47).

CyTM5 labeling of collagen

CS (10 mls) was reacted with bis-functional dye Cy5TM (0.2 mg, Amersham Biosciences, UK) dissolved in DMSO (200 μ l), stirring continuously for 24 hours at 4°C) and the labeled collagen solution was used as described.

Cells

GFP-tFbs: Human dermal fibroblasts immortalized by ectopic expression of hTERT were a kind gift from Dr. J.W.Shay (Department of Cell Biology, UT Southwestern Medical School, Dallas Texas). These cells were kindly transduced in the laboratories of Dr. Victor Gonzales (Howard Hughes Medical Center, Dallas Texas) using enhanced GFP and the stable transfectants were isolated by cell sorting. (106)

GFP expressing hTERT dermal fibroblasts (GFP-tFbs) were cultured in DMEM (GIBCO, Invitrogen, Carlsbad, CA) containing fetal bovine serum (FBS, 10%, Atlanta Biologicals, Lawrenceville, GA) in a humidified incubator (37°C, 5% CO₂) with medium changes every second day.

hMSC: Bone marrow derived hMSC (Lonza, Switzerland) were cultured in MEM α (GIBCO, Invitrogen, Carlsbad, CA, USA) containing FBS (10%, Atlanta Biologicals, Lawrenceville, GA), 1% Penicillin-streptomycin (GIBCO, Invitrogen, Carlsbad, CA, USA) and FGF (10 nM, R&D Systems, Minneapolis, MN), with medium changes every second day. hMSC were passaged at 80-90% confluence using trypsin (0.05%) with 0.53 mM EDTA in HBSS (GIBCO, Invitrogen, Carlsbad, CA, USA) and plating at 3000 cells/cm². Cells were counted using hemocytometer and Trypan blue (Sigma-Aldrich, St. Louis, MO, USA) dye exclusion viability stain.

hOST: Primary human osteoblasts (hOST, Lonza, Switzerland) were cultured in osteoblast growth medium (OGM, Lonza, Switzerland) which maintains the proliferative phenotype. hOST were expanded as described above for hMSC. Osteogenic differentiation of hMSC was induced using MEM α (GIBCO, Invitrogen, Carlsbad, CA, USA) containing FBS

(10%, Atlanta Biologicals, Lawrenceville, GA, USA), ascorbate-2-phosphate (200 mM, Sigma-Aldrich, St. Louis, MO), dexamethasone (10nM, Sigma-Aldrich, St. Louis, MO, USA), and β -glycerol phosphate (10mM, Sigma-Aldrich, St. Louis, MO, USA). This medium is referred to as osteogenic differentiation medium (ODM) and was changed every other day.

Impregnation of The Collagen Scaffold

After preparation, dispensing accuracy of CS, was determined by pipetting 50 μ l into plastic weigh-boat weighing (OHAUS GA110 analytical balance, Pine Brook, NJ, USA). The collagen type I scaffold - Ultrafoam[®] cubes were immersed in medium, the excess medium blotted on filter paper and the cell suspension in CS (10^5 cells/ml, 250 μ l) seeded on to the scaffold. The impregnated Ultrafoam[®] cubes were incubated at 37°C to allow collagen solution to gel and will be thereafter referred to as collagen gel impregnated collagen scaffold (CGCS).

Retrieval of Cells from CGCS

To release the cells, collagen type I foam scaffold (Ultrafoam[®]) or CGCS were treated with collagenase P (1ml / 5x5x5 mm cube, Roche, Germany) for one hour at 37°C. Collagenase P was reconstituted as directed by Roche in Hanks Buffered Salt Solution to a concentration of 2 mg/ml.

Confocal Microscopy

The distribution of the cells in the CGCS was studied using scanning laser confocal microscopy (Zeiss, LSM-410) by analyzing the cellular content of the model at various optical planes throughout the specimens. Images were obtained using a 10 X objective, while keeping the pinhole and other parameters constant. GFP expression in GFP-tFbs was observed

using 488nm and Cytotracker™ Orange (Invitrogen, Carlsbad, CA) labeled hOST cells were observed using 568 nm excitation laser.

Neutral Red Staining

Neutral red (3-Amino-7-dimethylamino-2-methylphenazine hydrochloride, Sigma-Aldrich, St. Louis, MO, USA) was dissolved in distilled water (1 gram in 100 ml) CGCS with GFP-tFbs was maintained in culture for 30 days and then placed in serum free DMEM with 10% neutral red and incubated for 2 hours at 37⁰C. At the end of the incubation period CGF was washed with phosphate buffered saline (0.256g/L NaH₂PO₄ H₂O, 1.19g/L Na₂HPO₄, 8.76g/L NaCl, pH 7.4, in distilled water) (PBS) and examined by confocal microscopy.

MTT Assay

The CGCS 3-D constructs, placed in wells of a 24-well plate, were washed with PBS (1 ml/well), and incubated with 3-(4,5-Dimethylthiazol-2-yl)-2,5-diphenyltetrazolium bromide, (MTT, 0.2 mg / ml of PBS - 500 µl /well, Sigma-Aldrich, St. Louis, MO, USA) for two hours at 37⁰C. The formazan from metabolized MTT was dissolved in solubilization solution (250 µl, MTT assay kit) by rocking for 90 minutes, and 100 µl aliquots were transferred to wells of a 96-well plate (duplicate wells/specimen). The 96-well plate was examined using the plate reader (Molecular Devices Spectramax 340 PC, MDS Analyticals, Toronto, Canada) and the absorbance at 570 nm recorded. Using a monolayer of hMSC (seeding density 7.5 x 10³ - 2.5 x10⁵ cells per well in a 24 well plate) the standard curve for the conversion of MTT into formazan (a straight line with Spearmans correlation statistic of 1, and $p < 0.05$) was used to calculate the cell number from the formazan absorbance. The standard curve was used to determine the cells that had “escaped/overflowed” the CGCS impregnation and subsequently the

cell numbers residing in CGCS.

Alkaline Phosphatase Assay (ALP)

The CGCS 3-D model containing hMSC (5mm cubes) were cultured in 24-well plate with medium (ODM) changed every other day. Samples were removed from culture weekly during the period of four weeks. The specimens washed with PBS (1 ml /well) in the wells in which they were cultured and were pulverized (small pestle) in the tissue lysis buffer (250 μ l, 1x component of ALP assay kit, Anaspec Enzolyte™, San Jose, CA). Aliquots of tissue lysate (50 μ l) were transferred to a 96-well plate and each well was treated with p-nitrophenyl phosphate solution supplied in ALP assay kit (50 μ l/well, pNPP). After incubation (30 min at 37°C) the 96-well plate was examined at 405 nm (Molecular Devices Spectramax 340 PC, MDS Analyticals, Toronto, Canada). DNA content of tissue lysates was determined using an Eppendorf Biophotometer (Eppendorf, Westbury, NY) with the built in settings for measuring double stranded DNA in solution.

Tissue Processing

Samples of CGCS were fixed in buffered formalin (10% formalin/formaldehyde 10 mls, PBS, Fisher Scientific) at 4 °C for 24 h, dehydrated through a series of ethanols and xylenes and embedded in paraffin. Embedded specimens were sectioned (~30 μ thickness), and sections were deparaffinized by incubations in xylenes and ethanols. After rehydration for 30 min in PBS and distilled water washes (3x10 min), sections were used for histochemical / immunohistochemical analysis. Mounted specimens were examined on Olympus AX70 fluorescent microscope (Olympus, Center Valley, PA) using SPOT® TWAIN software (Microsoft, Issaquah, WA).

Immunohistochemistry

Rehydrated tissue sections were washed in Amplifying buffer (1x, 3 ml/slide, IHC Kit, Prohisto, Columbia, SC, USA), 5 minutes rocking at room temperature (RT, amplifying chamber, IHC, Prohisto). Slides were treated with epitope unmasking solution (1x, IHC Kit, Prohisto), covering all slides in the slide rack, and the slide rack heated in boiling water for 20 minutes. After cooling to RT, the slides were transferred to amplifying chamber (IHC Prohisto) in which all the subsequent steps were performed. Slides were washed with rocking (5min at RT) with amplifying buffer (1x, 3mls/slide, IHC Kit, Prohisto), blocked with 1% BSA (3 ml per slide, EMD Chemicals, Gibbstown, NJ, USA) in PBS, rocking for 30 minutes at RT. The slides were incubated with rocking for 24 hours at 4°C with mouse anti-osterix antibody (Novus Biologicals, Littleton, CO, USA) diluted to 1:500 or rabbit anti-osteopontin antibody (Abcam Inc., Cambridge, MA, USA) diluted to 1:800 dilutions in amplifying antibody dilution buffer (1x, 3 ml/slide IHC Kit, Prohisto). The slides were then washed 3 times in amplifying wash buffer (1x, 3 ml per slide, IHC Kit, Prohisto), rocking for 5 minutes at RT and then treated with 3 ml antibody solution per slide for 24 hours at 4°C on a rocker with Alexa Fluor 594 labeled goat anti-mouse and Alexa Fluor 488 labeled goat anti-rabbit (both from, Invitrogen, Eugene, OR, USA) secondary antibodies were diluted in PBS, 1:4000. After washing 3 times in amplifying wash buffer (1x, 3 ml per slide, IHC Kit, Prohisto), rocking for 5 minutes, at RT, and 3 distilled water washes, 3 ml per slide and rocking for 5 minutes at RT, the slides were covered with glass coverslips and mounted using Prolong Gold Antifade Reagent containing DAPI (Invitrogen, Eugene, OR, USA). After drying overnight the slides were examined by fluorescent microscopy as described above.

Alcian Blue Staining

Rehydrated tissue sections were immersed in Alcian blue stain solution (Alcian blue 8GX, 1 gm/100mls 3% acetic acid pH 2.5, Sigma-Aldrich, St. Louis, MO) for 15 minutes, and then rinsed with distilled water and counterstained with neutral red solution (1g in 100 ml water containing 100 µl glacial acetic acid, Sigma-Aldrich, St. Louis, MO) for one minute. After washing in distilled water the sections were covered with glass coverslips, sealed at the edges using nail polish and immediately examined by microscopy as previously described.

Von Kossa Staining

The staining solution was freshly prepared by mixing: naphthol AS MX-PO₄ (0.005g, Sigma-Aldrich, St. Louis, MO, USA), N,N-dimethylformamide, (200µl, DMF, Fisher, Fair Lawn, NJ, USA), Tris-HCl (25 ml, 0.2 M, pH 8.3), distilled water (25 ml), red violet LB salt (0.03 g, Sigma-Aldrich, St. Louis, MO, USA). Filtered staining solution (Whatman's No.1 filter paper) was applied to cover the slides and the slides incubated at RT for 45 min, rinsed in distilled water 3-4 times and left to stand in distilled water for 1 hour. Finally the slides were counterstained with silver nitrate (2.5% aqueous, Sigma-Aldrich, St. Louis, MO, USA) for 30 min. The excess silver nitrate was aspirated, the slides rinsed with distilled water 3 times and dried overnight, covered with a glass coverslips, sealed at the edges (nail polish) and immediately examined microscopically as previously described.

Statistical analysis

Graphical presentations of the results were generated using GraphPad Prism 4 (GraphPad Software, LaJolla, CA), and the same software used for statistical analysis. The area of calcification was calculated using Matlab (The Mathworks, Natick, MA, USA). In all the experiments the “*n*” indicates biological replicates.

Results

Characterization of Collagen Scaffold

The collagen type I foam scaffold (Avitene Ultrafoam[®]) had variable pore size (Fig 1a). Its high porosity was demonstrated by saturation with four times its dry weight of water (Fig. 1b) after 24 hour of immersion (fractional change in weight, mean = 4.0, SD= 0.26, $n=3$). Significantly, saturation of dry Ultrafoam[®] with 5 times its dry weight of neutralized collagen type I (CS), which was allowed to gel for 24 hours at 37°C was essential for assembly of CGCS (fractional change in weight, mean = 5.3, SD = 0.56, $n=3$). The absence of cross-linking of the Ultrafoam[®] was demonstrated by the “wetting time” that exceeded 20 seconds (47). No residue remained after the treatment of Ultrafoam[®] with collagenase P for one hour. These results support the fact that the Ultrafoam[®] is native collagen type I and has not been extensively cross-linked during the manufacturing process.

The Presence of Collagen Gel in CGCS Increases Cellular Seeding Efficiency and Loading

Pipetting 50 μ l of CS, dispenses a mean of 49.2 mg (\sim 49.2 μ l) with a standard deviation of 1.4 mg (\sim 1.4 μ l) ($n=6$). This ensures that collagen impregnation of the pores in Ultrafoam[®] scaffold to generate CGCS, can be precisely controlled and that the number of cells delivered to any porous scaffold can be accurately determined. The efficiency of delivering 50K cells suspended in the medium (500 μ l) during impregnation of the Ultrafoam[®] scaffold pieces was 80-85% (7,500 to 10,000 cells escaped delivery) ($n=2$). The efficiency of cell delivery using 50K cells suspended in CS was above 92% (less than 3750 cells escaped delivery) ($n=2$) however, the penetration of cells into the scaffold was much higher but was difficult to quantify.

Cells suspended in CS saturated the pores throughout the Ultrafoam[®] scaffold, as shown by formazan color formation (deep purple) after MTT staining of the CGCS (Fig 2a). The presence of hMSC suspended in gelled collagen solution was demonstrated by hematoxyline / eosin (H and E) staining of the scaffold sections of the scaffold cut orthogonally to the seeding surface (Fig 2b).

Using confocal microscopy and the models cells (GFP expressing, telomerised human dermal fibroblast, GFP-tFbs), suspended in Cy-5 labeled collagen prepared in our laboratories, it was shown that the cells were distributed throughout the CGCS (Fig 3).

Collagen supports proliferation and long-term survival

hMSC survive and proliferate for up to two months when cultured in CGCS (Fig. 4a). GFP-tFbs, cultured in the CGCS, showed normal morphology and viability at one month (neutral red staining - Fig. 4b). When GFP-tFbs were maintained in this 3-D model they were viable for a period of four months (data not shown).

Cell Proliferation in the CGCS

The presence of collagen gel in CGCS contributed significantly to cell proliferation and viability during one month of culture when compared with hMSC cultured in Ultrafoam[®] alone (Fig 5a, 2 way ANOVA). When the primary human osteoblasts (hOST) were seeded and cultured directly on the Ultrafoam[®], confocal microscopy showed Cytotracker[™] Orange labeled cells to be predominantly on or close to the surface of the scaffold (Fig 5b panels 1i,1ii). In contrast, when these cells were seeded as a component of CGCS, they were “delivered” to the interior of the CGCS (e.g. 100 μ above the non-seeded surface (Fig. 5b. panels 2i,2ii). After 14 days in culture hOST seeded on Ultrafoam[®], did not remain in the deeper

regions of the scaffold (Fig 5b. panels 1iii, 1iv) but hOST seeded as a component of CGCS were observed in the interior of the 3-D model, although more cells were present at the surface (Fig. 5b panels 2iii and 2iv).

Migration of the Cells that Populate CGCS

The cell migration model was set up as shown in Fig 6a by placing CGCS without cells close to the edge of a well in 12-well tissue culture plate and the well was filled with neutralized collagen type I solution (3 ml) and allowed to gel. A small cavity (5mm diameter) was created in the center of the well containing acellular, gelled collagen type I. A suspension of cells in neutralized collagen type I solution was added to the central cavity and the model was cultured and cell migration was observed over 14 days.

GFP-tFbs migrated from the central cavity and colonized / invaded the CGCS (located at the edge of the well) (Fig 6b, panel 1). When collagen type I impregnated CGCS containing GFP-tFbs was placed into the central cavity in acellular collagen gel, GFP-tFbs exited the CGCS and invaded the collagen gel (Fig 6b, panel 2). Repeating these experiments with Cytotracker™ Orange labeled hOST, showed similar migration of hOST into and out of the CGCS (Fig 6C).

CGCS is Mechanoresponsive

GFP-tFbs seeded on CGCS were randomly oriented after seeding (Fig 7a, panel 1). When the CGSS was stretched by hand for ten seconds and then studied after overnight incubation in the medium, the cells had realigned with their long axes parallel to the direction of the stretch (Fig 7a, panel 2). This change was observed throughout the scaffold as shown on gallery of images obtained by confocal microscopy (Fig 7b).

Osteogenic Differentiation of hMSC in CGCS

The expression of alkaline phosphatase (ALP) normalized to DNA increased to day 14 and then declined at day 28 (Fig 8a). Alcian blue staining demonstrated proteoglycan deposition around hMSC in CGCS after 28 days in culture under osteogenic differentiation conditions (Fig 8b).

Immunohistochemistry was performed to track expression of markers of osteogenic differentiation (Fig 9a and 9b). hMSC did not express osterix (transcription factor) or osteopontin (extracellular matrix protein) at the start of the experiment. However, hMSC expressed these markers by the 28th day of osteogenic differentiation in CGCS and when in Ultrafoam[®].

Collagen type I Dependence of Mineralization in CGCS

Calcium deposits were detected using a modified von-Kossa staining protocol. No foci of calcification were observed in case of hMSC seeded on CGCS and maintained under non-differentiation conditions (no dexamethasone, no ascorbate) (Fig 10a, panels 1i and 1ii). Very few foci were observed when hMSC were seeded directly on Ultrafoam[®] and maintained under differentiation conditions (Fig 10a, panels 2i and 2ii) for 28 days, but multiple foci of calcification were observed after 28 days of differentiation, when hMSC were the component of CGCS (Fig 10a, panels 3i and 3ii and Fig 10b).

Analysis of von Kossa stain positive areas showed that hMSC seeded on CGCS, and cultured under differentiation conditions for 14 days, 0.28% (mean, SD= 0.03%, n=3) of the image area was covered by calcium deposits. This area increased more than 10 fold (3.53%, mean, SD= 0.63%, n=3) when culture period was extended to 28 days (unpaired t-test $p < 0.001$).

The area of the image occupied by Ultrafoam[®] was 17.43% (mean, SD= 2.01%, n=3) and by gelled collagen was 60.34% (mean, SD= 3.67%, n=3). The remaining blank area of the image resulted from fixation, dehydration and paraffin embedding.

Figures and Legends

Figure 1. Characterization of collagen foam. Figure. 1a. Phase contrast light micrograph of collagen type I foam (Ultrafoam[®]) showing large irregular pores. **Figure. 1b.** Retention capacity after impregnation. Ultrafoam[®] retention capacity was determined as weight of water or gelled neutralized collagen type I solution held by dry Ultrafoam[®] after 24 hour immersion, expressed as the gain in weight. (Mean and SEM, n=3)

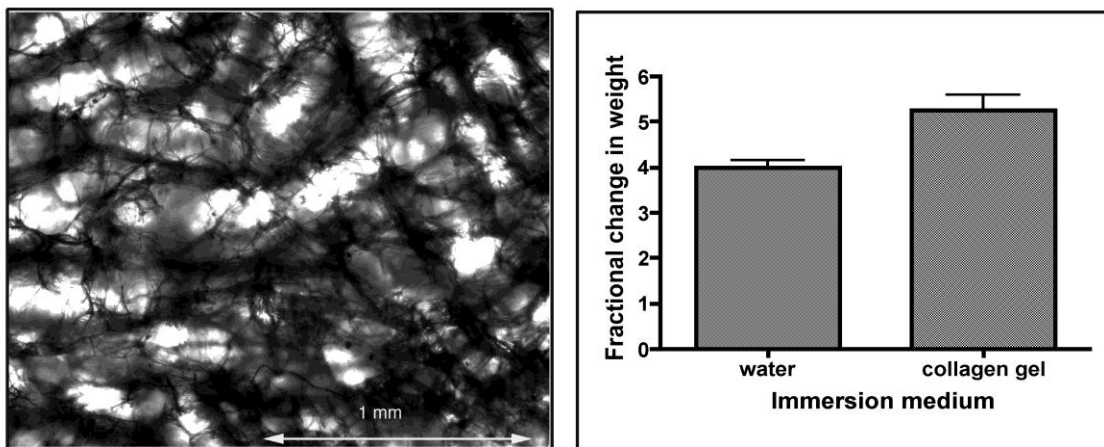


Figure 1a

Figure 1b

Fig. 2. Distribution of human bone marrow derived mesenchymal stem cells (hMSC) in Ultrafoam[®] impregnated with collagen type I (CGCS). Figure 2a. CGCS populated with hMSCs shows uniform distribution of cells labeled after MTT treatment when formazan stains

the entire specimen (dark purple). **Figure 2b.** H&E stained, cross section (10 μ) of paraffin embedded CGCS showing Ultrafoam[®] (dark purple), impregnating collagen gel (light pink), and hMSC (dark blue nuclei marked by black arrows). The specimen was sectioned orthogonally to the seeding surface.

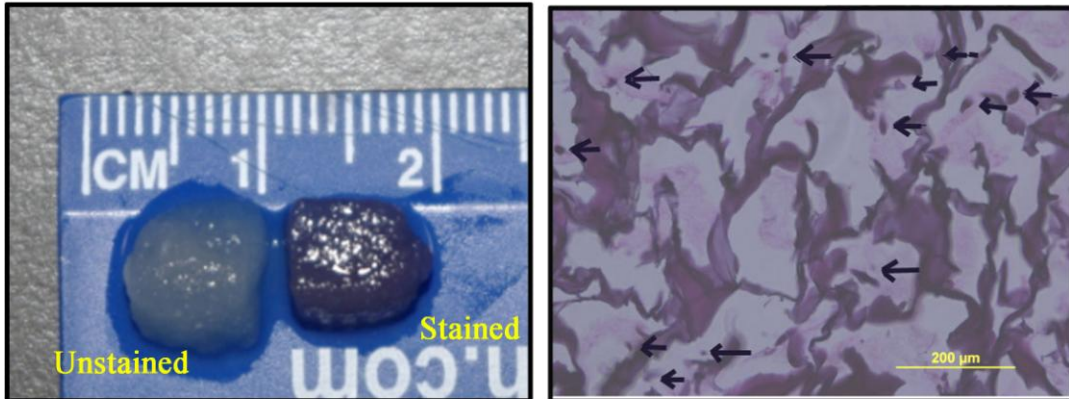


Figure 2a

Figure 2b

Figure 3. Confocal micrograph of CGCS 3-D model assembled with Cy5 labeled collagen type I and GFP expressing telomerized human dermal fibroblasts (GFP-tFbs). Uniform penetration and distribution of cells and collagen type I in the CGCS scaffold (Ultrafoam[®]). Unlabeled scaffold (Ultrafoam[®], dark areas) in which pores contain Cy-5 labeled gelled collagen type I (red) and GFP-tFbs cells (green). The figure represents an optical slice 100 μ m superior to the basal surface.

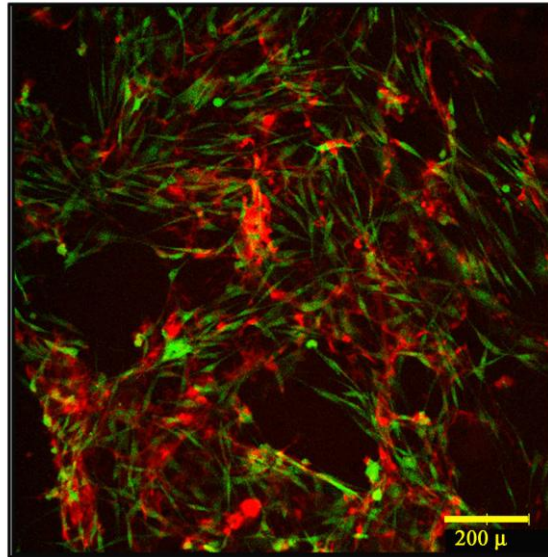


Figure 3

Figure 4. Proliferation and viability of GFP-tFbs and hMSC in CGCS. **Figure 4a.** Proliferation of hMSC over 56 days determined by MTT assay. Formazan formation and absorbance (570 nm) provides a quantitative measure of the number of viable hMSC residing in CGCS. (Mean and SEM, n=3). **Figure 4b.** Our 3-D model can support more long term viability of cell types other than hMSC as shown by neutral red stained CGCS populated with GFP-tFbs after 30 days of culture. Light microscopy shows normal cell morphology (fluorescence in image 1), and high cell viability (image 2) in the same optical section.

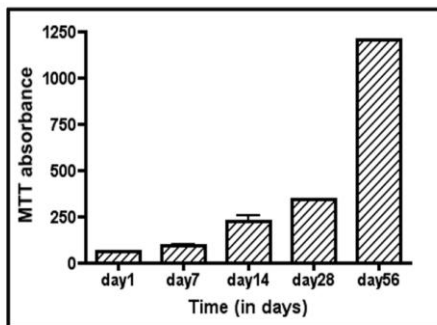


Figure 4a

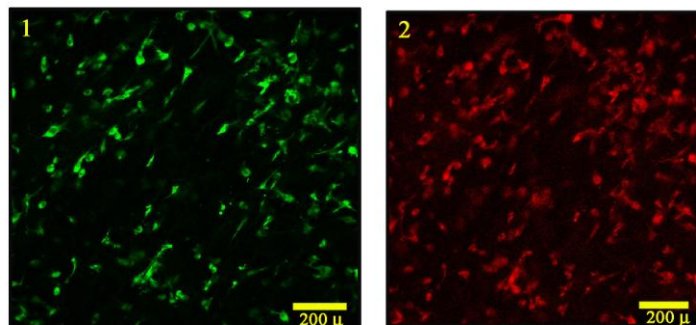


Figure 4b

Figure 5. The presence of collagen type I has a significant positive effect on distribution, survival and proliferation of hMSC and hOST cells in CGCS. Figure 5a. Cultures of hMSC (100,000/ml) seeded on CGCS results in significantly higher cell number (seeding efficiency and proliferation) when compared to cultures on Ultrafoam[®] alone (2 way ANOVA, mean, SEM graphed. $n=3$, $p < 0.05$). **Figure 5b.** Cytotracker[™] Orange labeled hOST seeded on Ultrafoam[®] (row 1) and on CGCS (row 2). Images obtained on day one at the surface (panel 1i) and 100 μ below the surface (panel 1ii) of Ultrafoam[®] show fewer cells and indicate inadequate delivery of cells in the absence of collagen solution. Images obtained on day 14 (panels 1iii and 1iv) show that prolonged culture of cells in the absence of collagen gel results in the cell migration from the interior to the Ultrafoam[®] surface (panel 1iii) since the cells are not detected at 100 μ below the surface (panel 1iv), and the overall increase in proliferation is not indicative of cell death in the interior of the Ultrafoam[®]. Confocal images captured on day 1 at the surface (panels 2i) and 100 μ below the surface (panel 2ii) of the 3-D model respectively. Confocal images on day 14 demonstrate the presence of cells on the surface (panel 2iii) as well as in the interior (100 μ below the surface, panel 2iv) of CGCS.

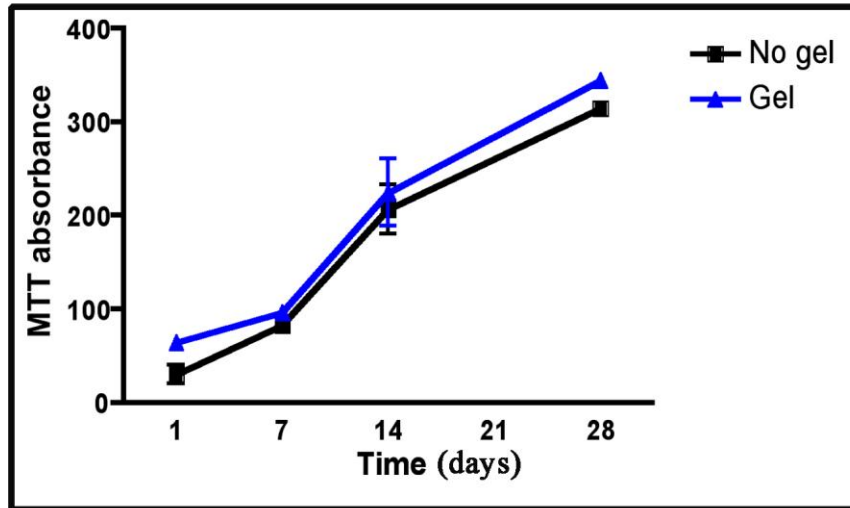


Figure 5a

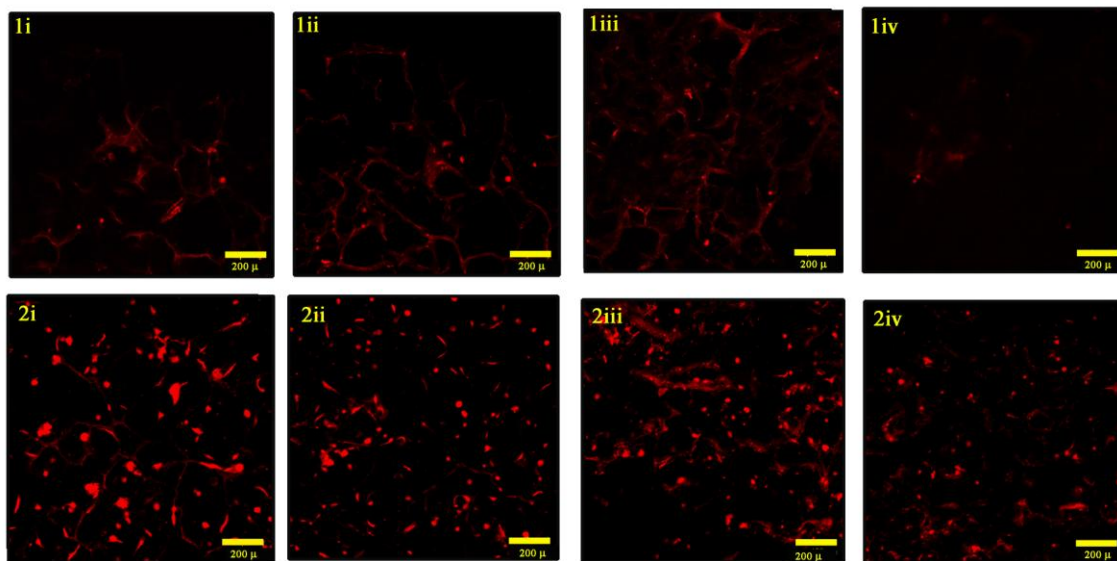


Figure 5b

Figure 6. Our CGCS 3-D model can be used for studies of cell migration in 3-D. The scale bars are 200 μ m in figures 6b and 6c. **Figure 6a.** Acellular CGCS was placed close to the edge of the well in a 12-well plate and was totally immersed in neutralized collagen type I solution,

which was allowed to gel. Cells suspended in neutralized collagen type I solution was added into a small cavity formed in the center of the well and the cell migration was observed over a 14 day period. **Figure 6b.** GFP-tFbs, used as model cells, migrated into the CGCS (from top left of image 1) from the central cavity (to bottom right image 1). GFP-tFbs could also migrate from CGCS populated with cells (from top left image 2) into surrounding acellular gel. **Figure 6c.** Using the same methodology Cytotracker™ Orange labeled hOST migrated from central cavity (from bottom right) into the acellular CGCS (to top left). Image 1 at start of experiment (day1) and image 2 is on day 14.

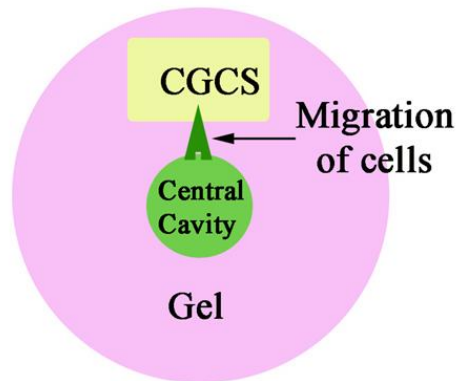


Figure 6a

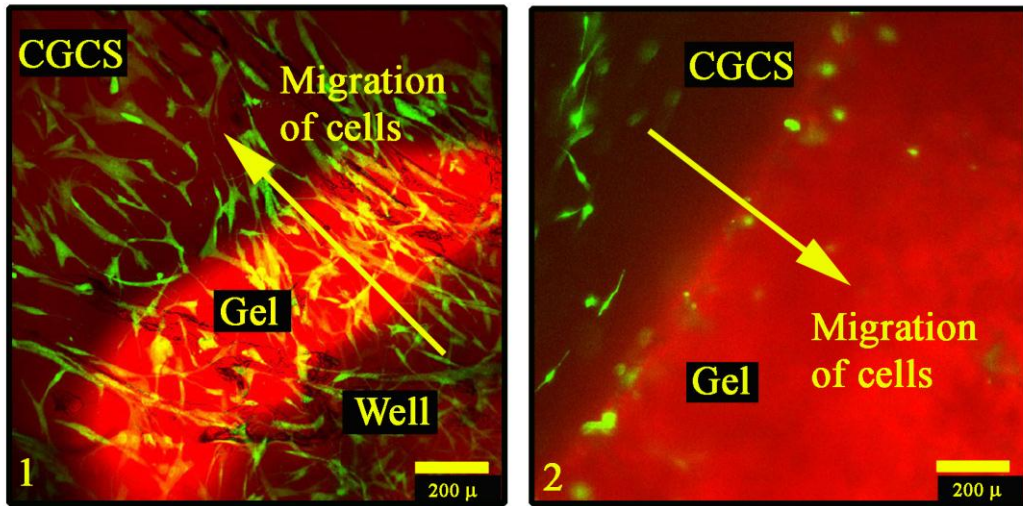


Figure 6b

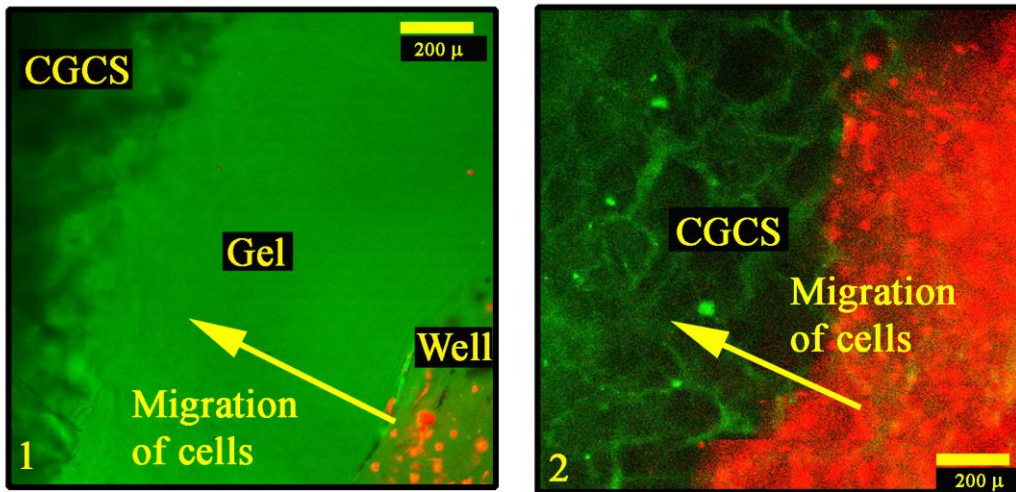


Figure 6c

Figure 7. The response of cells in CGCS (our 3-D model) to mechanical force. Figure 7a. GFP-tFbs populating CGCS are randomly orientated (image 1). After a brief stretch in the direction of the arrow, followed by 24 hours resting period the cells reorient with the long axes in the direction of the force (image 2). **Figure 7b.** Confocal microscopy shows that the cell alignment occurs throughout the scaffold as evident from the optical sectioning and assembly of

the gallery of images ranging from 50μ to 150μ below the surface (images 1 before and 2 after

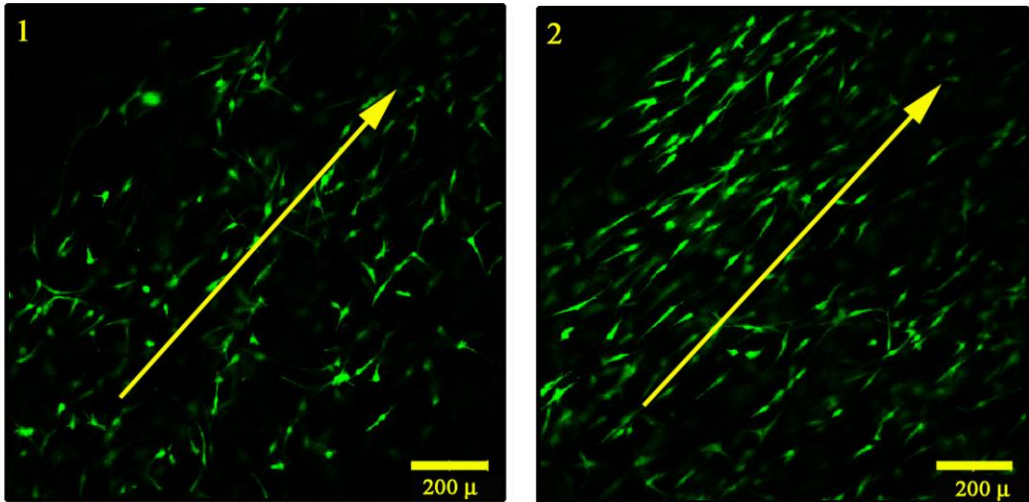


Figure 7a

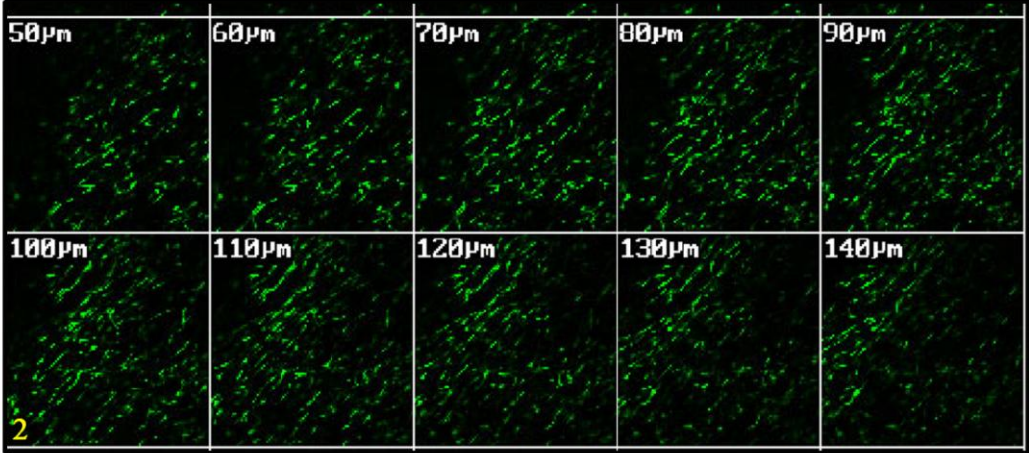
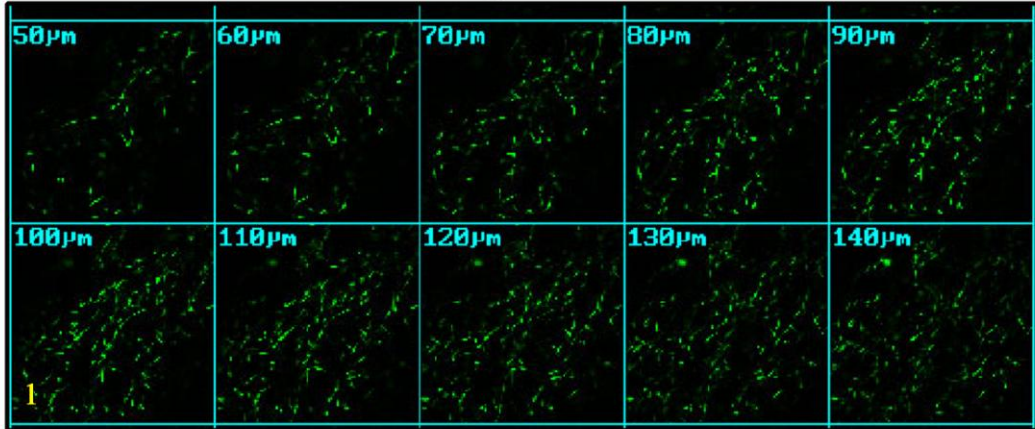


Figure 7b

stretching).

Figure 8. Differentiation of hMSC in CGCS. Figure 8a. Alkaline phosphatase (ALP) activity, an osteogenic differentiation marker, was assayed using colorimetric conversion of pNPP (normalized to cellular DNA to compensate for hMSC proliferation). The maximum ALP activity observed on day 14 was not sustained and decreased by day 28. (Mean and SEM plotted, $n=3$). **Figure 8b.** Deposition of extracellular glycosaminoglycan characteristic of osteogenic differentiation of hMSC, is shown by Alcian blue staining (marked by black arrow) in CGCS at day 28.

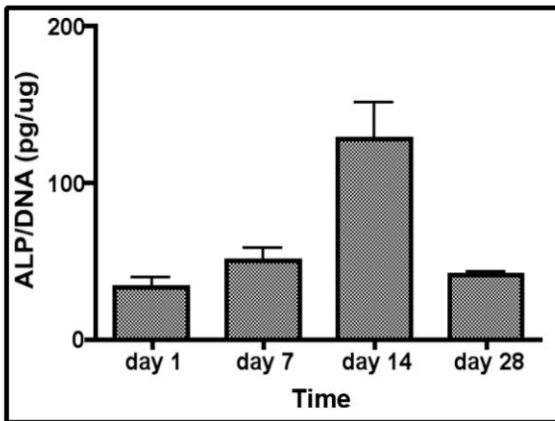


Figure 8a

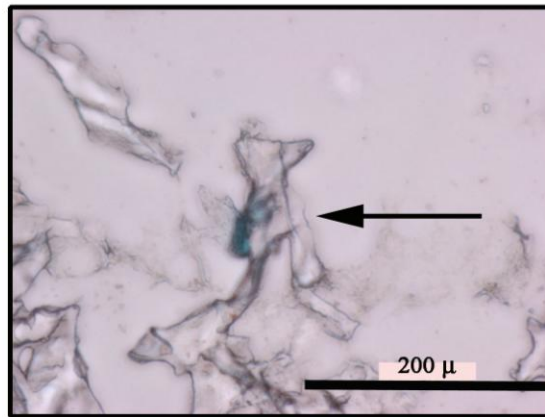


Figure 8b

Figure 9. Immunohistochemical analysis of hMSC differentiation in CGCS. Figure 9a. Expression of osterix, a transcription factor associated with late stages of differentiation (red fluorescence), is not expressed by hMSC on day 1 but is present after 28 days in culture in Ultrafoam[®] (panel 1) or CGCS (panel 2). Panel 3 is higher magnification of panel 2. Yellow arrowheads mark the positions of the cells as determined by DAPI staining **Figure 9b.** Expression of osteopontin (green fluorescence), is an extracellular protein deposited by osteoblasts late in the differentiation process. Its presence is not observed on day 1 but is present

after 28 days of culture under differentiation conditions (panel 2 - Ultrafoam[®] and panel 2-CGCS). Yellow arrowheads mark the positions of the cells as determined by DAPI staining.

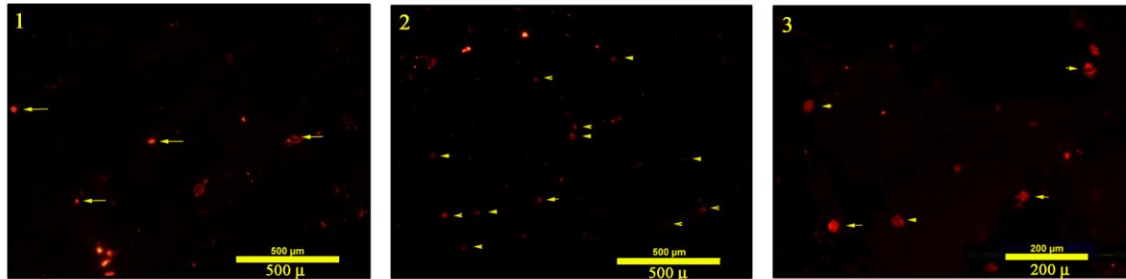


Figure 9a

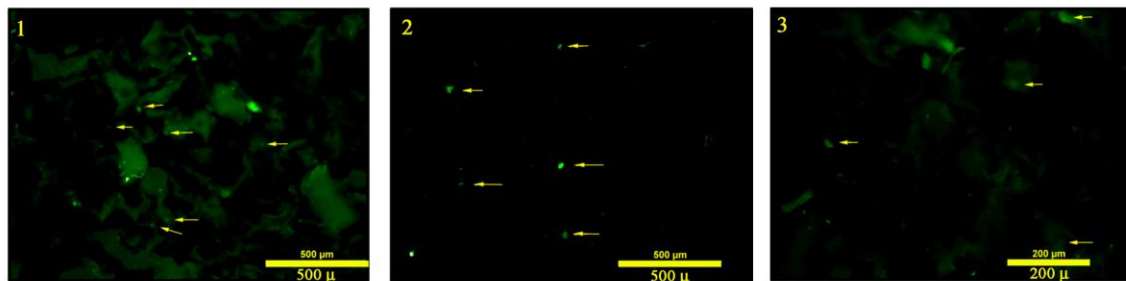


Figure 9b

Figure 10. Histochemical analysis (Von Kossa stain) demonstrated the requirement for collagen type I for *in vitro* mineralization in CGCS model. Figure 10a. Panels 1i (day1) and 1ii (day 28) are cross sections (10 μ) of paraffin embedded CGCS populated with hMSC and maintained under proliferation conditions. Panels 2i (day 1) and 2ii (28 day) are cross sections (10μ) of paraffin embedded Ultrafoam[®] (without collagen impregnation) populated with hMSC and maintained under differentiation conditions. Panels 3i (day 1) and 3ii (day 28) are cross sections (10 μ) of paraffin embedded CGCS with hMSC maintained under differentiation conditions. Positive Von Kossa staining (black staining) observed in panel 3ii only, indicated calcification - active ossification under differentiation culture conditions. **Figure 10b.** Shows higher magnification of panel 3ii. **Figure 10c.** A significant increase in mineralization was

observed after 28 days of differentiation in CGCS (cross section images analyzed using Matlab)
(Mean and SEM $n=3$, unpaired t-test $p < 0.001$).

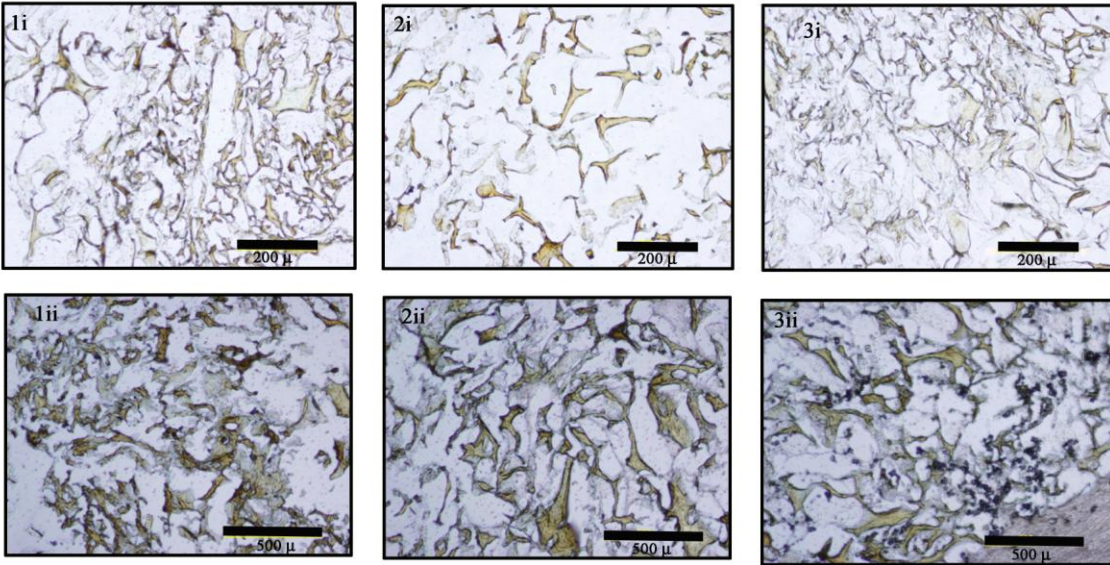


Figure 10a

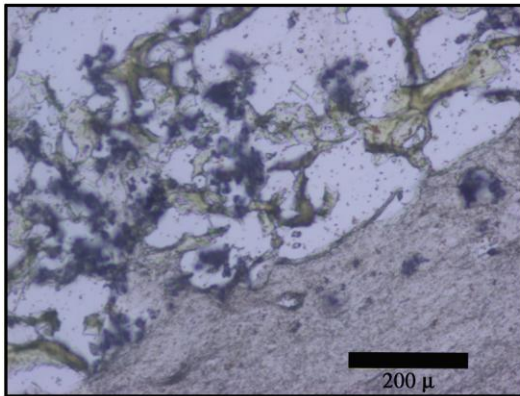


Figure 10b

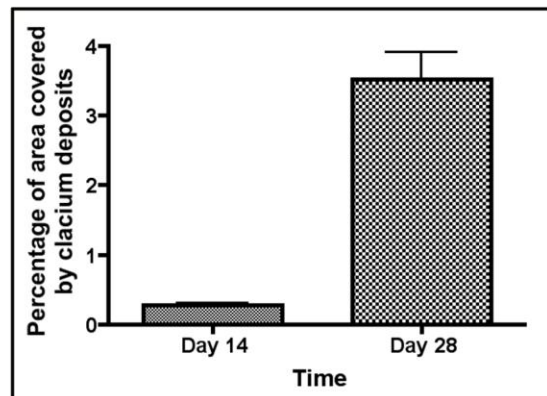


Figure 10c

Discussion

The ECM of bone contains 70 to 90% of collagen type I, the most abundant structural protein in higher living organisms (3), (4). To produce the characteristic hard bone

tissue and yet retain some measure of flexibility, microcrystalline hydroxyapatite (complex calcium phosphate) is deposited on the network of collagen fibrils that are further organized into bundles. Fulfilling its multifunctional physiological role the bone provides a compartment for the stem cells that maintain blood and immune system cell populations as well those that comprise the skeletal system (1). The cellular constituents of bone include osteoblasts, osteoclasts and osteocytes. Osteoclasts and osteoblasts are responsible for bone homeostasis (cycles of deposition and resorption of mineralized ECM) (1), bone repair (regeneration), and structural remodeling in response to hormonal and mechanical signals. The terminally differentiated osteocytes are the “mechanosensors” and the major cell population in bone.

The bone formation process during development is well documented but bone repair and regeneration is not as well understood (8). While 3-D morphology is essential for mineralization of collagen type I bone matrix (14), (18), differentiation of MSC to osteoblasts takes place in 2-D (12), (13) and 3-D cultures (14), (15). Following an injury (fracture) activated osteoblasts invade and mineralize and become embedded in the collagenous microenvironment and differentiate into osteocytes. In contrast 2-D osteoblasts cultures generate multilayered cell sheets and form nodules of calcification (14), (18) without terminal differentiation into osteocytes. The expression levels of osteogenic biomarkers are higher in 3-D cultures than in monolayer cultures (16), (17) and mineralization begins earlier and proceeds faster in a 3-D environment (15), (16), (17). Thus in a 3-D environment the process of differentiation and mineralization represents a more *in vivo* relevant ossification process (19). Although the course of osteoblast differentiation in 2-D is relatively uniform, the differentiation in 3-D is dependent on the model used because not all the models are truly three-dimensional. Cells seeded on various porous scaffolds form a monolayer on the pore surfaces, and although these surfaces are

tortuous and convoluted, the osteogenesis forms cell multilayers that synthesize collagen and form nodules of mineralization, a progression that is characteristic of 2-D cultures.

Our efforts in engineering of human tissue have lead to the development of three - dimensional (3-D) models (also known as tissue equivalents or organotypic cultures) of the skin, cornea and conjunctiva (64). In these 3-D models of living human tissue, appropriate connective tissue cells (usually fibroblasts) populate the acid solubilized non-denatured collagen type I gels (the extracellular matrix, ECM). In contrasts to similar tissue constructs that contract spontaneously (65), our patented connective tissue models are dimensionally stable. A benefit of the non-contractile matrix is the translucency of our 3-D models that allows morphological observation of the cellular behavior by non-intrusive microscopic methods. Furthermore, our constructs allow free exchange of nutrients and waste products, resulting in long-term (months) stability and cell viability, and support cell migration (64). Expanding our collagen-based tissue engineering, we here report assembly of an *in vitro* model of bone tissue that allows studies of poorly understood aspects of human osteogenesis in an *in vivo* relevant manner. We have examined the suitability of porous non-denatured commercially available collagen type I foam (Ultrafoam[®]), a scaffold stiffer than the collagen gel alone, yet cytocompatible, easy to handle and amenable to physical deformation. This approach is justified by the increasing interest in hydrogels as critical components that provide significant biological advantage to composite constructs and grafts (107).

Most of the current 3-D models are hydrogels that lack adequate mechanical strength (7). Human mesenchymal stem cells (hMSC, (57)) and osteoblasts (hOST, (14)) rapidly contract collagen hydrogels that they populate to one third of the initial size, which decreases cell viability and survival. In order to prevent compaction and allow long-term cell viability we

selected collagen foam (Ultrafoam[®]) as a stiff scaffold that will reinforce our patented collagen hydrogel (64). Stiffer scaffolds have also been reported to favor osteogenic differentiation (19), (40). Ultrafoam[®] is highly porous and accommodates five times its own weight of collagen type I gel (Figs. 1a and 1b). It is made from native (non-denatured) collagen type I that is not cross-linked as demonstrated by the long wetting time and complete, residue free, degradation after collagenase treatment. This is important because aldehyde based collagen cross-linking is one of the factors responsible for pathological calcification (foreign body reaction) that leads to structural deterioration and is a major reasons for failure of modified collagen implants (47). Ultrafoam[®] also provides a surface favorable for cell adhesion, is mechanically stronger, stable over long-term culture periods and easy to manipulate.

In order to generate consistent and uniform osseous structure and facilitate proper function a 3-D model requires homogeneous cell distribution. Penetration of cells into the interior of a scaffold at depths greater than 500 μ m has been a challenge (17), and has been approached by utilizing very high seeding densities (59). Introduction of cells suspended in a solution of neutralized collagen type I into Ultrafoam[®], and allowing the collagen to gel at 37°C, formed collagen hydrogel containing collagen scaffold (CGCS). This approach ensured that even at low seeding density, cells could penetrate into and be distributed throughout the scaffold. Thus MTT staining, that generates formazan dark blue color (108) (Fig 2a, 2b), hematoxylin-eosin staining of paraffin embedded sections of CGCS (Fig 2c), and confocal microscopy (Fig 3) demonstrated distribution of cells throughout the CGCS, although the cell density was higher at the surface than in the interior of the model. This picture was further clarified by using fluorescently labeled model cells (a human dermal fibroblast cell line with ectopic expression of telomerase and GFP, GFP-tFbs) and Cy5[™] labeled collagen and is shown in Fig 3. After 12 hrs

in culture the seeding efficiency in CGCS was increased from 85% when cells were seeded on Ultrafoam[®] without collagen gel to more than 92% in the presence of collagen gel. We therefore doubled the reported seeding efficiency (40%) reported with collagen diluted with culture medium as the cell delivery vehicle (61).

Since it has been shown that lower seeding density does not affect tissue formation (60), and that very high density inhibits proliferation in 3-D scaffolds (59), we used cell seeding density of 100,000 cells/ ml with 50,000 cells per scaffold for all our experiments. Lack of proliferation on collagen scaffolds, after one week in culture, was attributed to differentiation, (17), but as even early osteoblasts are proliferative, the arrested proliferation is more likely due to compromised nutrition and overcrowding. In our CGCS model hMSC proliferated for a period of 8 weeks under differentiation conditions (Fig 4a), a much longer survival and viability than has so far been reported. This demonstrates the suitability of our model for long-term studies (Fig 4b), and four-month viability was also observed but not recorded.

The presence of collagen did not suppress hMSC proliferation even after 4 weeks of culture under differentiation conditions [see growth curves for hMSC cultured in Ultrafoam[®] and in CGCS (Fig 5a)]. Osteoblasts cultured in Ultrafoam[®] for 4 weeks, migrated to the surface and very few cells were present in the Ultrafoam[®] interior (Fig 5b), probably due to a more favorable nutrient supply at the scaffold surface. In contrast, a greater number of osteoblasts were present in CGCS interior (Fig 5b), most likely because presence of collagen gel, stabilizes the growth factor access and availability, and maintains equally favorable nutritional conditions in the interior of the scaffold as at its surface. Regardless of the cell type (fibroblast, hMSC, osteoblast) the use of collagen gel impregnation facilitates total penetration into the scaffold, a

more uniform distribution of cells, higher seeding efficiency and improved cell survival and proliferation.

Osteoblasts can up-regulate matrix metalloproteinases (MMP) secretion to degrade and remodel the surrounding matrix (19). MMP activity is important for differentiation of osteoblasts into osteocytes, cell survival by creating cell migration pathways, production of matrix fragments that serve as signaling molecules, and the release of matrix bound latent growth factors (19), (40). Consequently the presence of non-degradable (stable) cross-links interferes with progression of ossification (48). Since the Ultrafoam[®] and the collagen hydrogel are native collagen type I (Fig 3) both are substrates for collagenase which was shown to completely dissolves CGCS. Thus cells populating the CGCS model are able to manipulate the collagen as needed, demonstrating the potential for degradation / remodeling *in vitro* and if used as a graft *in vivo*. Cells recovered after collagenase digestion of CGCS attach and proliferate when placed in culture.

To produce a seamless interface when serving as a graft, our 3-D model (CGCS) has to allow free movement of cells so that the graft-host interactions are facilitated. The schematic in fig 6A shows the design of the preliminary migration experiment, which we used to demonstrate qualitatively cell motility. The cells (fibroblasts and osteoblasts) were shown to migrate out of CGCS into surrounding acellular collagen gel (Fig 6b, panel 2) indicating the potential use of CGCS to deliver cells to the site of injury. Successful penetration by cells from collagen hydrogel into CGCS (Fig 6) indicates its ability to allow invasion by resident host cells during integration of graft with host tissue.

During the remodeling bone responds to mechanical forces by changing its

structure and shape to optimize its load bearing capacity (1). The effects of force at the cellular level are currently studied using cell monolayers cultured on elastic membranes and subjecting the membranes to a variety of stretching forces. When a tensile force is applied to fibroblasts populating our 3-D model - CGCS they realigned parallel to the direction of application of force within 24 hours (Fig 7a). The alignment occurs throughout the specimen (Fig 7b), validating the use of CGCS for mechanotransduction in 3-D. When the experiment was repeated with osteoblasts the alignment was not observed. This is likely to be due to the fact that the mechanosensing cells in bone are osteocytes, which instruct osteoclasts and osteoblast to remodel a specific area of need.

The exposure of hMSC populating CGCS to osteogenic differentiation conditions showed that alkaline phosphatase (AP) activity peaked at 14 days and decreased by day 28 (Fig 8a). This is an AP activity profile similar to that reported to take place during differentiation of hMSC in a monolayer culture and confirms that the AP activity is an early differentiation event (109) in our 3-D model also. Synthesis and pericellular deposition of glycosaminoglycans that occurs during chondrogenesis, also takes place during endochondral ossification and was observed by day 28 in Alcian Blue stained paraffin sections of CGCS (Fig 8b). Although demonstration of osteogenic differentiation monitors the changes in mRNA levels of several biomarkers, we favor demonstration of translation and presence of the proteins which is a more difficult process in 3-D models. While in histochemical analysis uniform distribution of cells translates into fewer numbers of cells within a field of view (particularly at higher magnification), in Western blot analysis the presence of collagen overwhelms the low concentrations of cellular proteins. Nevertheless, transcription factor osterix (Fig. 9a) and the extracellular matrix protein osteopontin (Fig 9b), were observed after 28 days of differentiation

in Ultrafoam[®] without collagen gel as well as in CGCS. These results support our conclusion that osteogenesis is taking place in our *in vitro* model.

hMSC cultured in collagen gel led to formation of bone like tissue, expressed differentiation markers at levels similar to those in bone and showed enhanced mineralization (44). Similar behavior was not exhibited by hMSC cultured in fibrin, alginate, or pluronic F127 hydrogels. Differentiation of hMSC on thin collagen films (6) and culture of osteoblasts in collagen gels (14) deposited calcium phosphate on collagen fibrils. Osteoblasts cultured in a compressed collagen hydrogel, survived predominantly on the surface of the thin dense matrix and rapidly deposited calcium hydroxyapatite on the collagen fibrils (19). These studies support our hypothesis that the presence of collagen type I is essential for *in vitro* ossification. Previous *in vitro* studies with cross-linked collagen scaffolds did not differentiate between physiological (cell-mediated) calcification and the crystallization due to spontaneous degradation of β -glycerol phosphate (62) in the monolayer culture controls. In our study one of the controls was the culture of hMSC in Ultrafoam[®] under differentiation conditions for 28 days (Fig 10a, panels 1i and 1ii). The second control was culture of hMSC in CGCS under non-differentiation conditions (no dexamethasone, no ascorbate) for 28 days (Fig 10a, panels 2i and 2ii). No calcification was observed in either of these controls supporting the fact that the calcification we observed in cultures of CGCS populated with hMSC under differentiation conditions for 28 days ((Fig 10a, panels 3i and 3ii) was the physiological mineralization. Higher magnification micrograph (Fig 10b) clearly shows mineral deposition within the pores in association with collagen hydrogel. Quantification of areas rich in calcium deposits shows ten fold increase from day 14 to day 28 (Fig 10c) corresponding in culture.

Data presented in this study demonstrated several findings critical to ossification. Our model is “cytocompatible” and supports the transition of our strategy from successful engineering of 3-D models of living “soft” human tissue to modeling bone morphogenesis. CGCS is not cross-linked, is biodegradable, and has sufficient mechanical integrity to facilitate easy handling and remains intact during prolonged culture periods. It retains its original shape and size without contraction, and supports invasion, proliferation, metabolic homeostasis, mechanotransduction and osteogenic differentiation of hMSC including calcification in a physiological manner. We further demonstrated that the presence of collagen is essential for effective cell delivery and long-term cell viability in the impregnated scaffolds and particularly the importance of collagen in the osteogenic mineralization. We have used of several cells types and differentiation along one lineage but the data supports the proposal that CGCS can serve as an excellent *in vitro* 3-D model to study variety of cells in an *in vivo* relevant manner. CGCS is particularly appropriate as an *in vitro* 3-D model for studies of osteogenesis.

CHAPTER IV

COLLAGEN IMPREGNATED BETA-TRICALCIUM PHOSPHATE - A 3-D MODEL FOR STUDY OF OSTEOGENESIS *IN VITRO*

Introduction

Bone is a multifunctional tissue that provides form to the human body, protection to the viscera, plays a role in calcium and phosphate homeostasis and is the site of hematopoiesis (1), (2). Bone is a unique tissue that heals by regeneration in contrast to other tissues that develop a scar when injured. If the injury is severe and a large amount of bone is lost, the repair process may not be able to heal the resultant void, which becomes a critical sized defect. Bone grafting is currently the gold standard of treatment for critical sized bone defects (1). Bone grafting constitutes a \$1 billion segment of the \$15 billion (in 2001) worldwide sales of orthopedic products. While autografting suffers from donor site morbidity and increased infection risk, the allografts perform inconsistently and further increase the risk of infection and disease transmission. As a potential solution of these challenges development of tissue engineered bone graft substitutes is an actively pursued strategy.

Ideally tissue engineered bone grafts should consist of the following components: the scaffold that can be remodeled, appropriate cells and biologically active entities (growth factors, cytokines) that improve the repair (2). Current tissue engineering strategies deliver the

preloaded cells into a scaffold and/or rely on the host cells at the site of scaffold implantation to augment the ossiointegration (38). For a tissue engineered bone graft to succeed the graft should mechanically strengthen the grafted area, support vascularization, recruit osteogenic cells, promote integration with host tissue, and finally be resorbed to provide a seamless repair. (1). Besides development of grafts for various tissues, another goal of tissue engineering research is to develop living 3-D models of various tissues. These models should be able to respond to applied controllable biochemical and physical stimuli and allow the study of physiological and pathological behavior of cells in an *in vivo* like environment (20). We (manuscript under review) and others (14) have shown that a 3-D scaffold and extracellular matrix (particularly collagen type I) are required for mineralization *in vitro*. Monolayer cultures of osteogenic cells have to develop multilayered nodules and deposit collagen before mineralization can take place (14). This underlines the need for valid 3-D models for studies of ossification and mineralization mechanisms. In this study we describe construction of a β -TCP and collagen type I gel based 3-D model, which addresses this need and which has the potential to be translated into an engineered graft.

Materials and Methods

Cells

GFP-tFbs: Human dermal fibroblasts immortalized by ectopic expression of hTERT were a kind gift from Dr. J.W.Shay (Department of Cell Biology, UT Southwestern Medical School, Dallas Texas). These cells were transduced with enhanced GFP (eGFP) imbedded in a lenti-viral vector in the laboratories of Dr. Victor Gonzales (Howard Hughes

Medical Center, Dallas Texas). The stable transfectants were isolated by flow cytometry / cell sorting. GFP - hTERT expressing dermal fibroblasts (GFP-tFbs) were cultured in DMEM (GIBCO, Invitrogen, Carlsbad, CA) containing fetal bovine serum (FBS, 10%, Atlanta Biologicals, Lawrenceville, GA) in a humidified incubator (37°C, 5% CO₂) with medium changes every second day.

hMSC: Bone marrow derived hMSC (Lonza, Switzerland) were cultured in MEM α (Invitrogen, Carlsbad, CA) containing FBS (10%, Atlanta Biologicals, Lawrenceville, GA) and FGF (10 nM, R&D Systems, Minneapolis, MN), with medium changes every second day. hMSC were passaged at 80-90% confluence using trypsin (0.05%) with 0.53 mM EDTA in HBSS (Invitrogen, Carlsbad, CA) and plating at 3,000 cells/cm². Cells were counted using hemacytometer and Trypan blue (Sigma-Aldrich, St. Louis, MO) dye exclusion viability stain.

Collagen Type I Gel

Cold (4°C) porcine collagen type I solution (Cellmatrix-A[®], Wako Chemicals, Richmond, VA, USA, 3mg/ml) (8 parts v/v) was mixed thoroughly with cold (4°C) 10 X MSCGM (1 part, v/v) and then neutralized (pH 7.4) with cold (4°C) reconstitution buffer (sodium hydroxide 0.5N, sodium bicarbonate 22g / l, HEPES free acid 47.7 g / l) (1 part v/v). This order of addition of reagents with thorough and careful mixing after each addition ensures formation of a homogeneous viscous solution free of air bubbles. All solutions and mixing steps were conducted at 4°C and the neutralized collagen solution remained liquid at 4°C. For cell-populated collagen gels, cells were dispersed in neutralized collagen solution by passing through a syringe and a needle (21 gauge). When incubated at 37°C under 5% CO₂ the solution gelled

within 30 min. All experiments were performed using the above mentioned collagen type I gel preparation protocol.

Impregnation of β -Tri-calcium Phosphate Scaffold

Porous scaffolds made of β -tri-calcium phosphate (β -TCP, chronOSTM preforms) were a kind gift from Synthes (Monument, CO, USA). The pore size of these scaffolds ranges from 100 to 500 microns, with a porosity of 70% (information provided by Manufacturer).

The β -TCP preforms were cut into cubical pieces (5mm sides) and immersed in phosphate buffered saline {0.256g/L NaH₂PO₄ H₂O, 1.19g/L Na₂HPO₄, 8.76g/L NaCl, pH 7.4, in distilled water} {PBS}) for 24 hours. The β -TCP cubes were blotted dry (filter paper), transferred into wells of 6 well plates and impregnated with neutralized collagen type I solution (with or without cells). The collagen type I solution loaded β -TCP cubes were incubated (humidified incubator at 37°C, 5% CO₂) overnight to allow the collagen to gel and will hereafter be referred to as **Collagen Gel Impregnated Porous Scaffold (CGIPS)**. The CGIPS used for all experiments were 5mm X 5mm X 5mm loaded with 250 μ l collagen type I gel. When populated with cells the collagen solution impregnating the CGIPS contained 100,000 cells /ml unless otherwise indicated.

CyTM5 labeling of collagen

Collagen type I solution (10 mls) was reacted with bis-functional fluorescent dye Cy5TM (0.2 mg, Amersham Biosciences, UK) dissolved in DMSO (200 μ l), with continuous stirring for 24 hours at 4°C. The labeled collagen solution was then used to impregnate β -TCP preforms as described above for unlabeled collagen.

Confocal Microscopy

The distribution of the cells in the cell-populated CGIPS was examined using laser scanning confocal microscopy (Zeiss, LSM-410, Thornwood, NY, USA) by determining the cellular content of the model at various optical planes throughout the specimens. Images were obtained using a 10 X objective, while keeping the pinhole and other parameters constant. GFP expressing GFP-tFbs were detected after excitation at 488 nm and Cytotracker™ Orange (Invitrogen, Carlsbad, CA) labeled hOST cells were observed using 568 nm excitation laser.

MTT Assay

The CGIPS 3-D constructs, placed in wells of a 24-well plate, were washed with PBS (1ml/well), and incubated with 3-(4,5-Dimethylthiazol-2-yl)-2,5-diphenyltetrazolium bromide, (500µl /well, MTT, 0.2 mg / ml of PBS, Sigma-Aldrich, St. Louis, MO, USA) for two hours at 37°C. The formazan (metabolized MTT) was dissolved in solubilization solution (250 µl, MTT assay kit) by rocking for 90 minutes, and 100 µl aliquots were transferred to wells of a 96-well plate (duplicate wells / specimen). The 96-well plate was examined using the plate reader (Molecular Devices Spectramax 340 PC, MDS Analyticals, Toronto, Canada) and the absorbance at 570 nm recorded. Cells from a monolayer culture of hMSC (seeding density 7.5×10^3 - 2.5×10^5 cells per well in a 24 well plate) were used to generate the standard curve for the conversion of MTT into formazan. A straight line with Spearman's correlation statistic of 1, and $p < 0.05$) was used to calculate the cell number from the formazan absorbance.

Micro CT

CGIPS and β-TCP (without collagen) with cells were fixed in buffered formalin (10% formalin/formaldehyde 10 mls, PBS, Fisher Scientific) at 4 °C for 24 h and transferred to

70% ethanol. Specimens (10mm X 10mm X 5mm each) were scanned in a GExplore μ CT scanner (GE, Piscataway, NJ, USA). 3D reconstructions of the scans were analyzed using Microview Software (GE, Piscataway, NJ, USA). The volume external to the CGIPS was assigned to be the “blank”, and its the highest grayscale value was used as threshold to determine unoccupied pores in CGIPS. The “calcified / mineralized” tissue was identified using the auto threshold function of the software. The regions with the intermediate density were considered as “soft tissue” (cells with collagen type I ECM). Eight volumetric regions (3mm x 3mm X 3mm) were studied in each specimen and three biological replicates were used for each of the eight groups.

Response of CGIPS to Pressure (Load)

CGIPS specimens were placed in an inverted cover of a 10 cm tissue culture (petri) dish. The bottom part of the petri-dish was placed on top of the CGIPS without touching the cover. One and two pound weights were placed on top of the bottom half of the petri-dish (transmitting the pressure to the three CGIPS placed below it simultaneously spaced equidistantly from the center and one another) for 10 minutes and 1 hour. The application of pressure was maintained daily for ten days. The number of cells within each of the CGIPS specimen exposed to varying pressures were determined using MTT assays.

Statistical analysis

GraphPad Prism 4 (GraphPad Software, La Jolla, CA) was used to graphically represent and statistically analyze the results. Two-way ANOVA followed by Bonferroni post comparison tests were used to compare individual groups. In all the experiments the “*n*” indicates biological replicates.

Results

Porous Beta-Tricalcium Phosphate Scaffold can Absorb and Retain Native Fibrillar Collagen Gel

Scaffolds composed of β -TCP (chronOSTM preforms) have pores ranging in size from 100 μ m to 500 μ m (shown in Figure 1A) with porosity of 70% (manufacturing specifications). During a 24 hour immersion, β -TCP absorbed 50% of its dry weight in water, and 75% of its dry weight of collagen type I solution (Figure 1B). Neutralized collagen type I solution gelled within the pores of β -TCP preforms and attained a native fibrillar hydrogel conformation (Figure 1C). β -TCP loaded with collagen gel containing cells will be referred to as **Collagen Gel Impregnated Porous Scaffold (CGIPS)**.

CGIPS Populated with Cells

When a suspension of GFP-tFbs, in neutralized collagen type I solution was applied to the top surface of β -TCP preforms, the collagen solution, which later gelled, was shown to fill the pores (Figure 2A, panel 1). The penetration of the cell suspension throughout the specimen was evident on confocal micrographs shown in Figure 2B (panel 2). Examination of the sectioned surfaces, after the CGIPS was sectioned in half, confirmed that the cell-populated gel had penetrated into the specimen (Figure 2B, panel 1). A depth coding reconstruction of a CGIPS after z-section confocal (optical) scan showed the presence of cells at various depths and their attachment to the pore surfaces (Figure 2B, panel 2). The cells also populated the gel filling the pores as evidenced by concentric circles of fluorescent signal at various depths .

When β -TCP performs were treated with hMSC, labeled with cytotrackerTM orange, without collagen as the carrier, most cells attached near the surface with very few cells penetrating to a depth of 200 μ (figure 3A, panel 1). After two weeks in culture very few cells were observed in confocal optical sections at a depth of 200 μ from the surface, (Figure 3A, panel 2). However, when collagen was delivery vehicle for hMSC, cells were found at 200 μ depth from the surface (figure 3A, panel 3) and continued to occupy the pores deep in the specimen (figure 3A, panel 4) after 2 weeks in culture.

If GFP-tFbs, were located at a distance from CGIPS, and both are embedded in collagen gel, the cells migrated into the CGIPS (Figure 3B).

Porous metallic scaffolds such as tantalum can also absorb and retain collagen gel (supplementary figure 1A). A cross-section from the central part of a tantalum pillar showed uniform seeding of cells in the pores of tantalum (supplementary figure 1B).

Proliferation of hMSC in CGIPS

CGIPS populated with hMSC (50,000 to 400,000 cells / ml of collagen solution) when incubated with MTT converted it to formazan in the pores of the scaffold (supplementary Figure 2A). The amount of formazan formed in CGIPS was directly related (Pearsons statistic 0.96) to the number of cells in the collagen gel (supplementary figure 2B). At the time of seeding hMSC on β -TCP, cells seeded in medium and cells seeded in collagen solution were contained within the scaffold (100% seeding efficiency, no cells escaped - overflowed into the well).

When hMSC in CGIPS were cultured under differentiation conditions the cell number slowly increased from 25 K to 50K (mean, SD=1.5 K, n =3) for the first two weeks. Thereafter hMSC proliferated rapidly for the next six weeks (Figure 4A), the longest time period under observation, to the final cell number of 333 K (mean, SD=88K, n=3). CGIPS with hMSC cultured in MSC growth medium started proliferating rapidly after one week in culture and had reached a significantly greater ($p<0.05$) cell number at the end of eight weeks as compared to MSC cultured in ODM (Figure 4B).

CGIPS supported cell proliferation without collagen gel contraction

CGIPS populated with hMSC (200,000 cells / ml collagen gel), proliferated when cultured in ODM (Figure 5A). At higher cell density hMSC started proliferating rapidly at the end of one week, whereas cells at 100,000 cells per ml started rapid proliferation at the end of two weeks. hMSC at 400,000 cells per ml proliferated rapidly even during their first week in culture (data not shown as only one week data point was obtained). At all cell densities the weight of CGIPS stabilized after some initial fluctuation during the first two weeks and stayed relatively constant thereafter (figure 5B).

Calcification in CGIPS *in vitro*

MicroCT scanning analysis revealed significantly different ($p<0.01$) “empty volume” (pores not occupied by soft tissue) for all the sample groups (Figure 6A). The control samples (β -TCP without either cells or collagen gel) had the maximum empty volume, while the cell-seeded β -TCP had more empty volume than the CGIPS. CGIPS and hMSC-seeded β -TCP had less empty volume at day 56 than on day one. The control sample had the minimum pore volume occupied by non-calcified tissue (cells and extracellular matrix) (Figure 6B) with each

group (control, hMSC-seeded β -TCP and CGIPS) being significantly different ($p < 0.01$) from the other. CGIPS had more volume of non-calcified tissue than hMSC-seeded β -TCP and day 56 samples had more pores occupied by non-calcified tissue than day one samples. As would be expected the amount of calcified tissue in the control sample, the β -TCP and CGIPS on day one were not significantly different (Figure 6C). CGIPS on day 56 had significantly more ($p < 0.01$) calcified tissue when compared to β -TCP on day 56 or CGIPS on day one. Table 1 lists the morphological parameters obtained from microCT scanning of the samples. Morphological parametric values for CGIPS at day 56 are indicative of a stronger trabecular bone as compared to values obtained for β -TCP at day 56.

Response of hMSC in CGIPS to “load”

When hMSC in CGIPS were subjected to 6 kilopascal (KPa) for 10 minutes daily for three days greater cell proliferation was observed when compared to CGIPS not exposed to pressure, exposed to 6 KPa for 1 hour daily for three days or to 12 KPa for 10 min daily for three days (Figure 7). The cells in control CGIPS were more proliferative during the next seven days. All of the applied pressures suppressed proliferation of hMSC during the three to ten day time period.

Figures and Legends

Figure 1. Impregnation and retention by β -TCP of collagen type I gel. Figure 1A. Phase contrast micrograph of a thin slice of β -TCP shows multiple pores with large interconnections. **Figure 1B.** After 24 hours immersion β -TCP absorbed 50% of its own weight in water and

absorbed and retained 75% of its dry weight of collagen type I solution. This indicated excellent penetration of collagen type I solution into the porous β -TCP and confirmed a high porosity of β -TCP. **Figure 1C.** Cy-5TM labeled collagen type I filled all the pores of the β -TCP (panel i) and adopted a fibrillar morphology resembling native collagen type I (panel ii).

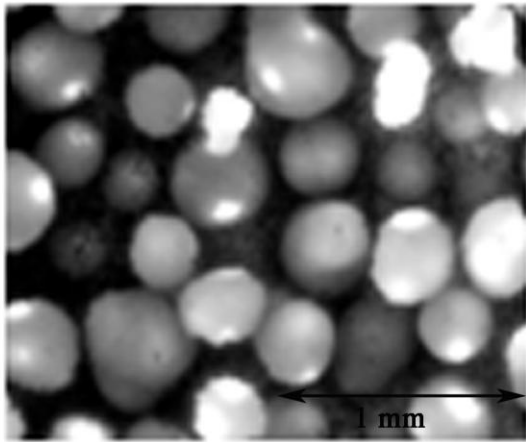


Figure 1A

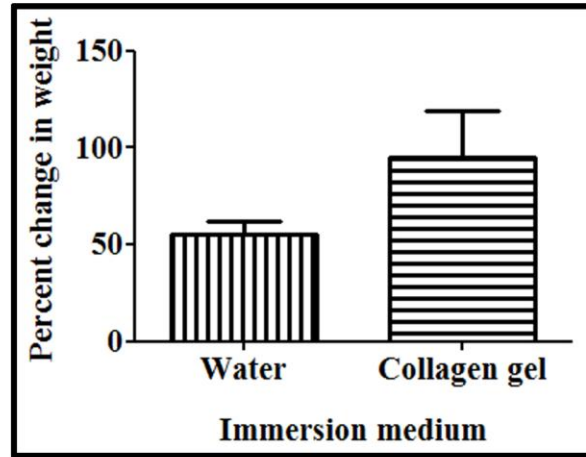


Figure 1B

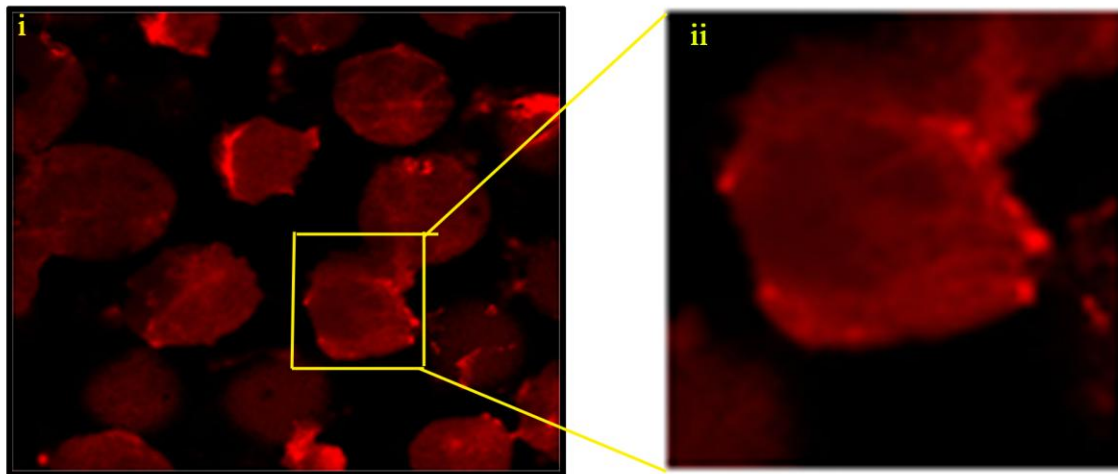


Figure 1C

Figure 2. Distribution of GFP-tFbs throughout the 5 mm x 5mm x 5mm β -TCP scaffold.

Figure 2A Panel i. A z projection of confocal images from the top section of β -TCP scaffold on

which GFP-tFbs in collagen type I solution were seeded. The cells are shown to line the surface as well as filling the pores. **Panel ii.** A z projection from the bottom section of CGIPS (opposite to the surface on which cells were seeded), showing that the cells have penetrated all the way through the scaffold. **Figure 2B.** The confocal micrograph of a cross-section through the center of CGIPS. **Panel i.** A confocal image confirming the presence of GFP-tFbs in the central section of the CGIPS scaffold. **Panel ii.** A depth coding of a series of images of the central section of the CGIPS scaffold, demonstrating presence of cells in pores at various depths (observed as concentric circles due to spherical morphology of the pores).

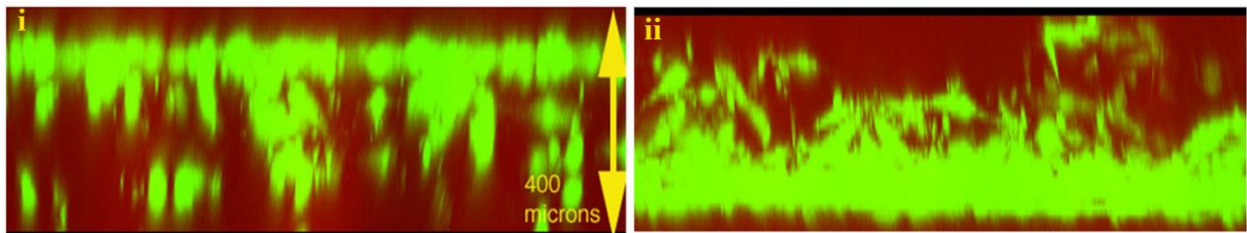


Figure 2A

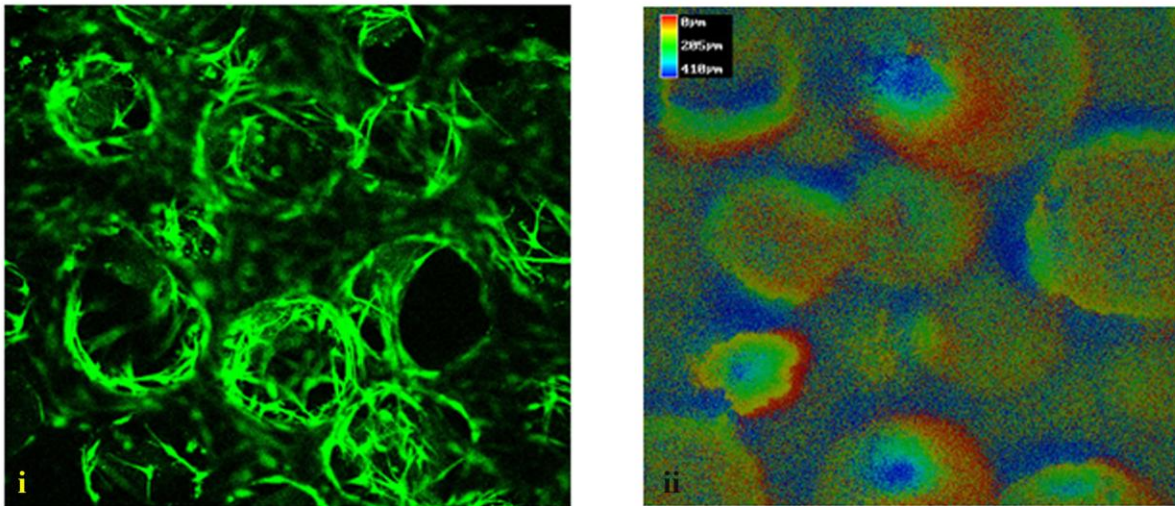


Figure 2B

Figure 3. Retention and migration of cells in CGIPS. Figure 3A. Panel i. When hMSC were applied to β -TCP in culture medium, they remained close to the surface and very few cells were observed in confocal sections 200 μ m below the surface. **Panel ii.** After two weeks almost all the cells had migrated to the surface and no cells were observed in confocal images 200 μ m below the surface. **Panel iii.** In contrast, when collagen type I solution was used to deliver hMSC, the cells penetrated much deeper into the porous β -TCP, and were present in confocal images from 200 μ m below the surface. **Panel iv.** After culture of the CGIPS for two weeks cells were still present in the pores at 200 μ m below the surface. **Figure 3B.** A z projection of series of confocal images captured at the interface of CGIPS and surrounding collagen type I gel demonstrating migration of GFP-tFbs into the CGIPS. When GFP-tFbs in collagen gel, which also contained distal they migrated radially away from the implant site and migrated into the CGIPS after two weeks of culture.

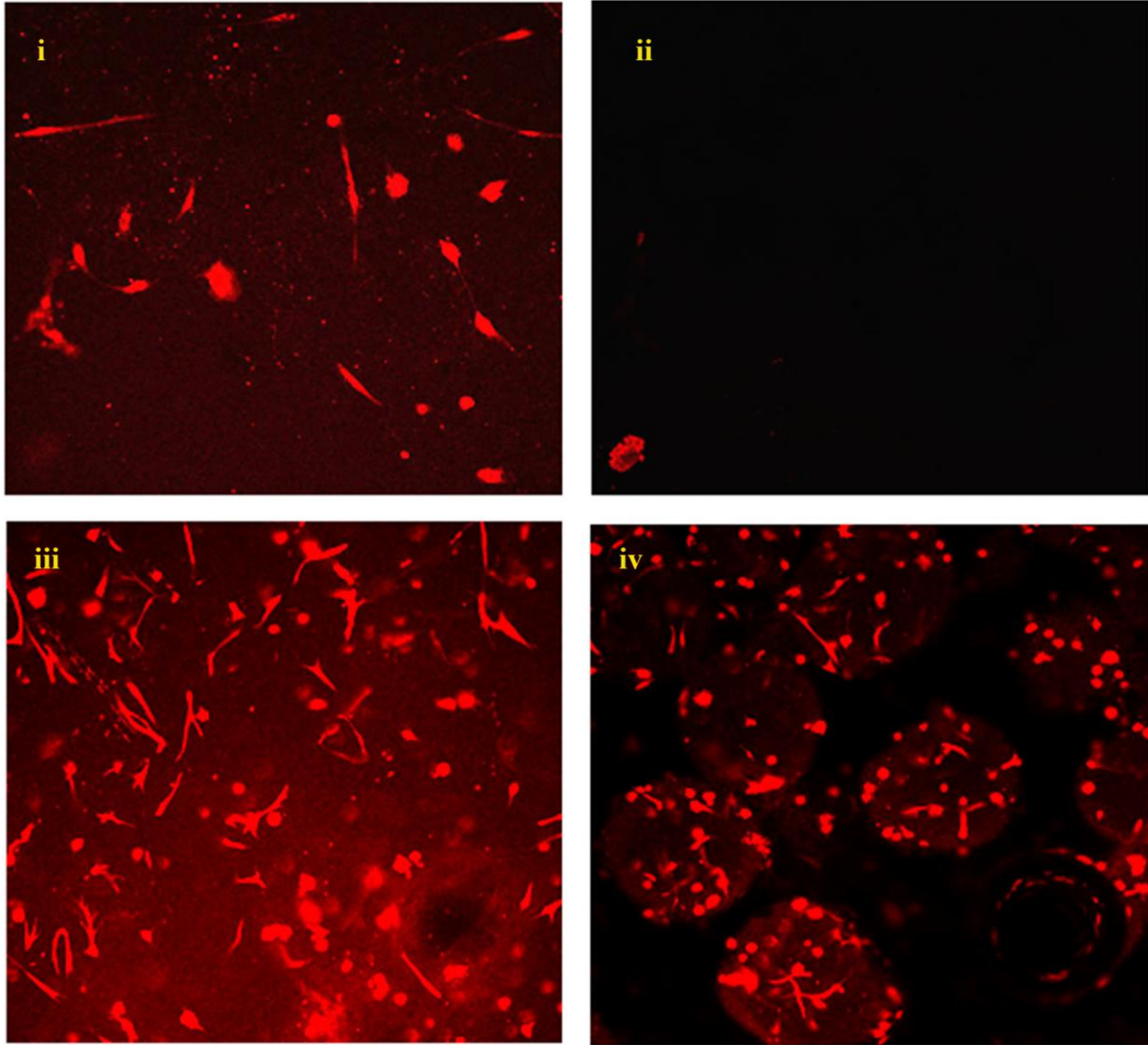


Figure 3A

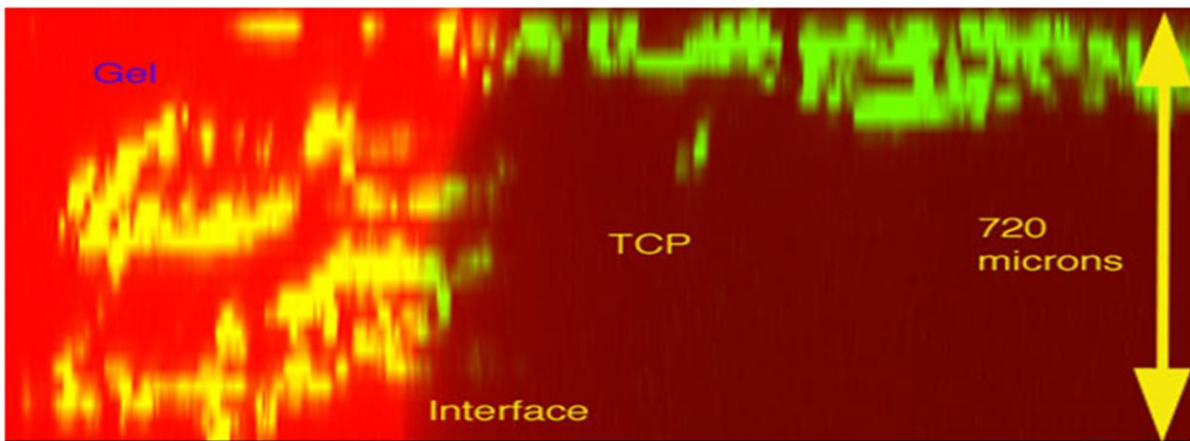


Figure 3B

Figure 4. Proliferation of hMSC in CGIPS. **Figure 4A.** hMSC cultured in CGIPS under differentiation conditions (ODM), proliferated from 25K cells to more than 300K after eight weeks (mean, SEM plotted, $n=3$, $p<0.05$). **Figure 4B.** hMSC in CGIPS cultured under proliferation conditions (MSCGM), achieved higher proliferation than hMSC in CGIPS cultured under differentiation conditions (ODM). (mean, SEM plotted, $n=3$, $p<0.05$).

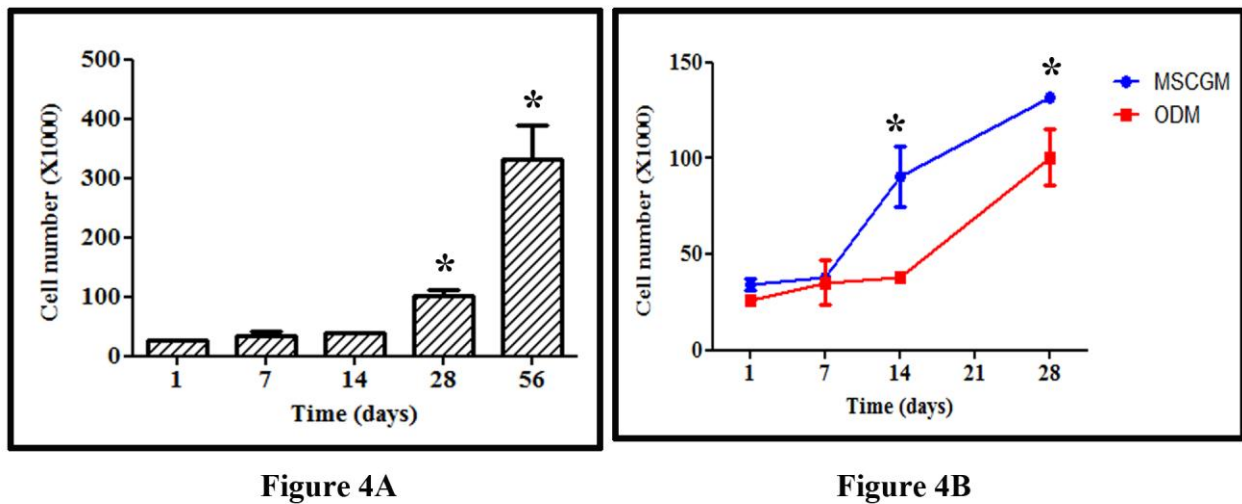


Figure 5. Collagen gel does not contract in CGIPS. **Figure 5A.** When cultured under differentiation conditions hMSC seeded at 200K cells / ml of collagen gel proliferated more than cells seeded at 100K/ml (mean, SEM plotted, $n=3$, $p<0.05$). **Figure 5B.** The weight of CGIPS stabilized after two weeks in culture and remained uniform thereafter. The absence of contraction was independent of cell seeding density (mean, SEM plotted, $n=3$, $p>0.05$).

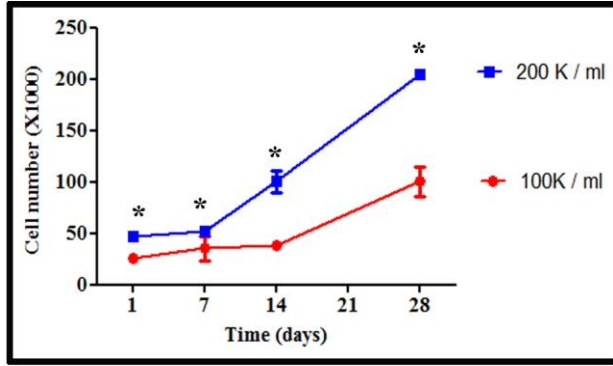


Figure 5A

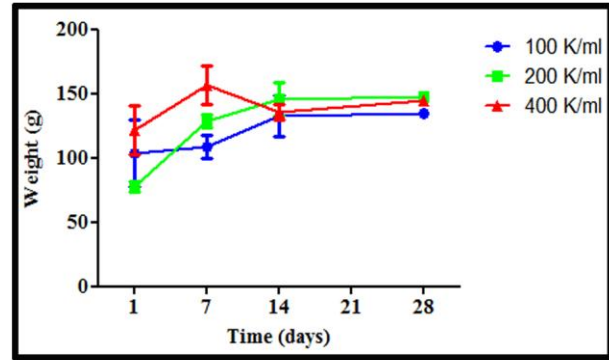


Figure 5B

Figure 6. microCT scanning analysis of CGIPS. Figure 6A. Maximum “empty volume” (volume not occupied by β -TCP scaffold or tissue) is observed in control specimens. Significantly less empty volume was observed in β -TCP populated with cells and CGIPS. ($p < 0.05$) (Mean, SEM graphed, $n=3$, $p < 0.05$). **Figure 6B.** CGIPS had significantly more ($p < 0.05$) soft tissue than β -TCP, indicating that a higher pore volume was occupied by cells and collagen type I ECM in CGIPS as compared to β -TCP. (mean, SEM graphed, $n=3$, $p < 0.05$). **Figure 6C.** CGIPS at day 56 had significantly greater ($p < 0.05$) calcified tissue than any of the other groups. In this respect the other groups were all similar to each other ($p > 0.05$). (mean, SEM graphed, $n=3$)

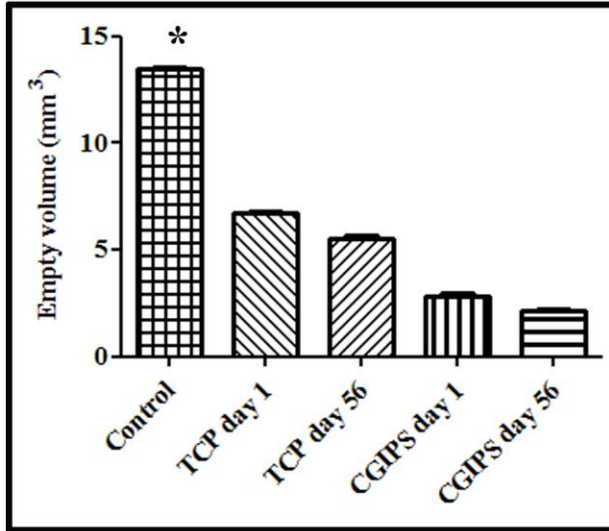


Figure 6A

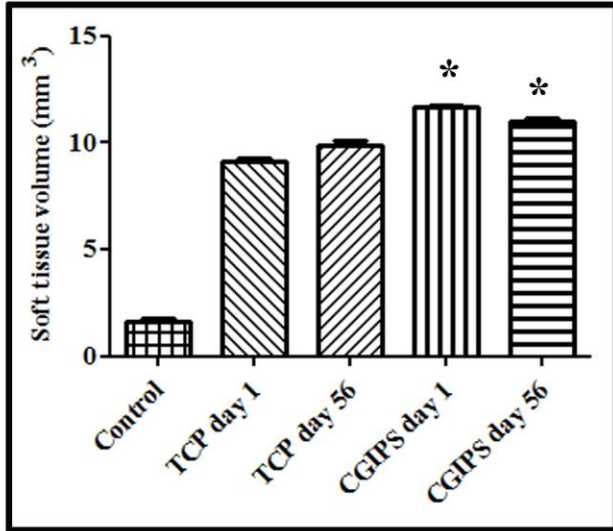


Figure 6B

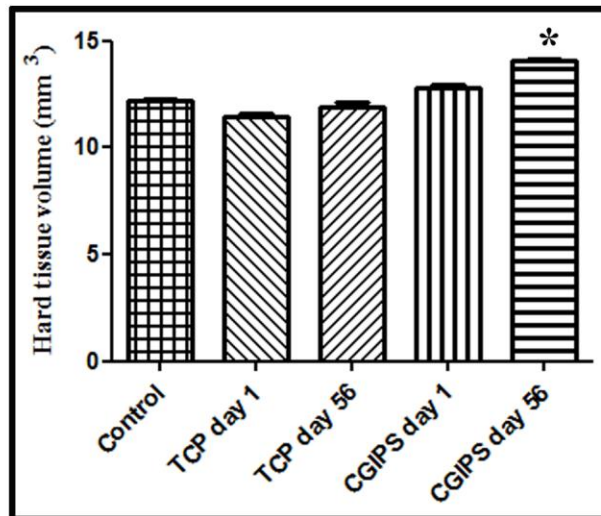


Figure 6C

Figure 7. Response of hMSC to load (pressure). Three days (bars with cross hatches) after exposure to 6 kPa for ten minutes there was a significant hMSC proliferation in CGIPS ($p < 0.05$) than in the untreated controls. 6 kPa for one hour or 12 kPa for ten minutes (daily for three days) did not cause a difference in proliferation. 10 days (bars with horizontal stripes) after exposure to pressure all the treated groups had not proliferated above the number of cells at 3

days while the control group had proliferated significantly more ($p < 0.05$). (mean, SEM graphed, $n=3$)

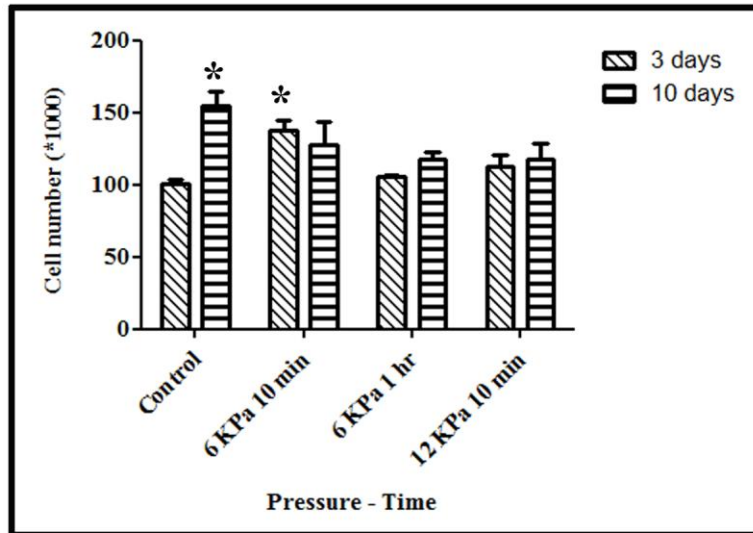
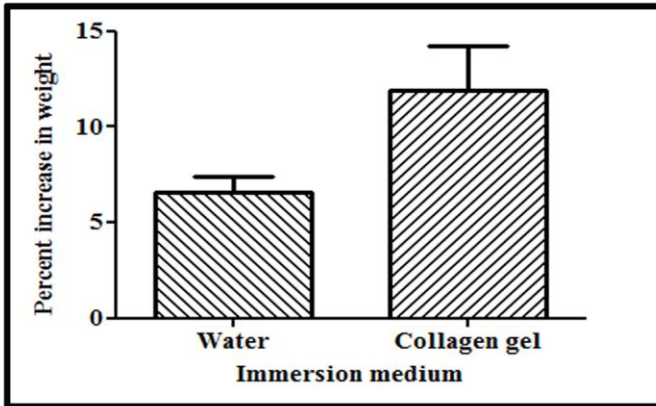
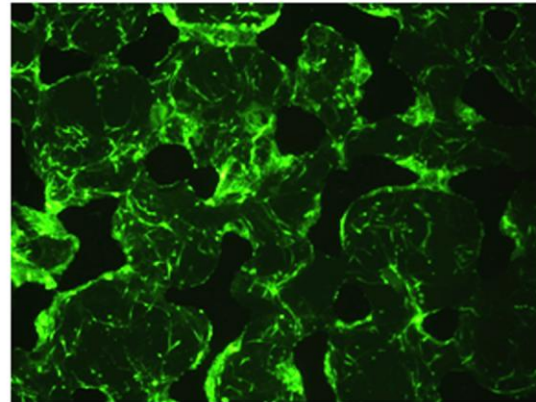


Figure 7

Supplementary figure 1. Impregnation of collagen gel in porous tantalum. Supplementary figure 1A. After a 24 hour immersion porous tantalum absorbed 5% of its own weight of water and 10% of its own weight of collagen gel (mean, SEM graphed, $n=3$). **Supplementary figure 1B.** Section obtained from central part of porous tantalum impregnated with collagen type I gel containing GFP-tFbs demonstrates the uniform distribution of cells in the pores.

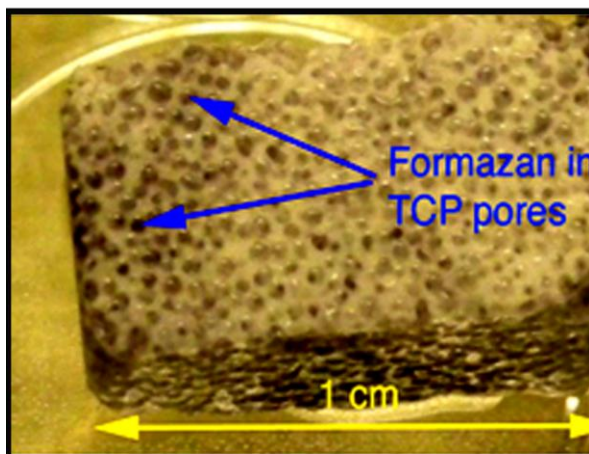


Supplementary figure 1A

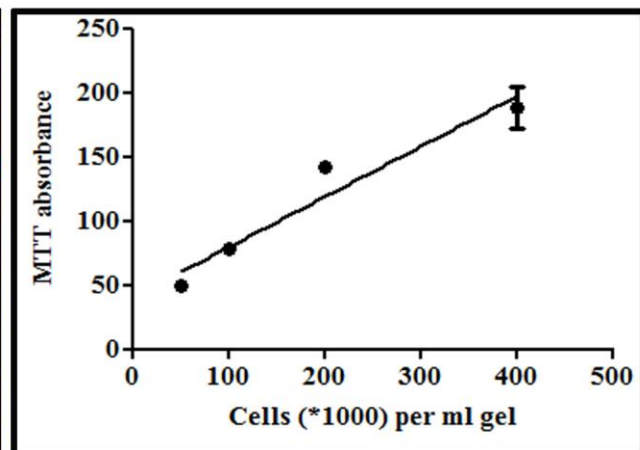


Supplementary figure 1B

Supplementary Figure 2. MTT assay for CGIPS. **2A.** CGIPS block sectioned through the center shows coloration due to formazan in the pores indicating the presence of viable cells. **2B.** Graphical representation cell number plotted against absorbance of light by formazan is a straight line with statistically significant linear correlation. This validates MTT assay for determination of the number of cells in CGIPS.



Supplementary figure 2A



Supplementary figure 2B

Table 1. Morphological parameters obtained from microCT scanning of specimen.

SV/TV: Fraction of volume occupied by soft (cells and matrix) tissue

BV/TV: Fraction of volume occupied by hard (bone) tissue

BS/BV: Ratio of bone surface to bone volume

Tb.Th: Thickness of the trabeculae

Tb.N: Number of trabeculae

Tb.Sp: Trabecular separation

Parameter	Control		TCP day 1		TCP day 56		CGIPS day 1		CGIPS day 56	
	Mean	SD	Mean	SD	Mean	SD	Mean	SD	Mean	SD
SV/TV	0.061	0.015	0.335	0.021	0.363	0.032	0.428	0.015	0.401	0.025
BV/TV	0.446	0.013	0.420	0.025	0.436	0.048	0.468	0.021	0.516	0.023
BS/BV	22.976	0.882	25.641	1.987	24.930	3.006	23.013	1.328	21.432	1.332
Tb.Th	0.087	0.003	0.078	0.006	0.081	0.010	0.087	0.005	0.094	0.006
Tb.N	5.117	0.201	5.363	0.219	5.368	0.212	5.379	0.259	5.516	0.211
Tb.Sp	0.109	0.006	0.108	0.006	0.105	0.009	0.099	0.007	0.088	0.005

Discussion

One of the key principles of tissue engineering is to assemble a structure that mimics the tissue of interest biologically as well as physically. Bone is composed of a network of parallel arrays of collagen type I fibers on which are deposited microcrystals of a stable yet reactive, hydroxyl deficient carbonate substituted calcium phosphate - hydroxyapatite (HA) (1). This particular collagen-HA combination is responsible for the bone strength and elasticity. Calcium phosphate based ceramics are commonly utilized scaffolds in bone tissue engineering. Calcium sulfate and calcium carbonate dissolve too rapidly to be of clinical use while hydroxyapatite is degraded too slowly (66). Beta-tricalcium phosphate (β -TCP) is a sintered hydroxyapatite (hydroxyl deficient calcium phosphate). It has similar mechanical properties to bone, can fuse directly with bone (67), and is almost completely resorbed *in vivo* in 6 to 9 months with no adverse reactions (66).

Rat mesenchymal stem cells (rMSC) seeded directly on β -TCP and cultured under static conditions did not proliferate but differentiated along osteogenic lineage. When this system was cultured under flow perfusion the cell number decreased (67). Human mesenchymal stem cells (hMSC) cultured on β -TCP substratum spontaneously differentiated along osteogenic lineages (75). Osteogenic cells proliferate at a faster rate on β -TCP than on HA and cell apoptosis is reduced (76). These results demonstrated that although β -TCP can support hMSC differentiation along osteogenic lineage to some extent proliferation is not facilitated.

Collagen type I is the major protein constituent of bone ECM and can bind proteins present in the serum (e.g. fibrinogen, fibroblast like growth factor) to stimulate hMSC proliferation and osteogenic differentiation (6). hMSC attachment on collagen based scaffolds

was more efficient than on β -TCP (17), (110). hMSC cultured on collagen substratum show a greater osteogenic differentiation potential and bone formation *in vivo*, than hMSC cultured on β -TCP (6), (17), (110). Interaction of collagen type I with cell surface $\alpha 2\beta 1$ integrin receptors on hMSC, stimulates osteogenic differentiation and blockade of this interaction hinders it (5). The tissue formed by porcine MSC differentiated *in situ* in collagen gel most closely resembled bone, demonstrated greater calcium deposition and was stronger when compared to that formed by pMSC in fibrin, alginate or pluronic gels (44). These data emphasize the potential suitability of collagen as a component of *in vitro* 3-D model and engineered grafts.

Hydrogels lack mechanical strength to carry out experiments involving application of force/load without compromising cell viability. We here propose that a combination of β -TCP and collagen type I would be superior to either alone in terms of cytocompatibility and mechanical strength. Various combinations and stand alone products of animal collagen and calcium phosphate have been approved by FDA for clinical use (51). Human osteosarcoma cells cultured on mineralized collagen composites expressed higher levels of differentiation markers than those cultured on β -TCP or collagen alone (79).

In porous scaffolds the presence of pores facilitates cell invasion, cell migration and complete population of the scaffold, and these are preferred to non-porous scaffolds. Porous scaffolds also allow cell proliferation, diffusion of nutrients into throughout and hence faster and more extensive vascularization and integration with the host tissue. Thus a stronger and more seamless interface develops between the graft and bone because of the larger surface area available in porous scaffolds for bonding (1), (7), (71), (72). The most important physical parameters in a 3-D model / graft assembly and engineering are pore size, pore volume and pore

interconnectivity. Thus pore size of more than 100 microns with a porosity greater than 70%, large pore interconnections and rougher pore walls with microporosity have been shown to be beneficial for bone formation (1), (7), (72). β -TCP scaffolds can be manufactured to satisfy these requirements without compromising the strength. Figure 1A shows the presence of large pores with large pore interconnections in chronOSTM β -TCP a commercially available FDA approved material that is used clinically. The large volume of water and collagen that can be accommodated by this material (Figure 1B) attests to the high pore volume.

Cross-linking collagen is a strategy commonly employed to increase its strength but cross-linked collagen elicits a foreign body reaction *in vivo* and can trigger spontaneous calcium phosphate crystallization (47). Spontaneous calcium phosphate deposition interferes with the experiments that use calcium deposition as a measure of mineralization by osteoblasts. hMSC adhere rapidly and in greater numbers to native collagen than to hydroxyapatite or cross-linked collagen (46). The ability of cells to degrade the gel by MMPs is critically important for differentiation (19), (111), and poor bone formation occurs when a gel is not cleavable. Cross-linking collagen results in the formation of inert fibrillar bonds and the use of denatured collagen substratum favored adipogenic differentiation while native collagen favored osteogenic differentiation (49). Our patented technique results in the formation of a non-contracting native collagen gel (64) and Figure 1C demonstrates that the collagen hydrogel impregnating β -TCP pores is in a native fibrillar form.

One of the difficulties associated with using a porous scaffold is delivery of cells throughout the scaffolds. rMSC (67) and hMSC (17) seeded directly on β -TCP did not penetrate into the porous scaffold but stayed near the surface as a monolayer producing a non 3-

dimensional environment (51). Even when scaffolds with larger pores were used the cells could only penetrate into the scaffold by seeding high densities (in the order of a million cells per scaffold) (59). The strategy employed by some research groups in which the pores are filled with collagen gel prior to seeding cells prevented the perfusion of cells deep into the scaffold interior (46), (51). When we suspended hMSC in neutralized collagen type I solution, applied this suspension to the porous β -TCP scaffolds, and allowed the impregnated collagen to gel *in situ*, even a density of 100,000 cells per ml collagen was shown to penetrate deep into the β -TCP scaffold. Thus Figure 2A and 2B show a cross-section through the center of the Collagen Gel Impregnated Porous Scaffold (CGIPS) demonstrating that the cells are present throughout the entire scaffold. When cells were seeded in CGIPS, the cells that had reached the deeper parts were observed to be present there after two weeks of culturing in ODM (Figure 3A) while no cells were detected in the deep interior of β -TCP after two weeks.

When non-biodegradable implants are used (e.g. stems of replacement joints implants) sub-micron wear particles created by the micro-motion may trigger an immune response leading to implant loosening and failure (1). A strategy that we outlined above can be used to impregnate porous metal with collagen gel to facilitate stronger bonding between metal implant and bone. This should reduce the microdamage and subsequent implant failure. Supplementary figures 1A and 1B demonstrate the feasibility of using this strategy in tantalum metal cylinders.

Rabbit MSC seeded on collagen gel were observed to migrate into the gel and both populations could proliferate and differentiate under appropriate culture conditions (42). We also show the migration of cells into the porous CGIPS (Figure 3B) demonstrating potential for invasion of host tissue as well as study of cell migration in 3-D.

Cell adhesion, proliferation and functional differentiation are important criteria in evaluating the suitability of a scaffold for tissue engineering (77). Cell adhesion to biomaterial is a critical step that affects the function of the tissue engineered graft, since the cells can sense mechanical stimuli via their interaction with the ECM / scaffold to which they are attached. Cell proliferation and differentiation are also affected by the scaffold biomaterial. Hydrophilicity of scaffold can affect multiple steps like cell adhesion, cell migration and adsorption of growth factors. Differentiation of SV40 transformed osteoblasts was not as efficient on hydrophobic surfaces as on hydrophilic substrata (77). When collagen was added to the cell suspension medium seeding efficiency of mouse MSC on alginate-gelatin- β -TCP was improved from 30% to 40% but still most of the cells either did not attach or migrated out of the scaffold after one day in culture (61). Rabbit adipose tissue derived stem cells, were seeded using collagen carrier into PLGA- β -TCP scaffolds with 100% efficiency and the cells were distributed in the pore spaces (51). In our experiments with hMSC 100% efficiency was achieved when engineering CGIPS.

Determination of the cell numbers populating 3-D models is a challenge. Conversion of MTT to dark blue formazan and can be used not only to visualize the distribution of viable cells (59) but also determine the cells number in the 3-D model. Supplementary Figure 2A shows the hMSC populating the pores of β -TCP (formazan color within the pores) (i.e. CGIPS), while Supplementary Figure 2B establishes the validity of using MTT assay to determine the cell number. The relationship between light absorption by formazan (generated by cell respiration) bears a linear relationship to the number of cells present in the CGIPS. This linear relationship is not affected by osteogenic differentiation (manuscript in preparation) and a

given number of mesenchymal stem cells produce the same amount of formazan as the same number of osteoblasts.

When hMSC were seeded at a low seeding density on mineralized collagen sponge they proliferated well but the cells seeded at high seeding density did not proliferate (59). From our experience we believe that limitation of cell proliferation in 3-D scaffolds noted by previous researchers was due to restriction in diffusion of nutrients into the scaffold (17), (59). We observed proliferation of hMSC in CGIPS for upto 8 weeks of culture under proliferation conditions (Figure 4A). Even when the cells were cultured under differentiation conditions as would be expected proliferation was reduced but not inhibited. (Figure 4B).

A significant contraction of collagen gel was observed when it was used as a carrier for introduction of porcine MSC into β -TCP. This collagen contraction may have proved detrimental to long term survival of the cells located in the interior of the scaffold (44). Although dynamic culture conditions prevent the contraction, static culture conditions are a better representation of *in vivo* conditions. Data from our laboratory (manuscript in preparation) demonstrated that populating scaffolds at low cell density decreases collagen gel contraction during osteogenic differentiation of hMSC. It has been reported that decreasing the seeding density does not interfere with the formation of mineralized tissue over a culture period longer than 6 weeks (59), (60). Cell density of 100,000 and 200,000 cells / ml collagen proliferated in CGIPS (Figure 5A) with the higher density starting to proliferate earlier. Population density of 400,000 cells / ml, can cause collagen gel contraction (manuscript in preparation). Measuring contraction by loss in wet weight of CGIPS, the collagen gel did not contract as shown by stable weights of the CGIPS with different seeding densities (100K, 200K and 400K per ml) over a culture period of four weeks (Figure 5B). If the collagen gel had contracted, the weight of

CGIPS would have varied with seeding density, as the collagen gel contraction is seeding cell density dependent (manuscript in preparation).

Rabbit adipose tissue derived stem cells (rADSC) when introduced using collagen gel into PLGA- β -TCP scaffolds deposited more calcium than the cells seeded directly on PLGA- β -TCP scaffold (51). hMSC proliferated faster and formed more bone on porous β -TCP - HA with collagen gel as compared to uncoated β -TCP - HA, or porous β -TCP -HA containing alginate gel, fibrin gel, hyaluronate gel, pluronic gel, agarose gel (43). When the collagen gel was introduced into the porous HA scaffold prior to seeding the cells inferior bone formation was observed.(46). The mineralized tissue formed by pMSC in collagen gel in β -TCP scaffold was found mostly on the surface of the scaffold when cultured under static conditions (44). The design of the scaffold was such that none of the cells were deeper than 1 mm from the surface that was in contact with the medium. Although this design would improve the cell survival *in vitro*, it would decrease the stringency of the test conditions. For example *in vivo* cells in an implant are in a relatively anaerobic, nutrient deficient environment until extensive vasculogenesis takes place.

High concentration of inorganic phosphate can stimulate mineralization by osteogenic cells (69). Mineral deposition can occur spontaneously in the presence of high concentrations of calcium and phosphate, which then serve as the nidus for further crystalline growth. The degradation process of β -TCP generates high concentrations of calcium and phosphate ions in the immediate vicinity which can stimulate mineralization of surrounding osteoid tissue and enhance the bonding between grafted β -TCP and bone. This demonstrates the utility of β -TCP as a scaffold.

The depth of field of when observing specimens using confocal microscopy, is limited in opaque ceramics; also ceramics can be autofluorescent. MicroCT technique allows the reconstruction of 3-D images from a series of 2-D images obtained at multiple observation planes (112). Since quantitative parameters are important in defining bone morphology, density and hence bone strength (113), parameters like bone volume density (BV/TV, relative volume of mineralized tissue to total volume), bone surface density (BS/TV, relative volume of bone surface to total volume), trabecular thickness (Tb.Th, average thickness of the individual pillars forming the scaffold wall), trabecular separation (Tb.Sp, distance between trabeculae) and trabecular number (Tb.N, number of trabeculae per unit length) are used to compare bone graft specimens with trabecular bone. Figure 6A shows that CGIPS had significantly less empty volume than β -TCP. CGIPS had more volume occupied by soft tissue (cells and collagen ECM) than β -TCP at the start as well as at the end of eight weeks culture period. CGIPS showed significantly more calcium deposition at the end of eight weeks culture period whereas when cells were cultured on β -TCP a increase in calcium deposition was not observed (Figure 6C).

A unique feature of bone is its ability to change its shape and structure (remodel) in response to the mechanical forces acting on it (1). Mechano-transduction describes a series of events wherein mechanical forces acting through the extracellular matrix regulate gene expression in cells that is reflected in alterations in cell function. MSC bind extracellular matrix via integrin receptors and osteogenic differentiation is accelerated by dense ECM where the opportunities for such interaction are increased (19). Mechanical cues stimulate bone resorption by osteoclasts and deposition by osteoblasts (49) both of which processes have a pivotal role in fracture healing.

During the first phase of fracture healing, pluripotent tissue proliferates and forms the fracture callus (11). The proliferation of cells that are involved in wound repair is directed not only by biochemical signals but also by mechanical signals. Thus in the second phase, application of hydrostatic compressive forces (that change volume) stimulate the differentiation of the pluripotential callus tissue along chondrogenic lineage while octahedral shear stress (that causes deformation) leads to ossification. The third phase, the remodeling, takes place in response to the direction of force acting on the newly formed osseous tissue. Figure 7 shows the ability of CGIPS to reflect response of hMSC to mechanical forces. While application of 6 kPa pressure for ten minutes every day resulted in increased proliferation of hMSC over the first three days, continued application of the same pressure prevented further hMSC proliferation. Use of higher pressure (12 kPa) or longer duration of application of pressure (1 hour) led to prevention of proliferation of hMSC. It is possible that application of pressure led to rapid differentiation of hMSC and prevented proliferation. Although multiple factors are involved in bone remodeling, these experiments provide a proof of principle for the use of CGIPS as mechanosensitive 3-D models for study of ossification.

Thus CGIPS is superior to β -TCP alone with respect to cell distribution throughout the entire scaffold, retention of seeded cells, migration of cells into CGIPS, proliferation of hMSC and mineralization by osteogenically differentiated hMSC. Furthermore, we have provided a proof of concept for the use of CGIPS in studies involving mechanotransduction in 3-D.

CHAPTER V

CALCIFICATION OF COLLAGEN IMPREGNATED

B-TRICALCIUM PHOSPHATE *IN VIVO*

Introduction

The musculoskeletal system provides form to the human body, protects soft internal organs, serves as attachment for muscles facilitating locomotion, acts as a storehouse of calcium and phosphate and is the site of formation of blood and immune cells. (1), (2). The extracellular component of this vital organ system (comprised chiefly of bone tissue) is formed primarily by collagen type I with micro-deposits of bone-hydroxyapatite (a calcium phosphate mineral with minor carbonate substitution). The cellular components of bone, osteoblasts, osteoclasts and osteoblasts are responsible for deposition, resorption and maintenance of osseous tissue. Bone has the unique capability to heal by formation of new bone tissue after fractures. The first part of this process involves mesenchymal stem cell (MSC) invasion from the surrounding bone marrow and periosteum into the hematoma formed at the fracture site and differentiation into osteoblasts. Concurrently mononuclear cells invade the hematoma, fuse and differentiate into multinucleated osteoclasts. Both osteoblasts and osteoclasts are closely associated with the invading vasculature.

Although bones can heal by regeneration, the ability to repair a wound is limited and large bone voids may not heal unassisted (1), (2). These critical-sized bone defects can be

repaired only by means of grafting. Autologous bone graft is considered the gold standard of treatment against which new therapies are compared (21). The amount of autograft that can be harvested is limited and harvesting is associated with bleeding, infection and pain at the donor site in an already suffering patient. Allograft material from bone banks addresses these issues but suffers from lack of consistent performance and possibility of transmission of infectious agents. Bone grafting was responsible for more than US\$ 3 billion in health care costs and accounted for over 600,000 procedures in the US and more than 400,000 procedures in Europe (81).

Tissue engineering is a branch of science that attempts to utilize various artificial and natural materials to help repair tissues and organs in the body (2). For a tissue engineered product to meet FDA approval and be a successful bone graft substitute, it has to be cost effective, sterile, radiographically distinguishable, totally biodegradable with non-toxic degradation byproducts, mechanically strong, and finally remodellable into native bone tissue (23). Bone cements and other non-biodegradable graft substitutes that were previously developed to repair bone voids are not resorbed and replaced by bone tissue (44). Gels and other soft scaffolds lack mechanical strength and are inappropriate for use in a mechanically active environment. We studied the osteogenic capacity and biocompatibility of a bone graft substitute formed from β -TCP, collagen gel and MSC.

Materials and Methods

Cells

Telomerase transfected human bone marrow derived mesenchymal stem cells (TMSC) (a kind gift from Dr. Dario Campana, St. Jude Children's Research Hospital, Memphis,

TN, USA) (35) were cultured in MEM α (GIBCO, Invitrogen, Carlsbad, CA) containing FBS (10%, Atlanta Biologicals, Lawrenceville, GA) and FGF (10 nM, R&D Systems, Minneapolis, MN), with medium changes every second day. MSC were passaged at 80-90% confluence using trypsin (0.05%) with 0.53 mM EDTA in HBSS (GIBCO, Invitrogen, Carlsbad, CA) and plating at 3000 cells/cm². Cells were counted using hemocytometer and Trypan blue (Sigma-Aldrich, St. Louis, MO) dye exclusion viability stain.

Collagen Type I Gel

Cold (4°C) porcine collagen type I-A solution (Cellmatrix[®], Nitta Gelatin, Wako Chemicals, Richmond, VA, USA, 3mg/ml) (8 parts v/v) was mixed thoroughly with cold (4°C) 10X medium (1 part, v/v) and then neutralized (pH 7.4) with cold (4°C) reconstitution buffer (sodium hydroxide 0.5N, sodium bicarbonate 22g / l, HEPES free acid 47.7 g / l) (1 part v/v) with thorough mixing. Careful mixing after each addition was required to prevent air bubble formation in the viscous solution. All solutions and mixing steps were conducted at 4°C and the neutralized collagen solution stayed liquid at 4°C. Cell pellet could be suspended in neutralized collagen solution by passing through a syringe with 21 gauge needle. When incubated at 37°C under 5% CO₂ the solution gelled within 30 min. All experiments were performed using the above mentioned collagen gel.

Beta-Tricalcium Phosphate Scaffolds

Porous scaffolds made of β -tricalcium phosphate (chronOS[™], abbreviated as β -TCP) were a kind gift from Synthes (Monument, CO, USA). The pore size of these scaffolds ranges from 100 to 500 microns, with a porosity of 70% (Manufacturer provided information).

Impregnation of the β -TCP Scaffold

β -TCP scaffolds were cut into 4mm X 4mm X 2mm pieces and immersed in

phosphate buffered saline {0.256g/L NaH₂PO₄ H₂O, 1.19g/L Na₂HPO₄, 8.76g/L NaCl, pH 7.4, in distilled water} {PBS}) for 24 hours. The β -TCP pieces were blotted on filter paper and 250 μ l collagen solution (with 1 million TMSC/ ml collagen) was seeded on to the scaffold. Each β -TCP cube prepared in this fashion was placed in a well of a 24 well plate with 1.5 ml of collagen solution with TMSC. The culture plates were incubated at 37°C overnight to allow the collagen to gel and the β -TCP impregnated with collagen gel containing TMSC will hereafter be referred to as **Collagen Gel Impregnated Porous Scaffold (CGIPS)**.

Control group of β -TCP cubes with collagen but without cells was prepared as described above using neutralized collagen type I gel without any cells and will be referred to as β -TCP-Gel. Control group with cells seeded directly on β -TCP without any collagen gel was also prepared as described above by substituting cell culture medium for collagen solution at all steps. These controls will be referred to as β -TCP-Cells. The final control group consisted of β -TCP treated as described above with cell culture medium not containing collagen gel or cells and will be referred to as β -TCP-Empty.

Animals

Eight week old male Sprague-Dawley rats were purchased from Charles-River laboratories after protocol approval from the Institutional Animal Care and Use Committee (IACUC). The rats were used for surgical implants at ten weeks of age with bodyweights between 350 to 400 grams..

Surgical Procedure for Implantation in Rats

Rats were administered preoperative analgesic (Caprofen 4mg oral) on the night prior to surgery and food was withdrawn. On the morning of the surgery rats were anesthetised by inhalation of 5% isoflurane with oxygen at a flow of 4 literes per minute. After induction the

anesthetic agent was reduced to 2%. Antibiotic ophthalmic ointment was instilled in the eyes and the upper backs of the animals shaved. Animals were draped and surgical site prepared with betadine and ethanol. Incisions (1 inch) were made on the skin above the spine of the scapula and parallel to the spine. Intramuscular pockets were formed dorsal to the infrascapular region and CGIPS were placed on the left sided pocket and β -TCP-Empty specimen placed on the right. The intramuscular grafts were retained in place using fine 6,0 ethicon sutures. Subcutaneous pouches were formed and the implants were placed in these pouches. Left lateral pouch- CGIPS, Left medial pouch- β -TCP-Gel, Right medial pouch- β -TCP-Empty, Right lateral pouch- β -TCP-Empty. The skin was closed using metal clips. Rats were administered 4 mg Caprofen twice a day for 2 days postoperatively.

Retrival of Grafts

Animals were sacrificed by CO₂ asphyxiation at the end of one month and grafts removed from the implantation sites. The grafts were immediately placed in Neutral formalin buffer (10% formalin/formaldehyde 10mL, in Na₂HPO₄ 1.6g and NaH₂PO₄.H₂O 0.4g/100 mls of distilled water, all from Fisher Scientific), for two hours and in PBS with 30% sucrose overnight at 4°C. This was followed by freezing in Tissue-Tek and sectioning with cryostat.

Immunohistochemistry

Tissue sections were stained according to recommendations of IHC kit manufacturer (Prohisto, Columbia, SC, USA). Slides were transferred to amplifying chamber (IHC Prohisto) in which all the subsequent steps were performed. Slides were blocked with 1% BSA (3ml per slide, EMD Chemicals, Gibbstown, NJ, USA) in PBS, overnight at RT. Primary antibodies were diluted in amplifying antibody dilution buffer (1x, 3 ml per slide IHC Kit, Prohisto) as follows: mouse anti-osterix antibody (Novus biologicals, Littleton, CO, USA), to

1:500 and rabbit anti-osteopontin (Abcam Inc., Cambridge, MA, USA) to 1:800. The slides were incubated overnight at 4°C. The slides were then washed 3 times in water for 5 minutes at RT. Alexa Fluor 594 labelled goat anti mouse and Alexa Fluor 488 labelled goat anti rabbit (both from, Invitrogen, Eugene, OR, USA) secondary antibodies were diluted in PBS to 1:4000 and slides were incubated with 3 ml antibody solution per slide overnight at RT.. Slides were then washed 3 times in water for 5 minutes at RT. Coverslips were mounted on the slides using Prolong Gold antifade reagent with DAPI (Invitrogen, Eugene, OR, USA). After allowing the slides and coverslips to dry overnight the slides were examined by fluorescent microscopy as described earlier. All immunohistochemistry or histochemical stained specimens were examined on Olympus AX70 fluorescent microscope (Olympus, Center Valley, PA) using SPOT[®] TWAIN software (Microsoft, Issaquah, WA).

Hematoxylin & Eosin

Tissue sections were hydrated in water. Stained with Hematoxylin (Sigma-Aldrich, St. Louis, MO, USA) for 2 minutes, differentiated with 0.3% acid-alcohol (0.3% conc. hydrochloric acid in 70% aqueous ethanol) for 30 seconds, stained with Eosin (Sigma-Aldrich, St. Louis, MO, USA) for 10 minutes, dehydrated with 100% ethanol, cleared with xylene and mounted.

Alizarin Red

Slides were stained with 2% aqueous solution of Alizarin Red S, (pH adjusted to 4.5 with 10% ammonium hydroxide) (all reagents from Sigma-Aldrich, St. Louis, MO, USA) for five minutes. Sections were blotted, dehydrated in acetone, cleared with xylene and mounted.

VonKossa

The staining solution was freshly prepared by mixing: naphthol AS MX-

PO₄ (0.005g, Sigma-Aldrich, St. Louis, MO, USA), N,N-dimethylformamide, (200µl, DMF, Fisher, Fair Lawn, NJ, USA), Tris-HCl (25 ml, 0.2 M, pH 8.3), distilled water (25 ml), red violet LB salt (0.03 g, Sigma-Aldrich, St. Louis, MO, USA). Filtered staining solution (Whatman's No.1 filter paper) was applied to cover the slides and the slides incubated at RT for 45 min, rinsed in distilled water 3-4 times and left to stand in distilled water for 1 hour. Finally the slides were counterstained with silver nitrate (2.5% aqueous, Sigma-Aldrich, St. Louis, MO, USA) for 30 min. The excess silver nitrate was aspirated, the slides rinsed with distilled water 3 times and dried overnight, covered with a glass coverslips, sealed at the edges (nail polish) and immediately examined microscopically as previously described.

X-ray

Implants were dissected from the rats and preserved in 2% glutaraldehyde in PIPES buffer for 24 hours. The implants were placed in a petridish and X-ray images obtained using Lumina XR imaging system (Caliper life sciences, Hopkinton, MA, USA).

Histomorphometric analysis

Image J software (NIH, Bethesda, MD, USA) was used for measuring the area occupied by blood vessels/ soft tissue/ empty area (in H&E stained sections at 10X) and calcification within the soft tissue (von Kossa stained sections at 10X). Three different sections from two rats were analyzed. For Xray density, samples from seven rats were used and the optical density of the X-ray image of the implants was measured using Image-J. A fixed box size of 30 X 30 pixels was used for analysis of each implant.

Statistical analysis

GraphPad Prism 4 (GraphPad Software, LaJolla, CA) was used to graphically represent and statistically analyze the results. One-way ANOVA (with matching data obtained

from different study groups harvested from the same animal, viz. repeated measures ANOVA) was used for analysis of subcutaneously implanted study groups and was followed by Bonferroni post comparison tests to compare individual groups. Paired t test was used to compare intramuscular implants. In all the experiments the “*n*” indicates biological replicates.

Results

TCP implantation and recovery

The TCP pieces (4mm X 4mm X 2mm, Figure 1A) belonging to the four different groups were implanted on the upper back of the rats, in the area over the scapulae (Figure 1B). The rats were sacrificed after one month and the implanted TCP recovered. All the subcutaneous implants stayed separate from one another in their respective subcutaneous pockets (Figure 1C) and the intramuscular implants stayed in their respective intramuscular pockets in the scapular musculature (Figure 1D). X-rays of the dissected upper back muscles and scapulae demonstrated the positions of the implants with respect to one another and the scapulae (Figure 1E).

Expression of markers of differentiation

Frozen sections of the implants showed numerous cells in the pores on DAPI staining in all the groups (All panel i in Figure 2). Subcutaneously implanted empty-TCP did not show presence of human cells (Figure 2A, panel ii) or expression of osteopontin (Figure 2A, panel iii). Subcutaneously implanted CGIPS demonstrated that human cells had survived in the implants (Figure 2B, panel ii) with rat cells and human cells present in the scaffold (Figure 2B, panel i and ii). Expression of osteopontin is observed in the same region where human cells are observed viz along the pore walls (Figure 2B, panel ii and iii).

Far more cells infiltrated the pores of Gel-TCP (Figure 2C, panel i) as compared

to Cells-TCP (Figure 2D, panel i). Gel-TCP did not contain any human cells (Figure 2C, Panel ii) and implanted human cells did not survive in Cells-TCP (Figure 2D, panel ii). Osteopontin expression is observed in Gel-TCP along the pore walls (Figure 2C, panel iii) but not in Cells-TCP (Figure 2D, panel iii).

In case of intramuscular empty-TCP implants fewer cells were seen in the pores as compared to CGIPS (Figure 2 E and F, panel i). No expression of osteopontin was observed in empty-TCP (Figure 2E, panel iii). Human cells were observed along the pores of the wall (Figure 2F, panel ii) colocalizing with osteopontin expression (Figure 2F, panel iii).

Expression of osterix was similar to osteopontin, viz. not observed in empty-TCP implanted subcutaneously (Figure 3A, panel i), Cells-TCP implanted subcutaneously (Figure 3B, panel ii) and empty-TCP implanted intramuscularly (Figure 3A, panel iii). Generalized expression of osterix was observed in the pores with higher expression along the pore walls, in case of CGIPS implanted subcutaneously (Figure 3B, panel i), Gel-TCP implanted subcutaneously (Figure 3A, panel ii) and CGIPS implanted intramuscularly (Figure 3B, panel iii).

Vascularization of implants

Host tissue had penetrated into the pores in all implants (Figure 4A) and different types of cells were densely distributed in the soft tissue along with blood vessels invading into the implants. The amount of tissue within the pores of CGIPS was not significantly different in case of subcutaneous implants (Figure 4B, panel i). For intramuscular implants CGIPS had significantly more tissue invasion than Empty-TCP (Figure 4B, panel ii). When sectioning the samples CGIPS and Gel-TCP held together and had tissue invading into the central pores. The Cell-TCP and Empty-TCP interior portions collapsed during sectioning. For the

histomorphometric analysis only the pores at the margins were compared and the central blank areas observed in sections of Cell-TCP and Empty-TCP were not considered (Supplementary Figure 1).

The number and size of blood vessels (total volume of vascular tissue) was significantly greater for subcutaneous CGIPS and Cell-TCP when compared to subcutaneous empty-TCP (Figure 4C, panel i). In case of intramuscular implants no difference was observed in the vascular invasion of CGIPS and empty-TCP (Figure 4C, panel ii).

Histomorphometric quantification of mineralization

Alizarin red S staining demonstrated no calcification inside the pores (within the soft tissue) for subcutaneously implanted Empty-TCP (Figure 5A, panel i), Cell-TCP (Figure 5A, panel iv) and intramuscular Empty-TCP (Figure 5A, panel v). Calcification within the pores was observed in case of subcutaneously implanted CGIPS (Figure 5A, panel ii), Gel-TCP (Figure 5A, panel iii) and intramuscular CGIPS (Figure 5A, panel vi).

von Kossa staining demonstrated calcium deposits within the tissue inside the pores of CGIPS implanted subcutaneously (Figure 5B, Panel ii) as well as intramuscularly (Figure 5B, Panel vi). Very few, small calcium deposits were seen within the soft tissue of subcutaneously implanted Empty-TCP (Figure 5B, panel i), Gel-TCP (Figure 5B, Panel iii), Cell-TCP (Figure 5B, panel iv) and intramuscular Empty-TCP (Figure 5B, panel v).

Calcium deposition in the soft tissue was significantly higher for subcutaneous CGIPS as compared to the other subcutaneous implants (Figure 5C, panel i). Intramuscular CGIPS had significantly higher calcium deposition (t test, $p < 0.05$) than Empty-TCP implanted intramuscularly (Figure 5C, panel ii).

X-ray quantification of density

Grafts were dissected and X-ray images obtained (Figure 6A). The X-ray density of subcutaneous CGIPS and Gel-TCP was significantly higher than Cell-TCP and Empty-TCP but not significantly different from each other (Figure 6B, panel i). X-ray density of intramuscular CGIPS was significantly higher than intramuscular Empty-TCP (Figure 6B, Panel ii).

Figures and Legends

Figure 1: Surgical implantation of bone graft substitutes. Figure 1A. The β -TCP was cut into cuboidal pieces measuring 4mm X 4mm X 2mm. **Figure 1B.** A half inch incision overlying the spine of the scapula was used to implant the study samples subcutaneously or intramuscularly. **Figure 1C.** One month after implantation, the subcutaneously implanted study samples had maintained their positions. CGIPS was implanted in a left lateral position, Gel-TCP in left medial, Empty-TCP in right medial and Cell-TCP in right lateral position. **Figure 1D.** The intramuscularly implanted bone graft substitutes were retained in the infrascapular intramuscular pockets in which they were placed at the time of the surgery. Muscle can be seen in close apposition with the implants which had to be dissected out from the muscular tissue. **Figure 1E.** After dissection of the scapulae with attached musculature and overlying tissue, X-ray films were obtained. X-ray pictures demonstrate the intramuscular implants lying above the scapulae in the infrascapular regions. The subcutaneous implants can be seen on either side of the intramuscular implant on the right and the left.

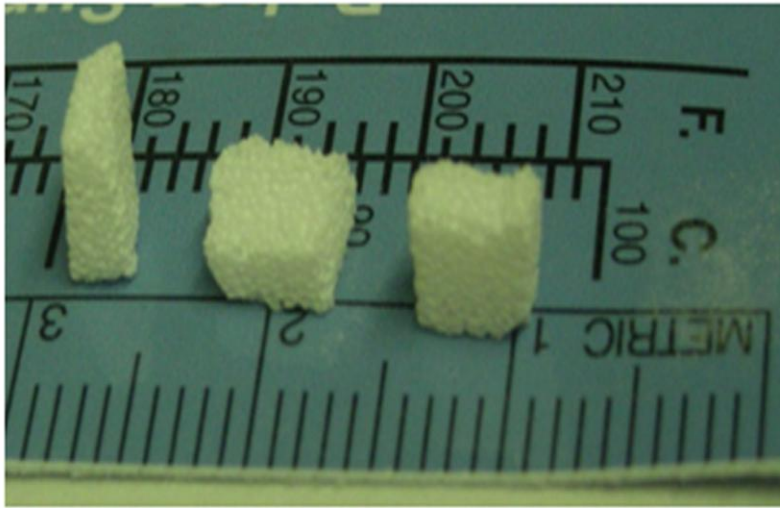


Figure 1A



Figure 1B

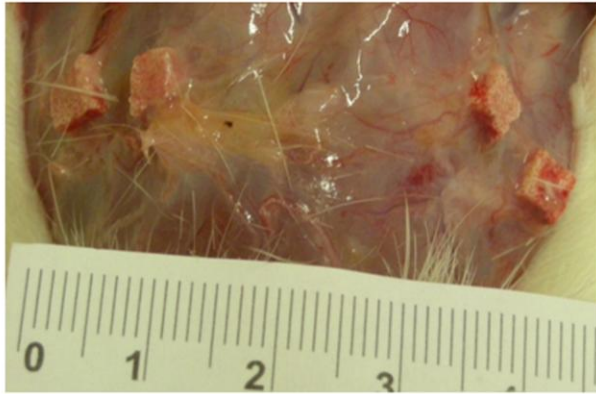


Figure 1C



Figure 1D

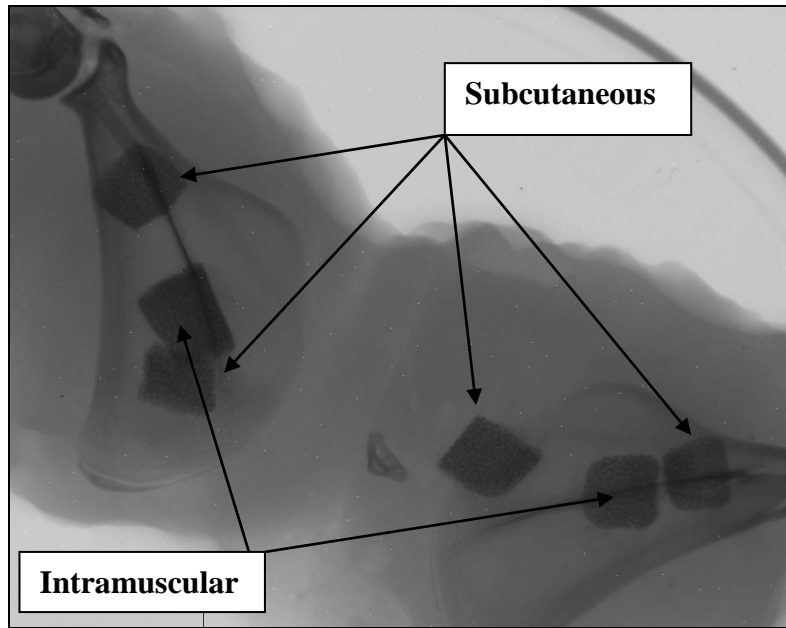


Figure 1E

Figure 2. Expression of osteopontin in various study samples. All scale bars are 500 microns.

Figure 2A. Cells invaded and populated the pores of Empty-TCP implanted subcutaneously seen by DAPI staining (Panel i). Human cells were not present in the pores (Panel ii). Very poor expression of osteopontin is observed in the pores (Panel iii). **Figure 2B.** A greater number of cells were observed at a higher density within the pores of subcutaneously implanted CGIPS (Panel i). Human cells (GFP expressing TMSC) survive and are seen within the pores (Panel ii). Osteopontin expression is observed along the pore walls in a distribution corresponding to the human TMSC distribution (Panel iii). The osteopontin expression in CGIPS is stronger than that in Empty-TCP. **Figure 2C.** Cells had penetrated into the pores of subcutaneously implanted Gel-TCP (Panel i). Green fluorescence indicative of human cells was absent (Panel ii). Osteopontin expression was observed along the pore walls in spite of absence of transplanted cells. (Panel iii). **Figure 2D.** Fewer cells were observed in the pores of subcutaneously implanted

Cell-TCP (Panel i) when compared to Gel-TCP. Although the scaffold had been seeded with green TMSC no fluorescence was observed implying absence of transplanted cells in the grafts (Panel ii). Very poor osteopontin expression was observed in Cell-TCP implants (Panel iii). **Figure 2E.** Cell invasion into the pores of Empty-TCP implanted intramuscularly was observed (Panel i). No human cells (Panel ii) and a very faint osteopontin expression (Panel iii) are observed. **Figure 2F.** A much greater number of cells are seen within the pores of intramuscularly implanted CGIPS (Panel i) as compared to intramuscular Empty-TCP. Human TMSC (green fluorescence) are seen lining the pore walls (Panel ii). Osteopontin expression is observed in a similar distribution viz. diffusely in the pores but stronger along the pore walls (Panel iii), as distribution of the human cells.

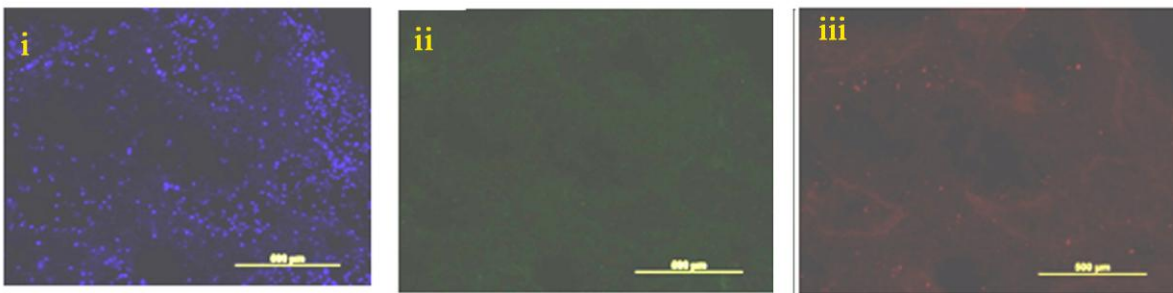


Figure 2A

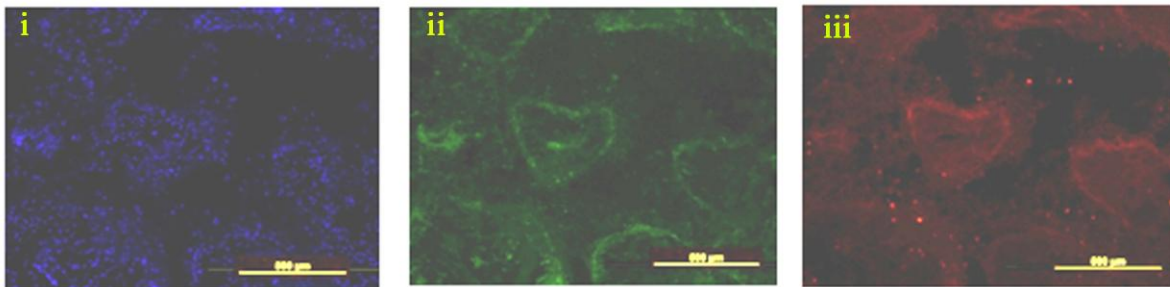


Figure 2B

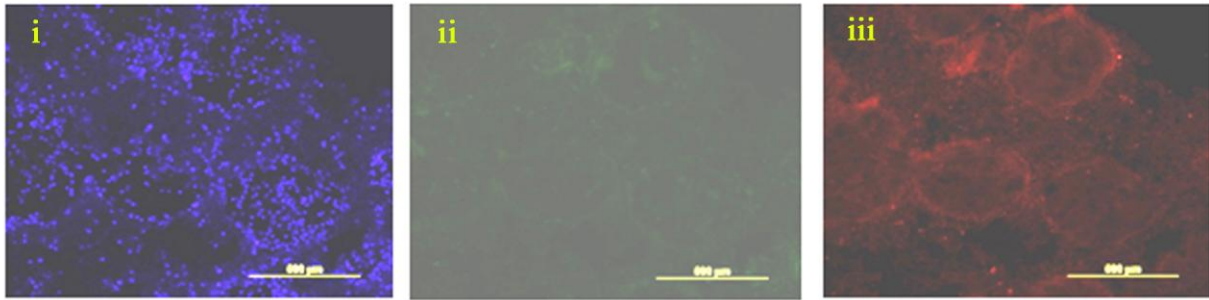


Figure 2C

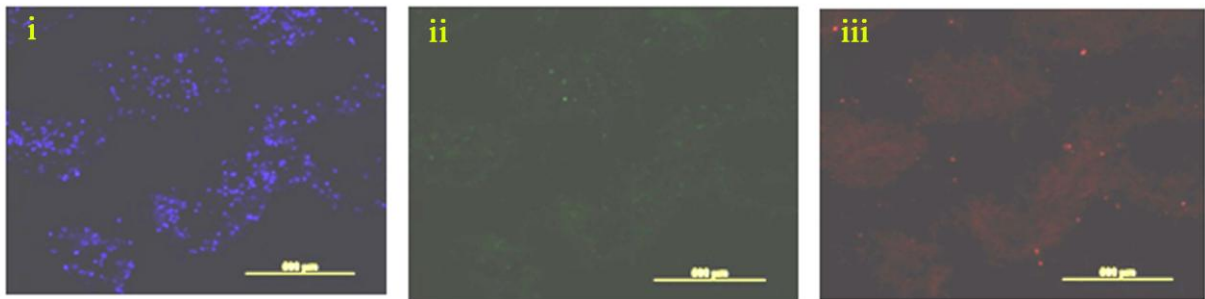


Figure 2D

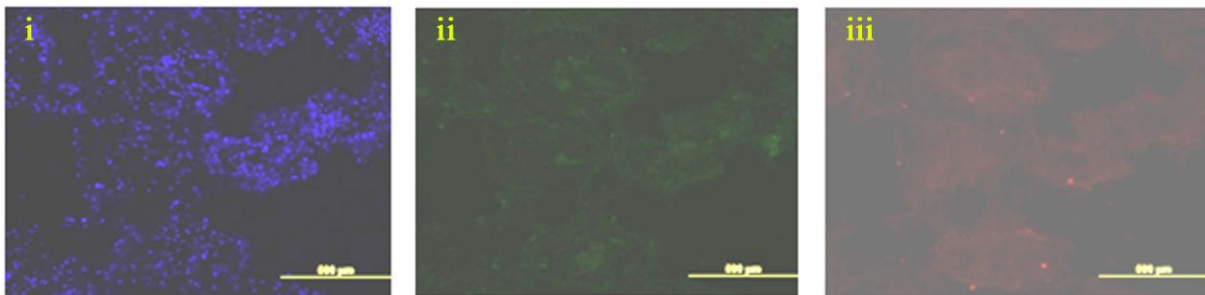


Figure 2E

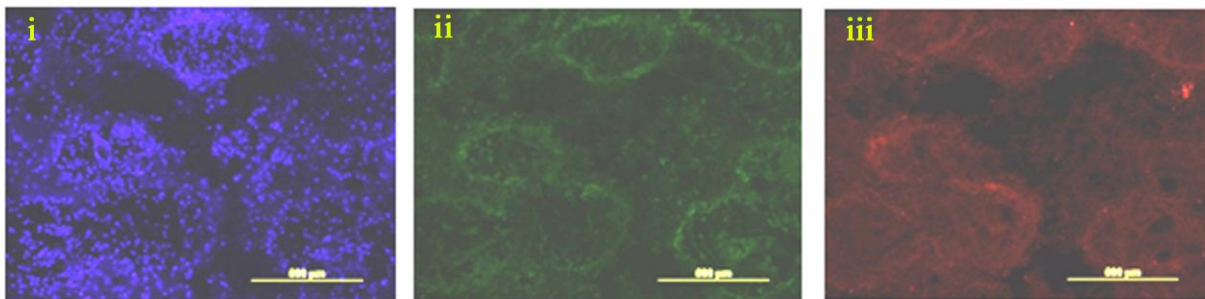


Figure 2F

Figure 3. Expression of osterix. (All scale bars 500 microns). **Figure 3A.** Osterix expression is not observed in subcutaneously implanted Empty-TCP (Panel i) and intramuscularly implanted Empty-TCP (Panel ii) but is observed in Gel-TCP (Panel iii) even in the absence of transplanted MSC. **Figure 3B.** Subcutaneously implanted (Panel i) and intramuscularly implanted (Panel iii) CGIPS demonstrate diffuse expression of osterix, which is stronger along the pore walls. Osterix expression is very poor in case of subcutaneously implanted Cell-TCP (Panel ii).

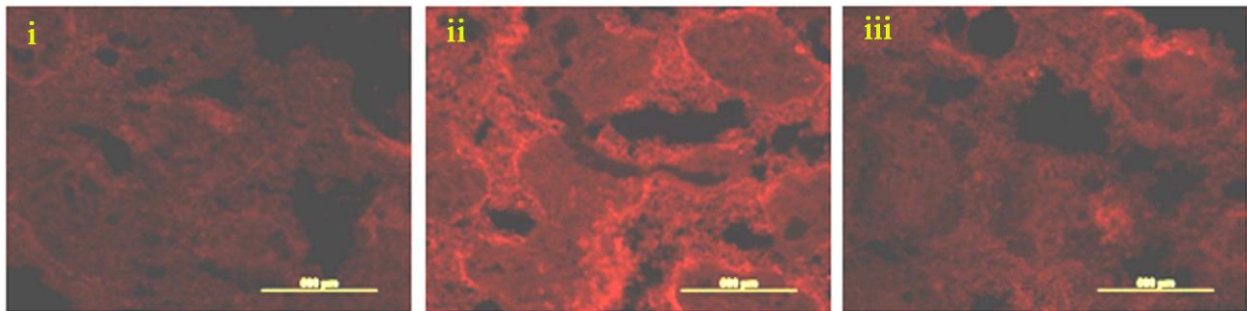


Figure 3A

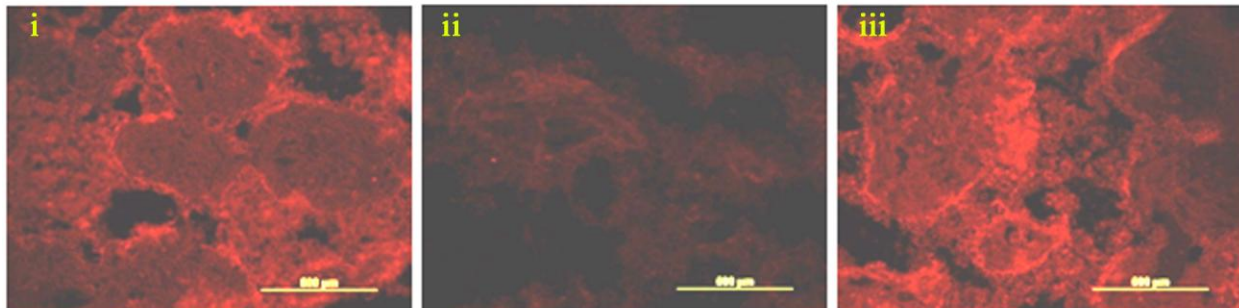


Figure 3B

Figure 4. Tissue penetration into porous scaffold. **Figure 4A.** Tissue can be seen penetrating into the pores of all the study groups: Subcutaneous Empty-TCP (Panel i), subcutaneous CGIPS (Panel ii), subcutaneous Gel-TCP (Panel iii), subcutaneous Cell-TCP (Panel iv), intramuscular Empty-TCP (Panel v) and intramuscular CGIPS (Panel vi). Blood vessels with erythrocytes inside the lumen are marked by yellow arrows. All scales bars are 200 microns. **Figure 4B.** No

statistical difference was observed with respect to amount of tissue invasion in any of the subcutaneously implanted study groups (Panel i) (Mean and SEM graphed, $n=3$, $p>0.05$). Significantly more tissue penetrated CGIPS when compared to Empty-TCP in case of intramuscular implants (Panel ii). (Mean and SEM graphed, $n=3$, $p<0.05$). **Figure 4C.** Vascular invasion was significantly greater in CGIPS and Cell-TCP when compared to Empty-TCP (Panel i) (Mean and SEM graphed, $n=3$, $p<0.05$). A significant difference was not observed for intramuscular implants (Panel ii). (Mean and SEM graphed, $n=3$, $p>0.05$).

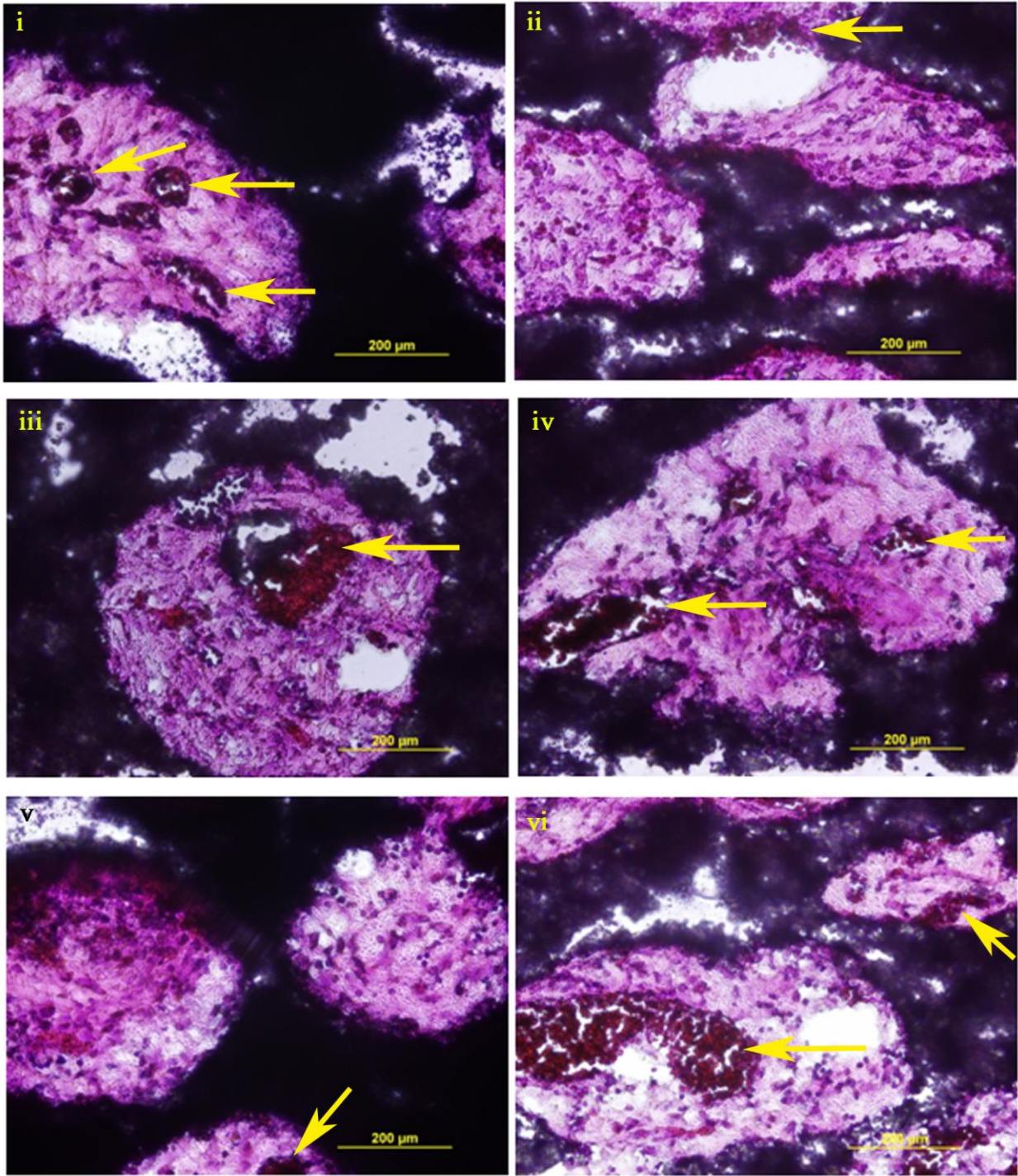


Figure 4A

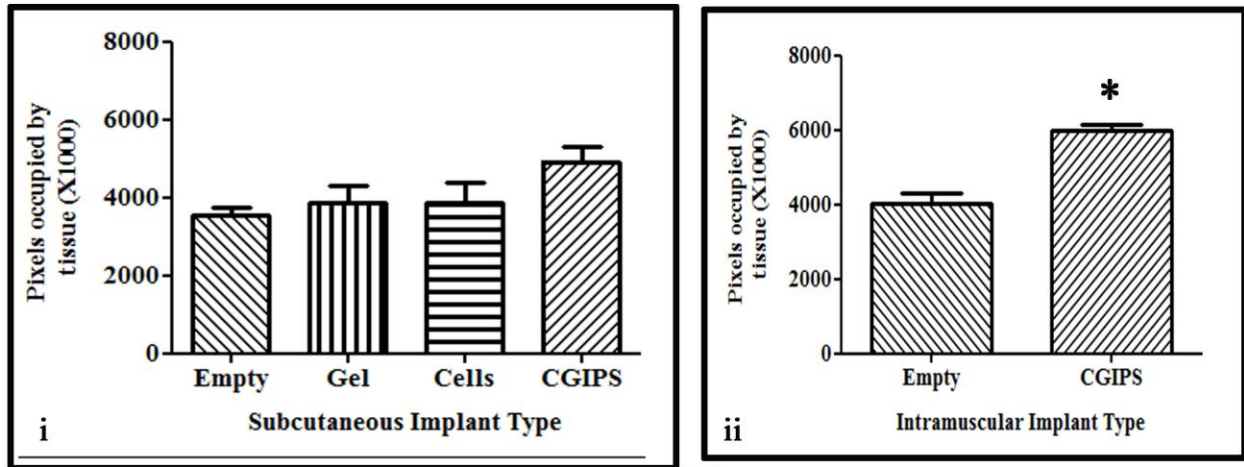


Figure 4B

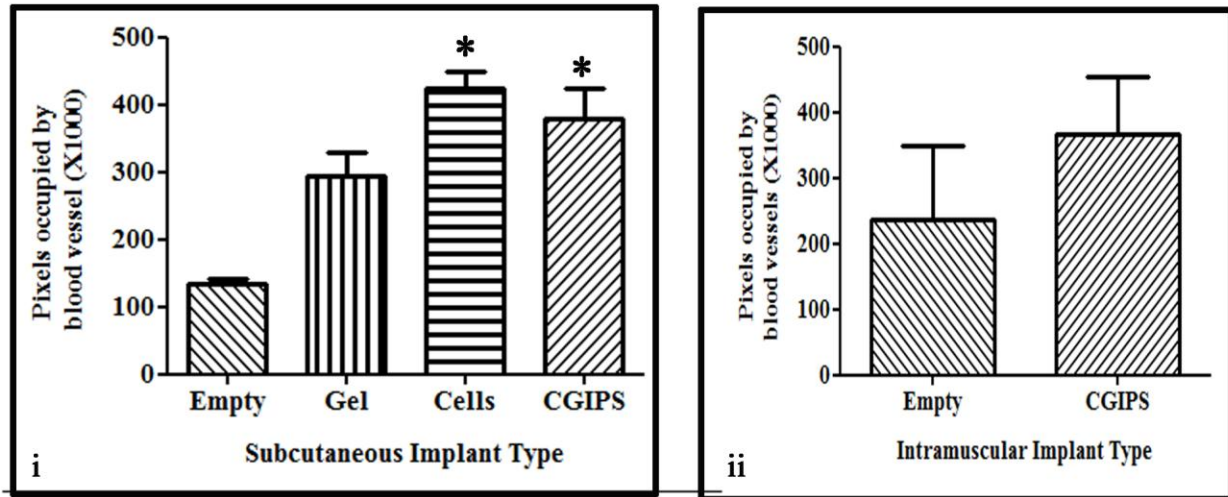


Figure 4C

Figure 5. Mineralization of scaffolds. Figure 5A. Alizarin Red S stained biological calcium deposits red and was used to demonstrate mineralization of the tissue within the pores. In case of subcutaneous Empty-TCP (Panel i), subcutaneous Cell-TCP (Panel iv) and intramuscular Empty-TCP (Panel v) red staining of the β -TCP scaffold is observed but the tissue within the pores is not stained red, indicating absence of mineralization of the invading tissue. On the other hand the tissue lining the pore walls is stained deep red in case of subcutaneous CGIPS (Panel

ii), subcutaneous Gel-TCP (Panel iii) and intramuscular CGIPS (Panel vi) indicating mineralization of the invading tissue. (All scale bars are 500 microns.). **Figure 5B.** VonKossa stained calcium deposits black. The deposits found inside the pores were considered as indicators of tissue mineralization. The origin of deposits seen near the pore walls is not certain (may be either due to extra-cellular matrix mineralization by cells or degradation of β -TCP with deposition of calcium phosphate). Calcium deposits within the soft tissue are proposed to be due to matrix mineralization by cells (solid black arrows in CGIPS implanted subcutaneously (Panel ii) and intramuscularly (Panel vi)). Very few and small foci of calcification were observed in subcutaneous Empty-TCP (Panel i), Gel-TCP (Panel iii), Cell-TCP (Panel iv) and intramuscular Empty-TCP (Panel v). **Figure 5C.** Calcium deposits within the pores were histomorphometrically measured as an indicator of active matrix mineralization by cells. Amongst subcutaneously implanted study samples, CGIPS had significantly greater matrix mineralization (Panel i). CGIPS implanted intramuscularly had significantly greater mineralization than Empty-TCP (Panel ii). (Mean and SEM graphed, $n=3$).

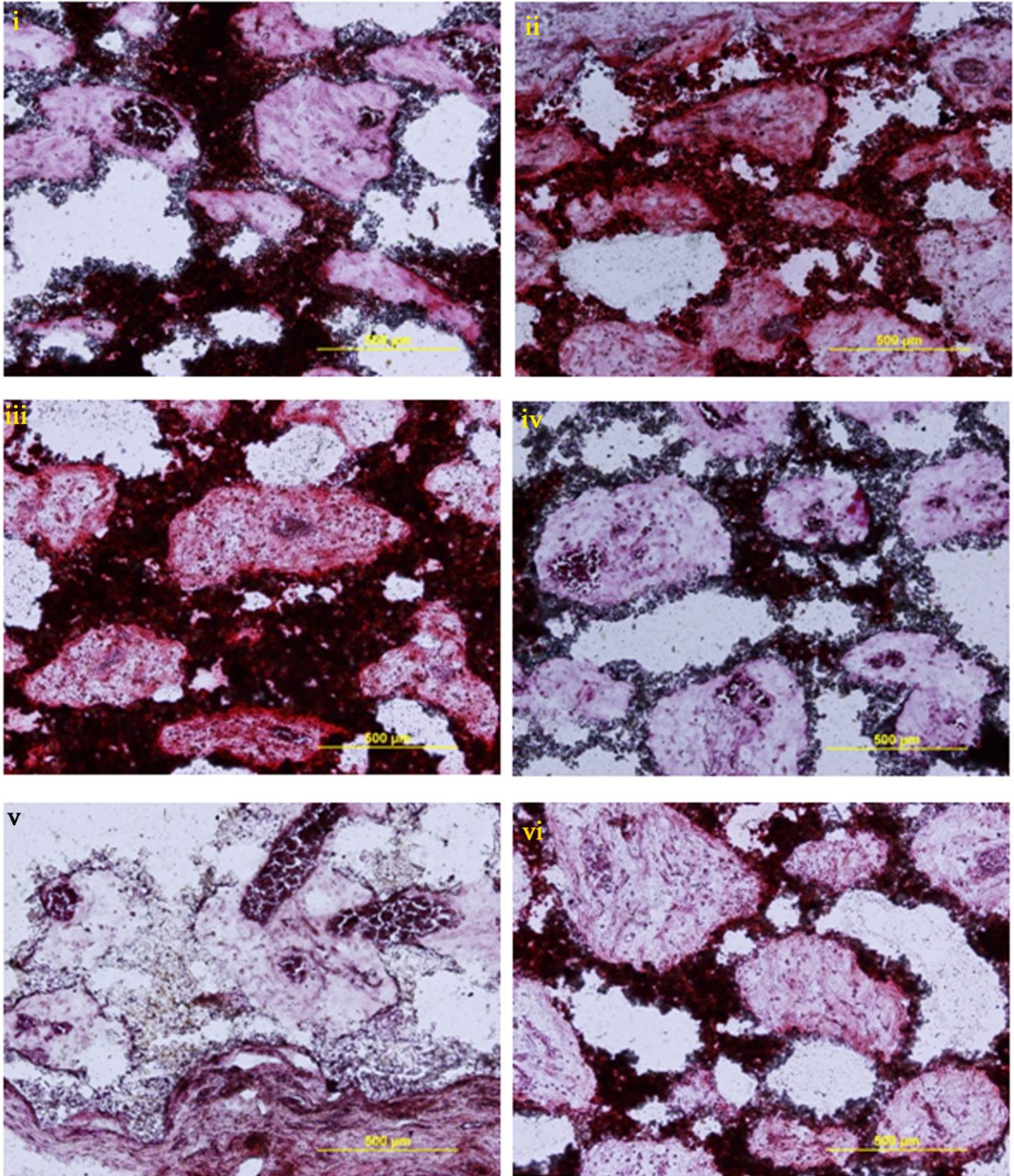


Figure 5A

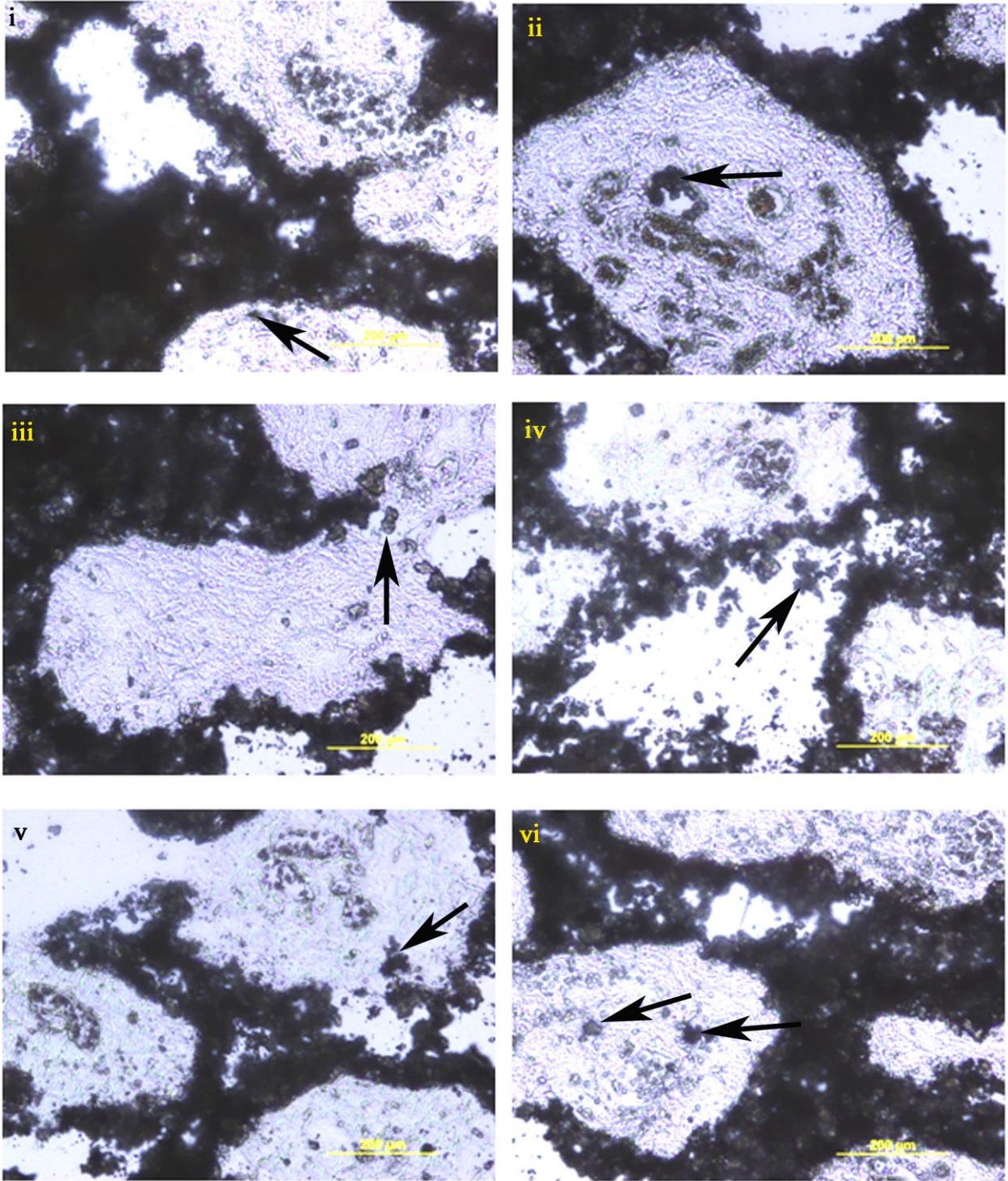


Figure 5B

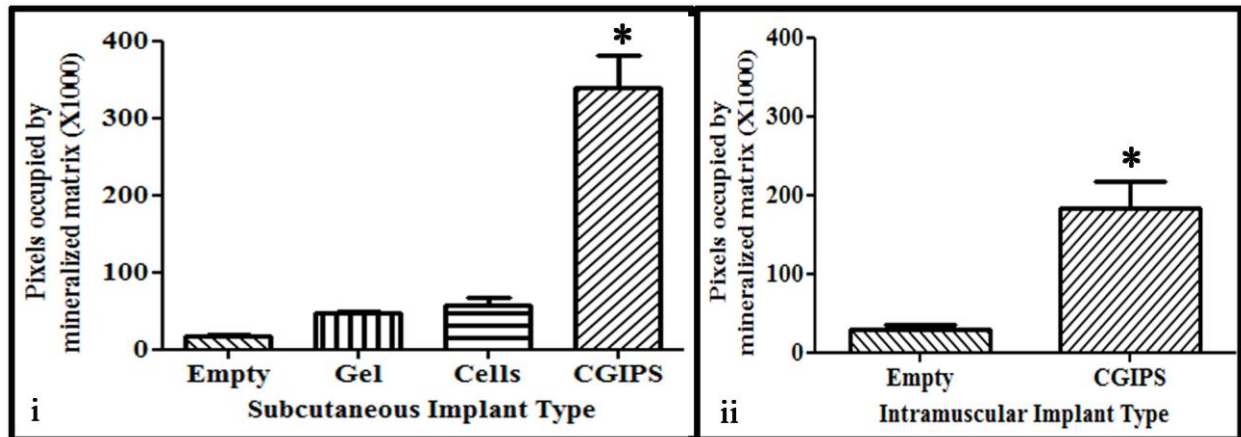


Figure 5C

Figure 6. X-ray densitometry of implants. Figure 6A. Implants were dissected out from the surrounding tissue and placed in a petri dish. X-ray images were captured. Denser calcium deposits appear darker on the X-ray. The CGIPS and Gel-TCP appear darker than the other implants. **Figure 6B.** Densitometric analysis with imageJ revealed that subcutaneously implanted CGIPS and Gel-TCP had significantly higher density than Cell-TCP and Empty-TCP (Panel i). Intramuscular CGIPS had significantly higher density than intramuscular Empty-TCP (Panel ii). (Mean and SEM graphed, $n=7$)

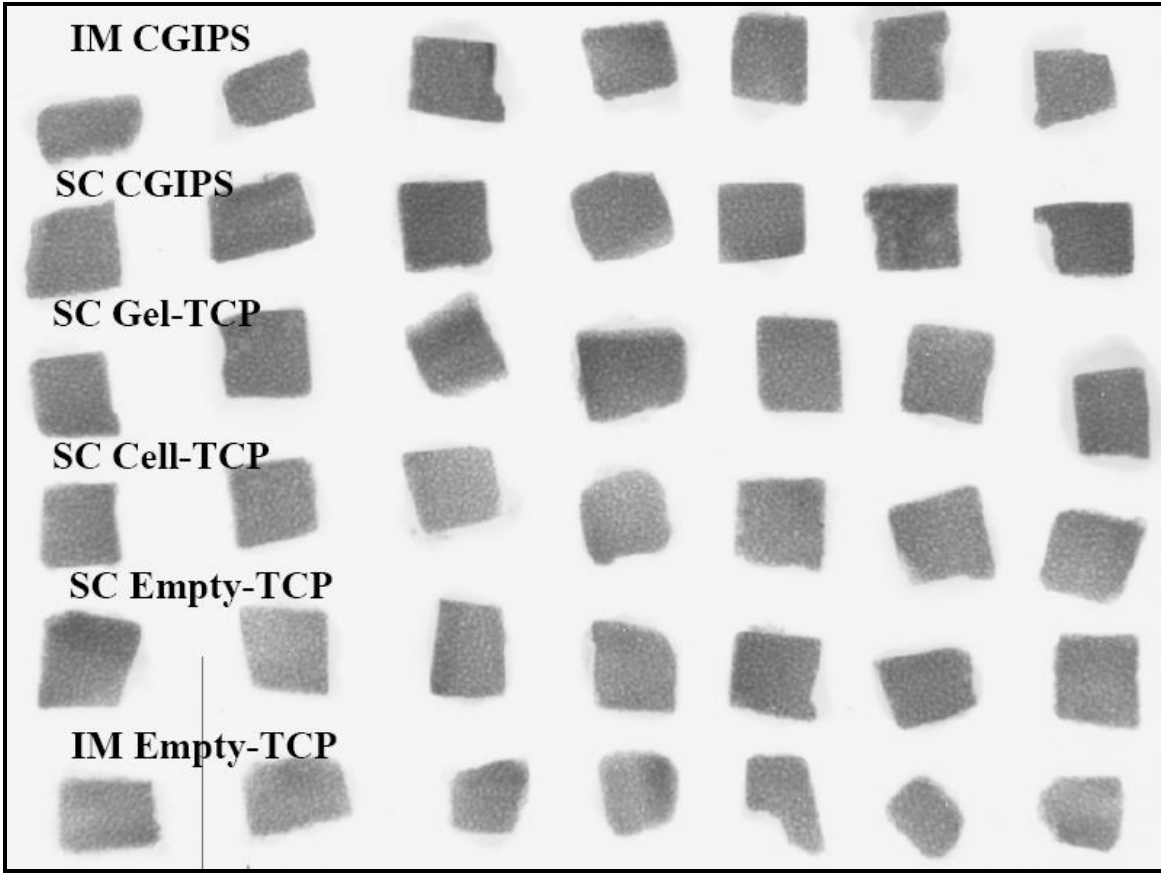


Figure 6A

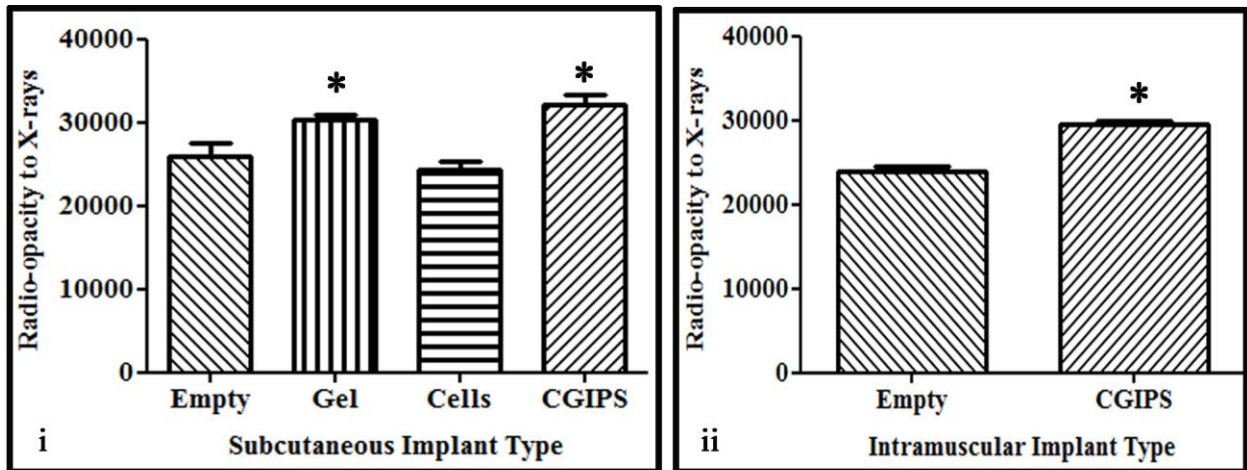
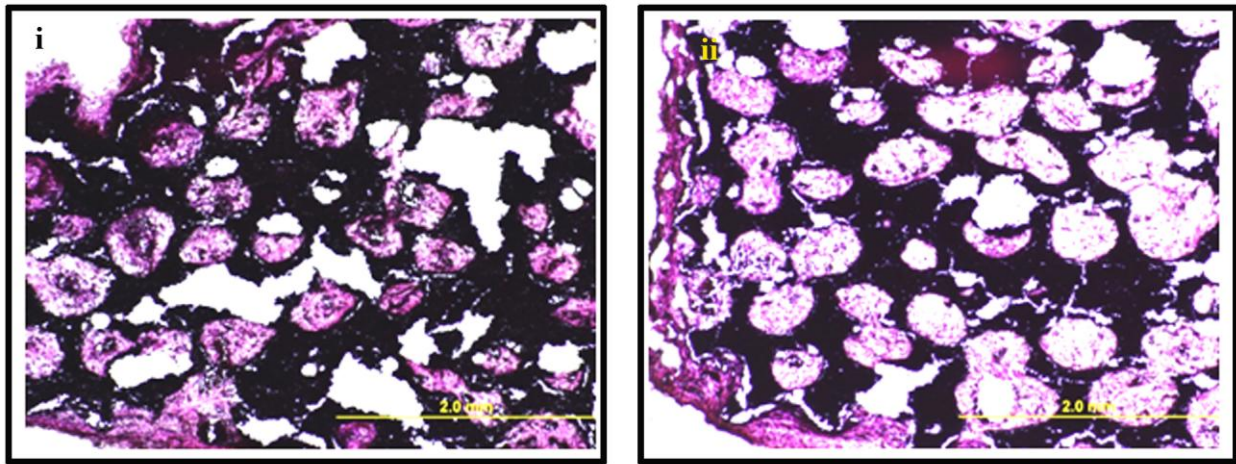


Figure 6B

Supplementary figure 1. Low magnification view of intramuscular implants. H&E stained sections observed at low magnification reveal that a greater part of the scaffold was lost during sectioning in case of Empty-TCP (Panel i) as compared to CGIPS (Panel ii) which held together well during sectioning. Most of the central part of Empty-TCP and Cell-TCP was lost during sectioning which may indicate absence of tissue invasion into the deeper parts. These blank areas were not taken into consideration while performing histomorphometric analysis for figure 4.



Supplementary Figure 1

Discussion

Beta tricalcium phosphate (β -TCP) is a dehydrated version of hydroxyapatite (HA) that is degraded within six to nine months of implantation (1). The high local concentration of calcium and phosphate ions released during degradation/ remodelling of β -TCP stimulates not only crystalline growth of calcium phosphate nuclei and active cellular mineralization of ECM by osteoblasts (69) but also stimulates osteoclast activity which in turn stimulates osteoblast activity, most likely through ephrin-eph signaling (70). This local mineralization process can enhance the bone-graft apposition and interface integrity and

strength. Although HA implants bonded directly with the host bone upon implantation in sheep tibia (7) and some degree of surface resorption is observed, remodelling does not occur with HA implants (52) which leads to micromotion and instability. The relatively rapid β -TCP resorption leads to high local calcium and phosphate concentration stimulating stronger bonding with native bone decreasing micromotion and forming a strong graft-tissue interface. β -TCP has been shown to integrate earlier with host bone than hydroxyapatite (114). Mesenchymal stem cells cultured on β -TCP demonstrated osteoblastic morphology, deposited collagen and mineralized collagen but not on hydroxyapatite.

Osteoinductivity is the property of a tissue engineered bone graft substitute to stimulate bone healing above that which would have been seen by the use of the scaffold alone (1). One of the strategies to make a bone graft substitute osteoinductive is to harness the proliferative and multi-lineage differentiation potential of MSC (2), (38). The two principal strategies are to either deliver cells to the site of injury within the scaffolding material or recruit host MSC to the implantation site of the scaffold.

Injections of rat bone marrow healed segmental bone defects in rats and the healing took place faster with a stronger bridge when more marrow was used demonstrating the utility of MSC (25). No difference was observed between rabbit MSC and rabbit osteoblasts cultured in a porous scaffold *in vitro* (18) or when implanted in critical sized bone defects in rabbits with respect to bone forming capacity (26). Thus MSC can be used directly without having to be predifferentiated *in vitro* prior to implantation.

Long term *in vitro* culture causes hMSC to lose proliferative potential (23), (35). This can be overcome by ectopic expression of telomerase, which improves *in vitro* proliferation and *in vivo* bone forming potential of hMSC and is switched off with differentiation (23).

Telomerase transfected human mesenchymal stem cells (TMSC) and primary hMSC underwent similar changes in gene expression when exposed to a differentiation inducing stimuli (unpublished data from our lab and (35). Thus TMSC are a good mimic of hMSC to study bone graft substitute function.

Ceramics alone can not heal long bone defects as adequate number of osteogenic cells are not available for the wound healing process (28). Use of calcium phosphate ceramic scaffolds with bone marrow healed long bone defect in dogs earlier than marrow alone (28), (29) and a combination of marrow and β -TCP formed bone in mice subcutaneous tissue whereas β -TCP alone failed (30). β -TCP with rat MSC had greater osteoclastin content, alkaline phosphatase activity, blood vessel invasion and bone formation than empty β -TCP after implantation in rats for eight weeks (31). HA with β -TCP and human MSC (hMSC) bound strongly to mouse bone while HA with β -TCP but without hMSC was encapsulated with fibrous tissue without bone formation (32). HA with β -TCP and hMSC formed more bone as compared to HA alone or HA with β -TCP but without hMSC when implanted into nude mice (33). Radiographic assessment of HA with β -TCP and hMSC showed a better antrum sinus healing in human patients as demonstrated by rapid host tissue invasion of the implant and integration with host tissue (34). All the studies discussed above confirm the improvement in osteogenic performance when hMSC are used as a component of bone graft substitutes.

hMSC survive after implantation into rat intervertebral discs whereas hematopoietic stem cells did not (36). MSC lack MHC-2 and lymphocyte costimulatory antigens rendering them immunoprivileged (37). Although MHC-1 is present MSC are not recognized by immune system and allogenic transplantation of MSC does not cause rejection. MSC also reduced the rejection of simultaneously transplanted other cell types like hematopoietic stem

cells, hence are considered immunomodulatory. Xenogenic transplantation of 20 million hMSC into sheep bone did not cause fever, weight loss, rise in inflammatory markers, leukocytosis or expression of acute phase reactants in the animals. Viable cells were detected even six weeks after the transplantation. hMSC could form bone when transplanted into not only immunodeficient mice (38) but also immunocompetent mice (32). These data form the basis of our use of human TMSC in immunocompetent rats.

Green fluorescent protein expressing human TMSC implanted within the scaffolds in rat subcutaneous tissue and intramuscularly survived for a period of one month as shown by the green fluorescence seen in frozen sections (Figure 2, Panel ii). These transplanted cells differentiated into osteogenic precursors as shown by the expression of osteogenic differentiation markers (osteopontin) which co-localized with the green fluorescence (Figure 2, Panels ii and iii).

The presence of TMSC in β -TCP (Cell-TCP) did not improve the host tissue invasion when compared to Empty-TCP (Figure 4B) but improved the ingrowth of vascular tissue into the implant (Figure 4C). Both Empty-TCP and Cell-TCP collapsed during sectioning (data not shown) perhaps due to inadequate invasion of tissue into the interior of the implant, but this could not be statistically verified. The increase in vascular invasion observed in case of cellular implants (Cell-TCP and CGIPS) over acellular ones (Empty-TCP and CGIPS) when implanted subcutaneously may be due to release of angiogenic factors from the implanted hMSC. Vasculogenesis precedes fracture repair and is prerequisite for osteogenesis (115), (116), (117). At the site of new bone formation osteoblasts are localized at the sites where endothelial cells have formed new blood vessels. (84). Presence of hMSC alone did not improve the mineralization of tissue by the cells (Figure 5C) or total calcification assessed by X-ray density

(Figure 6B) above that of Empty-TCP. Thus in our experiments subcutaneous and intramuscular xenogenic transplants of human cells, without collagen gel, into rats improved angiogenesis but did not affect osteogenesis.

The collagen type I network that forms the bone ECM provides attachment sites for bone cell integrin receptors, transmits mechanical signals to the cells, regulates growth factor and nutrient diffusion and is responsible for the physical characteristics of bone (38). Three dimensional morphology and collagen type I ECM are prerequisites for mineralization (14). Cells in a monolayer form a multilayered nodule, deposit collagen and then mineralize the matrix. Collagen can bind different integrins and circulating growth factors adsorbed on implanted material and act as a bridge between host cells and implant (118). CollagraftTM and HealosTM are collagen based bone graft substitutes approved by FDA (82). Collagen gel was superior to either alginate gel (43), (81), pluronic gel, agarose gel (43), matrigel, laminin gel, (45), fibrin gel (80), (81) RGD coating (118) with respect to bone formation when studied in various animal models of bone repair. In dog spinal fusion studies, collagen gel improved the interface bonding between fusion mass and native tissue (21) but bone volume and strength did not improve beyond that of an autograft. The collagen used in this study was very weak and was allowed to gel in situ. Liquid collagen can be diluted by tissue fluid before gelling and may have led to poorer results as it would not have been retained at original implantation site.

To overcome the problems posed by viscoelastic nature of collagen which causes it to liquify when exposed to mechanical stress crosslinked collagen is commonly used in collagen based devices and bioengineered products. However crosslinked collagen triggered inflammatory response and pathologic calcification when implanted subcutaneously in rats (47). This would confound the results of any study involving osteogenic capacity of a bone graft

substitute. Furthermore bone formation within gels depends on ability of MSC to remodel collagen gel (111). Crosslinking collagen causes masking of the hydrolytic sites used by matrix metalloproteinase and bone tissue will not form in gel. Our patented technique results in the formation of native collagen gels that do not trigger inflammation, are mechanically strong, easy to handle and translucent (64). hMSC cultured on β -TCP *in vitro* lose proliferative potential, osteogenic differentiation capacity and *in vivo* bone forming ability when compared to hMSC cultured on collagen (6). Thus we propose that a combination of ceramic with collagen will prove better than either alone.

When collagen type I gel impregnated β -TCP (Gel-TCP) was compared to Cell-TCP a greater cell density was present in the pores (Figure 2C and 2D). This finding is consistent with our *in vitro* observations that collagen gel facilitates migration of cells into porous scaffolds (manuscript in preparation). Cells that invaded Gel-TCP adopted an osteogenic lineage as evidenced by expression of osteogenic differentiation markers (osterix) (Figure 3A, Panel ii). This supports the published data supporting the osteoinductive nature of native collagen type I and β -TCP. In our experiments the presence of collagen gel did not improve mineralization of the matrix by the invading cells (Fig 5C) but the total calcium density of the implant was higher than Cell-TCP (Figure 6B). This may have been due to the re-deposition of calcium and phosphate ions derived from the β -TCP scaffold onto the collagen fibrils near the edge of the pores.

Collagen gel with porcine MSC formed bone after subcutaneous implantation in Polycapronolactone with β -TCP scaffold in nude mice (80), (81). Rabbit adipose stem cells suspended in collagen gel impregnated within porous Polylactateglycolate with β -TCP scaffold induced more bone formation and higher incidence of non-union healing when compared to

cellular scaffolds without collagen gel (82).

After implantation into rabbits, collagen gel alone triggered an inflammatory response (50), (51) but a combination of collagen gel with rabbit MSC did not and led to mineralization within the pores of PLGA-TCP composite scaffold into which the rabbit MSC-collagen gel was loaded (51). In human trial of CollagraftTM small percentage of patients developed antibodies to collagen but these did not react with human collagen or cause any adverse immunologic reaction (52). Even in those allergic to collagen, the use of collagen based bone marrow implants may not cause adverse clinical reactions (53).

Osteoblasts from the marrow enter the circulation and localize to the fracture site (83). Locally available (bone marrow derived) and circulating MSC/osteoblasts are vital for normal bone growth, remodeling and repair. Thus recruitment of MSC and osteoblasts to the site of injury is a critical event of the wound healing process and the invading vasculature provides a route for the recruitment of circulating MSC and osteoblasts (85), (86). Collagen with HA and canine MSC had greater healing rates for canine radius bone defect than HA with canine MSC without collagen gel (28). But collagen gel impregnated within HA with and without canine MSC performed at similar level. Multinucleated giant cells did not accumulate within the implant indicating absence of foreign body immune reaction. This data would suggest that transplanted MSC did not improve graft performance above the improvement observed in the presence of gel. Muschler also observed that transplanted MSC in collagen gel did not contribute to bone formation as much as the locally recruited MSC (2). Recruitment of local MSC into the collagen gel was important for bone formation. On the other hand in Weinand's study when porcine MSC suspended in collagen gel impregnated within β -TCP was implanted in nude mice, samples with cells had higher density and stiffness than those without cells (81). The new bone

was formed by the transplanted cells.

A greater cell density was observed in the pores of CGIPS as compared to Empty-TCP and cell-TCP (Figure 2) confirming the data from our *in vitro* experiments in which collagen gel facilitated cell migration. The expression of differentiation markers was more prominent in case of CGIPS as compared to Empty-TCP both in subcutaneous tissue implants (Figure 2A and 2B) and in intramuscular tissue implants (Figure 2E and 2F). Thus collagen gel and TMSC combination improved the survival of xenogenically transplanted cells (higher green fluorescence in CGIPS than in Cell-TCP, Figure 2B and 2D). The transplanted cells seemed to preferentially localize at the pore-gel interface and differentiate osteogenically as evidenced by expression of osteopontin, an ECM protein considered to be a marker of osteogenic differentiation (Figure 2, Panel iii) which colocalized with the transplanted cells (Figure 2, Panel ii). A higher expression of osterix was observed in CGIPS as compared to Empty-TCP (Figure 3).

CGIPS did not collapse during sectioning and host tissue was seen invading throughout the implant (Supplementary figure 1). This supports the conclusion that tissue invaded rapidly into the porous scaffold when it was impregnated with collagen gel in the pores. As the central core of all the β -TCP implants that did not contain collagen gel (Empty-TCP and Cell-TCP) collapsed during repeated attempts at sectioning we believe that tissue had not invaded into the central portion of the implant, leading to its collapse during sectioning. When we studied the pores at the margin we did not find any difference in tissue invasion between implants with collagen and those without collagen. A greater volume of vascular tissue was found in CGIPS and Cell-TCP as compared to acellular scaffolds (Gel-TCP and Empty-TCP, Figure 4C) indicating release of angiogenic factors by the transplanted cells.

CGIPS had significantly greater mineral deposits within the tissue inside the pores indicating active mineralization of the matrix by the cells within the pores (Figure 5C). This supports Rattners observation that collagen gel and a three dimensional morphology are prerequisites for mineralization (14) and our *in vitro* observation that mineralization occurs only in the presence of native fibrillar collagen (manuscript in preparation). The total calcium density of the CGIPS implants was significantly higher than acellular implants (Empty-TCP and Cell-TCP) (Figure 6B). This measurement takes into account the mineralization of the matrix by the cells as well as deposition of calcium phosphate on the collagen fibrils near the pore walls.

Bone can remodel according to the forces acting on it for optimum load bearing functionality (1). The ability of cells to sense mechanical forces and respond to the physical stimulus is known as mechanotransduction. The potential of using a bone graft in which cells can respond to the applied force would allow the bone to heal and adopt a structure that would be optimum for the physical function expected from it after healing of the site of injury. Although in the present study the placement of implants was not load bearing, future large animal studies will be able to study this aspect of bone physiology.

The first step towards clinical translation is biocompatibility, feasibility, non-toxicity and proof of principle testing in small animals (2). For bone the testing is most often performed in rats. Unfortunately rodent autografts contain a mixture of bone marrow and bone chips so can not be used as clinically relevant controls. Also rodent MSC are different from large animal MSC with respect to bone formation. Final testing of a bone graft substitute should be carried out in a large defect with relatively hypoxic environment eg a segmental bone defect in large animal. The defect has to be larger than 1 cm which is not feasible in rodent long bones. Technique of implantation and cell retrieval should closely mimic the clinical technique which is

possible only in large animals. The efficacy of the bone graft substitute has to be compared to autograft.

Thus enhanced mineralization near the pore walls and greater vascular tissue invasion would lead to a bone graft substitute that would rapidly integrate with the host tissue. A high graft tissue interface strength would result due to rapid invasion of surrounding tissue and mineralization at the surface of β -TCP, bonding it firmly with the native bone. Thus the results presented here indicate that CGIPS has the potential to form a mechanosensitive, completely resorbable, mechanically strong and osteoinductive bone graft substitute and merits further testing in large animal bone defect models.

CHAPTER VI

COLLAGEN IMPREGNATED POROUS SCAFFOLDS CAN SERVE AS DRUG DELIVERY DEVICES

Introduction

Bone repair is a complex process directed and modulated by the interplay between cells, extra-cellular matrix and cytokines (9). In pathological situations involving considerable bone loss such as compound fractures, treatment of bone tumors, osteoradionecrosis, joint replacement, congenital defect repair or spinal fusion surgeries, the bone defects can not heal unassisted. Autologous bone grafts have been considered as the gold standard of therapeutic intervention but harvesting the bone graft material can cause pain, infection and bleeding at the donor site (21). Allografts are less desirable due to possible transmission of infectious agents and inconsistent quality. A variety of tissue substitutes are being engineered around the world to address this need for bone graft substitutes.

Some of the factors that require careful consideration when engineering a bone graft substitute are biocompatibility, low toxicity/antigenicity, maintenance of cell functions pertinent to tissue regeneration, attachment/migration, vascularisation and ultimately complete degradation and replacement of implanted material with native tissue (9). It has been shown that collagen gel improved healing of rat cranial critical sized defects (45). A large number of collagen based devices have been approved for human use by FDA (21) and collagen gels have

been extensively used as matrices in tissue engineering (99). Crosslinking of collagen and other denaturing modifications lead to poor biocompatibility (47) and absorption and retention of growth factors (119).

For implantation in a mechanically active environment like bone, the graft must also have certain mechanical properties (9). As a stand alone graft material collagen gel is not strong enough and has to be reinforced by a suitable strategy (120). We impregnated various porous scaffolds with collagen gel to combine the mechanical strength of the scaffold with the cytocompatibility of collagen. Using collagen type I foam we showed that the presence of collagen type I gel is required for rapid mineralization *in vitro* (manuscript in revision). Another candidate for tissue engineering of bone grafts that we are exploring is a porous tri-calcium phosphate scaffold with pore size ranging from 100 to 500 microns, porosity 80% which is completely biodegradable *in vivo* in 6 months (ChronOS™ from Synthes – information provided by manufacturer). Hence we have used a native stable form of collagen hydrogel (64) and impregnated it into the porous ChronOS™ scaffolds to form collagen gel impregnated porous scaffolds (CGIPS).

Although the osteoconduction aspect of bone formation can be supported by a well designed scaffold – matrix combination, more optimal results depend on the presence of cells and signaling molecules (cytokines) to achieve osteoinductive status and speedy bone regeneration (9). A myriad of growth factors have been used in attempts to accelerate bone healing eg. BMP, TGF, FGF, PDGF, VEGF and IGF. Thus addition of BMPs to autologous bone graft improved the bone formation in spinal fusion in dogs (21). This and other similar studies support the role of biocompatible matrices which can serve as carriers of growth factors as well as being substrates for cell attachment/migration and vascular invasion (87). At the site of injury,

bone resorption (osteoclastic activity) is followed by influx of osteoblasts that generates new bone (70). It has been proposed that osteoblasts are recruited to the site of injury and their function stimulated by matrix immobilized growth factors which are released during bone resorption process (70). VEGF-A (88), BMP-2 (89), PDGF (90) have been proposed as mitogens and chemoattractants for MSC. However the interaction (coupling) between osteoblast and osteoclasts is pivotal for osteoblast recruitment. EphrinB2, which plays a role in bidirectional signaling between osteoclasts (bone resorbing multinucleated cells derived from mononuclear macrophages) and osteoblasts (bone depositing cells derived from mesenchymal stem cells) has been proposed as an important mediator of this coupling (96). We used EphrinB2 for this study as an adjuvant for CGIPS and studied the effect of ephrinB2 on stem cell migration and proliferation as this could improve the osteoinductivity of CGIPS when used as bone graft substitute.

Another serious complication which has an impact on repair of significant bone loss is infections (97). The infecting organism may be endogenous existing infection or may be introduced into the wound during injury and/or surgery. Intravenous antibiotic therapy is a requirement for long term management of foci of bone infection like open fractures or osteomyelitis. Serum levels have to be continuously monitored for cytotoxic levels of antibiotics but compromised blood supply at the site of injury leads to suboptimal delivery of antibiotics at site of infection. Local application of vancomycin has been shown to provide very high local concentrations at the wound site without exceeding safe systemic levels. FDA has approved clinical use of antibiotic containing bone cements at sites of infection after eradication of prior infection (98) It has been shown that powdered antibiotics mixed with bone cement can be released from bone cement after implantation. We studied the release of vancomycin from

CGIPS to test its potential for use as a drug delivery vehicle as well as a bone graft substitutes that can be used at a site of infection.

Materials and Methods

Collagen Type I Gel

Cold (4°C) porcine collagen type I-A solution (Cellmatrix[®], Nitta Gelatin, Wako Chemicals, Richmond, VA, USA, 3mg/ml) (8 parts v/v) was mixed thoroughly with cold (4°C) solution of molecule of interest (10 times the desired final concentration, dissolved in phosphate buffered saline {0.256g/L NaH₂PO₄ H₂O, 1.19g/L Na₂HPO₄, 8.76g/L NaCl, pH 7.4, in distilled water} {PBS}) (1 part, v/v) and then neutralized (pH 7.4) with cold (4°C) reconstitution buffer (sodium hydroxide 0.5N, sodium bicarbonate 22g / l, HEPES free acid 47.7 g / l) (1 part v/v) with thorough mixing. Careful mixing after each addition was required to prevent air bubble formation in the viscous solution. All solutions (maintained at 4°C) and mixing steps were conducted at 4°C and the neutralized collagen solution (CS) stayed liquid at 4°C. When incubated at 37°C in 5% CO₂ the collagen solution gelled within 30 min. All experiments were performed using the gelled collagen prepared as described above.

Beta-Tricalcium Phosphate Scaffolds

Porous scaffolds of β -Tricalcium phosphate (chronOSTM) were a kind gift from Synthes (Monument, CO, USA). The pore size of these scaffolds ranges from 100 to 500 microns, with a porosity of 60 to 80% (Manufacturer provided information).

Cells

Telomerase transfected human mesenchymal stem cells (TMSC) were a kind gift from Dr. Dario Campana, St. Jude Children's Research Hospital, Memphis, TN, USA (35). TMSC were cultured in MEM α (GIBCO, Invitrogen, Carlsbad, CA) containing FBS (10%, Atlanta Biologicals, Lawrenceville, GA) with medium changes every second day. TMSC were passaged at 80-90% confluence using trypsin (0.05%) with 0.53 mM Ethylene diamine tetra acetic acid (EDTA) in Hank's Balanced Salt Solution (HBSS) (GIBCO, Invitrogen, Carlsbad, CA) and plating at 3000 cells/cm². Cells were counted using hemocytometer and Trypan blue (Sigma-Aldrich, St. Louis, MO) dye exclusion viability stain.

Ephrin B2-Fc

The region encoding the extracellular domain of ephrin-B2 was amplified by PCR from a brain cDNA library and cloned into pFUSE-hIgGe3-Fc1 (InVivogen) in frame with the coding region for human Fc-gamma. The resulting construct was stably transfected into CHO-K1 cells (ATCC). Ephrin-B2 ectodomain/Fc recombinant protein was isolated from serum-free CHO cell-conditioned medium with protein A sepharose and stored in PBS.

Staphylococcus aureus

Green fluorescent protein expressing methicillin resistant *Staphylococcus aureus* (MRSA) strain RN6930 were a kind gift from Dr. Ambrose Cheung (Dept of Microbiology, Dartmouth Medical School, Hanover, NJ, USA). The bacteria were cultured in brain heart infusion broth (BHI, Hardy Diagnostics, Santa Maria, CA, USA) and streaked on mannitol salt agar culture plates (MSA, Hardy Diagnostics, Santa Maria, CA, USA). A colony was picked, cultured in BHI and this single bacterium progeny used for all the experiments.

Impregnation of the β -TCP Scaffold

The β -TCP scaffolds - chronOS™ cubes were cut into cubical pieces (5 X 5 X 5mm) and immersed in sterile PBS for 24 hours. The PBS was removed by blotting on sterile filter paper and each piece was moved to the wells of a 24-well tissue culture plate. CS (containing molecule being studied) was impregnated into the scaffold by dropping a known quantity of CS on the scaffold. The CS loaded β -TCP cubes were incubated at 37°C overnight to allow the CS to gel and will hereafter be referred to as Collagen Gel Impregnated Porous Scaffold (CGIPS).

Release of Bovine Serum Albumin

Bovine Serum Albumin (BSA Fraction V, Omnipur®, EMD Chemicals Inc., Gibbstown, NJ, USA) was dissolved in PBS at a concentration of 10 mg/ml. After addition to CS mix as described above the resultant concentration of BSA was 1 mg/ml. 500 μ l CS was dispensed in each well of a 12-well plate and allowed to gel overnight. PBS (1 ml, pH 7.4) was pipetted into each well containing collagen gel. The PBS solution was removed at predetermined time points (marked on the corresponding graphs) to provide quantitative release data for BSA from collagen gel under static conditions.

To study the release of BSA from collagen gel under dynamic conditions 1 ml of PBS was added into each well of 12-well plate containing 500 μ l collagen gel. At the predetermined time points indicated all the PBS was removed from the well, collected in 1 ml tubes and replaced with fresh PBS (1 ml). Both the release studies (static and dynamic) were carried out in triplicate (n=3) and at 37°C. Release of BSA from CGIPS (5 CGIPS placed in

each well of 12-well plate, each CGIPS containing 100 μ l collagen gel within the pores) was studied under dynamic conditions only.

Fluorometric determination of BSA

The samples of BSA release study were analyzed fluorometrically using intrinsic protein fluorescence of BSA using EclipseTM Spectrofluorimeter (Varian Inc., Victoria, Australia). Samples were excited at 280 nm and emission was scanned from 290 to 450 nm. BSA calibration curve was constructed using peak fluorescence intensity for different BSA concentrations and was fitted using linear equation ($R^2 = 0.996$). BSA free PBS was used as a background control and the BSA released from collagen gel or CGIPS was derived from calibration curve equation. Results of static and dynamic release study were plotted as percent cumulative release as a function of time. Data from dynamic study was plotted as amount of BSA released as a function of time.

Kinetics of BSA release

To determine the release mechanism from collagen gel, data obtained from *in vitro* drug release studies under static conditions was plotted as a component of different kinetic models namely, zero order representing cumulative amount of drug released vs time and first order as log cumulative percentage of drug remaining vs time. Higuchi's model for cumulative percentage of drug released vs square root of time and Hixson-Crowell cube root model to analyze if there is any effect of surface area and diameter of collagen gel on drug release were also tested. Plotted data was fitted using linear equations. Regression coefficient (r^2) and release constant (K) were calculated from appropriate graphs. Table below indicates the model and corresponding equations used to fit the data.

Model	Equation
Zero Order	$Q_t = Q_0 + K_0 t$
First Order	$\ln Q_t = \ln Q_0 + K_1 t$
Higuchi	$Q_t = K_H \sqrt{t}$
Hixson-Crowell	$Q_0^{1/3} - Q_t^{1/3} = K_{HC} t$

Q_t = Amount released at time t, Q_0 = Amount loaded in collagen gel, K = release constants

Release of EphrinB2 clusters from collagen gel

Ephrin B2 at a stock concentration of 1.98 mg/ml and clustering antibody (Fc) at a stock concentration of 2.4 mg/ml were used to combine 102 μ l of ephrin (200 μ g) with 20 μ l antibody (48 μ g) giving a mix ratio of approximately 4:1. The resulting mixture was further diluted with PBS to 500 μ l to provide a working concentration of 400 μ g/ml. This working solution of ephrinB2 was clustered by overnight incubation at 4^oC. Collagen solution was prepared as described previously was mixed with clustered EphrinB2 and contained ephrinB2 clusters at a concentration of 40 μ g/ml.

200 μ l of neutralized collagen solution (8 mg EphrinB2 total) was pipetted into each well of a 48-well plate. When incubated at 37^oC under 5% CO₂ the solution gelled within 30 min. After two hours of incubation 100 μ l of PBS was pipetted into each well.

For static release study the PBS was in contact with the collagen gels and was collected at predetermined time points (designated on the graph) and stored at -20°C. For the dynamic release study the PBS was removed from the gel at the time of collection and stored at -20°C. 100 µl of PBS was pipetted into the well from which the PBS was removed.

Western Blot analysis of Ephrin release

The collected PBS fractions were analyzed for EphrinB2 clusters by 12% SDS-PAGE, followed by Western blotting and detection with goat anti-human Fc antibody and HRP-conjugated anti-goat secondary (Jackson Immunolabs). Total ephrin released from the gels was calculated by densitometry of the resulting autoradiographs with ImageJ software (NIH, Bethesda, MD, USA).

Effect of Ephrin on TMSC proliferation

TMSC were seeded at a density of 10K/well of 12-well plate. EphrinB2 cluster in PBS (100 µl) was added to 900 µl medium in the positive control wells. EphrinB2 cluster in CGIPS (100 µl gel in one β-TCP cube) were placed in the experiment wells containing 900 µl medium. The resultant ephrinB2 concentration in the wells was 50, 250 and 500 ng/ml. Medium was changed on day 3 and fresh EphrinB2 cluster in PBS and CGIPS were added. On day 5 cells were fixed and a SRB assay was done.

The cells were fixed in 10% trichloro acetic acid (TCA, ICN Biomedicals, Aurora, OH, USA) for 10 min at 4°C. Cells were washed four times with distilled water and then stained with 0.4% sulforhodamine B (SRB, Sigma Aldrich, St. Louis, MO, USA) dissolved in 1% acetic acid for 10 min. The stained cells were washed with 1% acetic acid 4 times. Plates

were air dried at room temperature overnight. 250 μ l of 10mM Tris base unbuffered was added to each well and the plate was placed on rocker for 10 minutes. 100 μ l aliquots were taken from each well (duplicates) and placed in a 96-well plate. The absorbance at 560 nm was recorded using Tecan Infinite M200.

Effect of Ephrin on chemotaxis

TMSC (200,000) were suspended in 200 μ l collagen solution, placed in the well of a 96 well plate and gelled. CGIPS with 250 ng EphrinB2 per CGIPS (50 μ l collagen gel in one β -TCP) and CGIPS with 250 ng IgG control (50 μ l collagen gel in one β -TCP) were prepared. Two CGIPS from each group were placed at diametrically opposite ends of a well (12-well plate). The gel containing TMSC was removed from the 96-well plate well, placed in the center of the 12-well plate well, 3 ml collagen solution was added to the well and was allowed to gel overnight. MSCGM (2 ml) was added to each well and changed every 48 hours.

After 7 days medium was removed and gels washed with PBS (1 ml per well) and incubated with MTT (3-(4,5-Dimethylthiazol-2-yl)-2,5- diphenyltetrazolium bromide, Sigma-Aldrich, St. Louis, MO, USA) (0.2 mg per ml dissolved in PBS, 500 μ l per well) for two hours at 37°C. The central TMSC gel plug from the 96-well plate with TMSC was removed with a biopsy punch and transferred to a 1.5 ml tube. The rest of the gel was divided into one half containing the CGIPS with ephrin and the other half containing CGIPS with IgG. The CGIPS were removed from the gel and the gels were placed in 1.5 ml tubes and were treated with collagenase P (1ml, for each tube) for one hour at 37°C to release the cells. Collagenase P (Roche, Germany) was reconstituted as directed by supplier to a concentration of 2 mg/ml in Hanks Balanced Salt Solution (HBSS). Tubes were centrifuged to pellet the cells, the supernatant

was discarded, MTT solubilization solution was added (100 μ l per tube) and the tubes rocked for 90 minutes. 100 μ l of dissolved formazan was transferred to wells of a 96-well plate and the plate was scanned at 570 nm using Tecan Infinite M200 (Tecan Systems Inc., San Jose, CA, USA).

Statistical analysis

All the experiment were performed in triplicate. Graphical presentations of the results were generated using GraphPad Prism 4 (GraphPad Software, LaJolla, CA), and the same was software used for statistical analysis.

Determination of Vancomycin Minimum Inhibitory and Bactericidal Concentrations

Collagen solution was prepared with vancomycin at different concentrations (depicted in the graph, ranging from 2.5 to 100 μ g/ml), 100 μ l solution placed in each well of a 96-well plate and allowed to gel. This gel was detached from the well and used in the subsequent experiments. 100 μ l solution of collagen with vancomycin at different concentrations (same as above) was impregnated into each β -TCP scaffold, allowed to gel and the resultant CGIPS with vancomycin used in subsequent experiments.

After overnight incubation at 37°C, 100 μ l bacterial culture mixed with 800 μ l of fresh BHI was placed in each well of 24-well cell culture plate. In one set (n=3) of plates 100 μ l vancomycin in PBS was added, in the second set 100 μ l collagen gel containing vancomycin was added and in the third set vancomycin containing CGIPS were placed. Collagen gel and CGIPS had been prepared (as described above) on the previous day. The concentration of

vancomycin in PBS, collagen gel and CGIPS was adjusted so that the resultant concentration of vancomycin in the wells would be as desired (ranging from 100 to 2.5 $\mu\text{g/ml}$).

After incubation for 18 hours at 37°C, photographs were taken to determine presence of turbidity. The lowest concentration at which turbidity was not observed was recorded as the minimum inhibitory concentration (MIC). 100 μl aliquots were taken from each well (duplicates) and placed in a 96-well plate. The absorbance at 425 nm was recorded using Tecan Infinite M200 (Tecan Systems Inc., San Jose, CA, USA).

10 μl drops from each of the above wells were placed on MSA. After 36 hours of incubation, lowest concentration of antibiotic not showing any colonies was recorded as minimum bactericidal concentration (MBC).

Results

Release Kinetics of BSA

Under dynamic conditions over a 24 hr period BSA followed the same release pattern for collagen type I gel and from CGIPS. BSA release was biphasic, showing initial rapid release phase and a slow sustained phase. It took 24 hours to release about 80 % of the loaded BSA; the initial 60% being released over a 10 hours period with the remaining 20% being released in 14 hours. Release rate was slightly higher in case of collagen gel as compared to GGIPS. Figure 1 shows the BSA release from gel (1A) and from CGIPS (1B). It's evident from

the figure that peak BSA amount released at around 4 hr in both the cases. Results of the drug release kinetics model are shown in table 1.

EphrinB2 clusters release from collagen gel

EphrinB2-Fc clusters were released from collagen gel into PBS over a period of 120 hours (Figure 2A). Western blot analysis detected protein bands of the released clusters at the same molecular weight as control EphrinB2-Fc cluster that had not been incorporated into collagen gel. The release kinetics of ephrinB2-Fc clusters were similar to that of BSA but the peak release was delayed and release occurred for longer period of time (Figure 2B).

Effect of EphrinB2 on mesenchymal stem cell proliferation

EphrinB2 clusters in PBS stimulated telomerase transfected mesenchymal stem cell (TMSC) proliferation at all doses (50, 250 and 500 ng/ml) when added to the culture medium for five days (Figure 3A). When CGIPS containing EphrinB2 clusters were added to the medium proliferation was increased significantly at 250 ng/ml and above but not at 50 ng/ml (Figure 3B).

Effect of EphrinB2 on chemotaxis

After five days TMSC had moved radially outwards from the cell populated central collagen gel plug. Although most cells were still in the gel plug (Figure 4A), a significantly greater number of cells had migrated into the half of the gel containing CGIPS with ephrinB2 than into the half with IgG containing CGIPS (Figure 4B)

Vancomycin release from CGIPS

Turbidity was measured spectrophotometrically and represented graphically. The first significant values to demonstrate significant turbidity (2 way ANOVA) were 5 $\mu\text{g/ml}$ when vancomycin in PBS was added to the BHI culture medium (Figure 5A). Turbidity was observed at 7.5 $\mu\text{g/ml}$ (Figure 5A) and 15 $\mu\text{g/ml}$ (Figure 5A) when vancomycin was added in collagen gel and in CGIPS. Minimum bactericidal concentration for vancomycin in PBS was 15 $\mu\text{g/ml}$ (Figure 5B panel 1), for vancomycin in gel was 20 $\mu\text{g/ml}$ (Figure 5B panel 2) and for vancomycin in CGIPS was 25 $\mu\text{g/ml}$ (Figure 5B panel 3).

Figures and Legends

Figure 1. Release of BSA from collagen gels and CGIPS under dynamic conditions. Figure 1A. Amount of BSA released from collagen gel under dynamic conditions (PBS removed and replaced at indicated time points). The peak release of BSA is observed at four hours with sustained trailing release upto 24 hours. **Figure 1B.** The cumulative amount of BSA released under dynamic conditions expressed as percent of total BSA incorporated in collagen gel is seen to be a smooth curve represented by a one phase exponential equation with y_{max} of 75% and half life of 1.9 hours. **Figure 1C.** Amount of BSA released from CGIPS under dynamic conditions. The peak release of BSA is observed at four hours with sustained trailing release upto 24 hours. This is similar to the graph of BSA release from the collagen gel. **Figure 1D.** The cumulative amount of BSA released under dynamic conditions from CGIPS expressed as percent of total BSA incorporated in CGIPS is seen to be a smooth curve represented by a one phase exponential equation with y_{max} of 63% and half life of 2 hours.

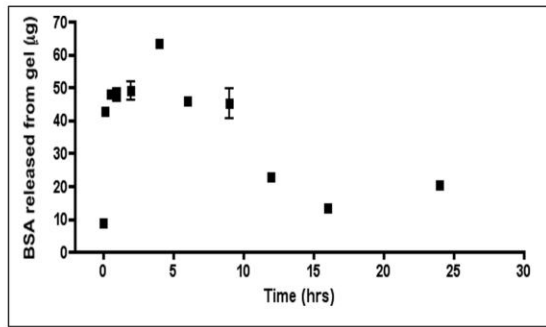


Figure 1A

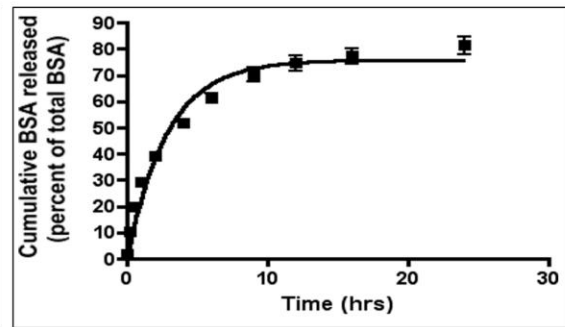


Figure 1B

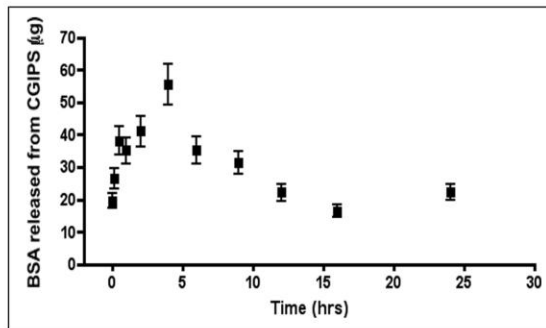


Figure 1C

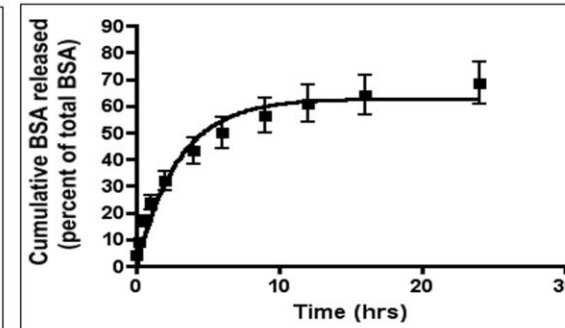


Figure 1D

Figure 2. Release of ephrinB2-Fc clusters from collagen gel. Figure 2A. Western blot on samples of PBS collected from wells containing collagen gels with ephrinB2-Fc clusters. The band of ephrinB2-Fc cluster is in the same position as the control band indicating release without degradation. Densitometric quantification allowed determination of amount of ephrinB2-Fc released from collagen gel by comparing density of band to control band with 5 ng ephrinB2-Fc cluster. **Figure 2B.** Peak ephrinB2-Fc release is observed at 24 hours with a sustained trailing release of ephrinB2-Fc over a period of 124 hours.

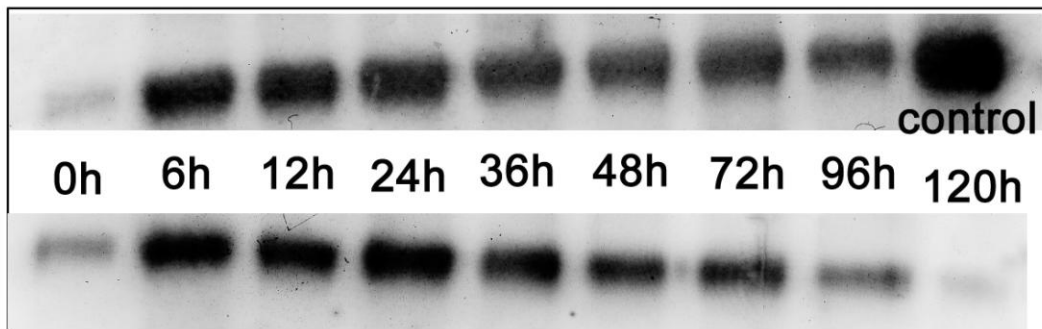


Figure 2A

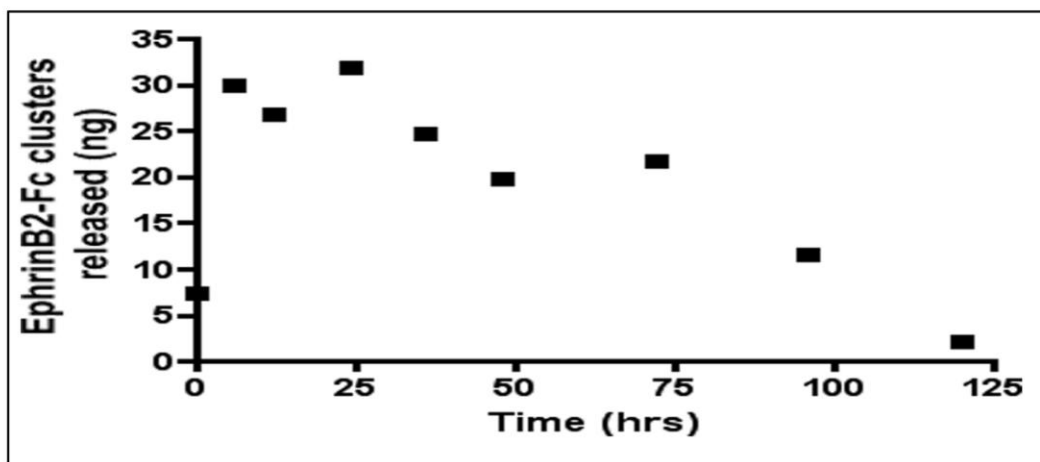


Figure 2B

Figure 3. EphrinB2-Fc stimulates proliferation of telomerase transfected mesenchymal stem cells (TMSC). Figure 3A. EphrinB2-Fc clusters added directly to the cell culture medium increase the cell proliferation significantly at all concentrations above 50 ng/ml. (Mean and SEM graphed, $n=3$, $p<0.05$) **Figure 3B.** CGIPS containing ephrinB2-Fc clusters were placed in the wells. Increased TMSC proliferation was observed in the presence of CGIPS containing ephrinB2-Fc clusters at concentrations above 250 ng/ml. This demonstrated that the ephrinB2-Fc clusters are released in a physiologically active form. (Mean and SEM graphed, $n=3$, $p<0.05$)

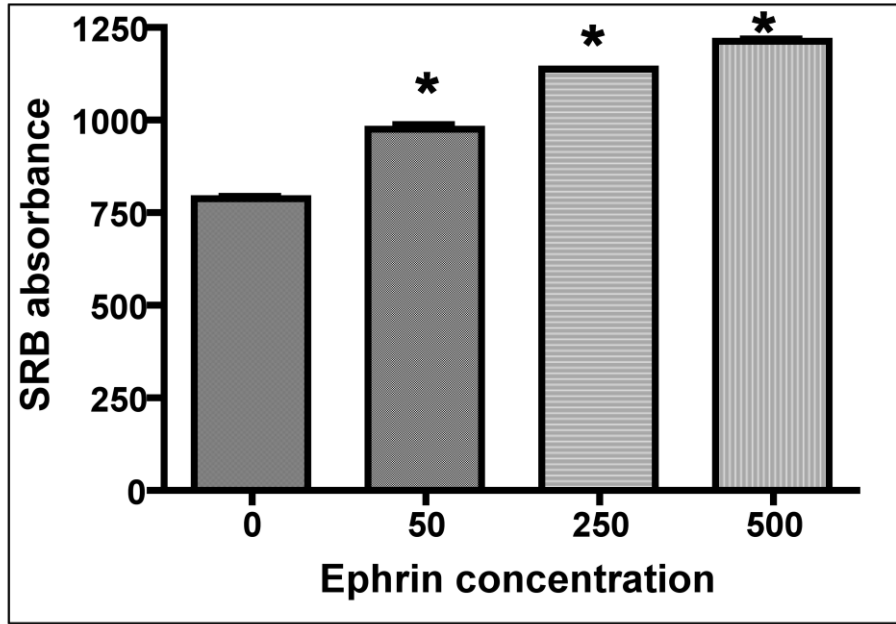


Figure 3A

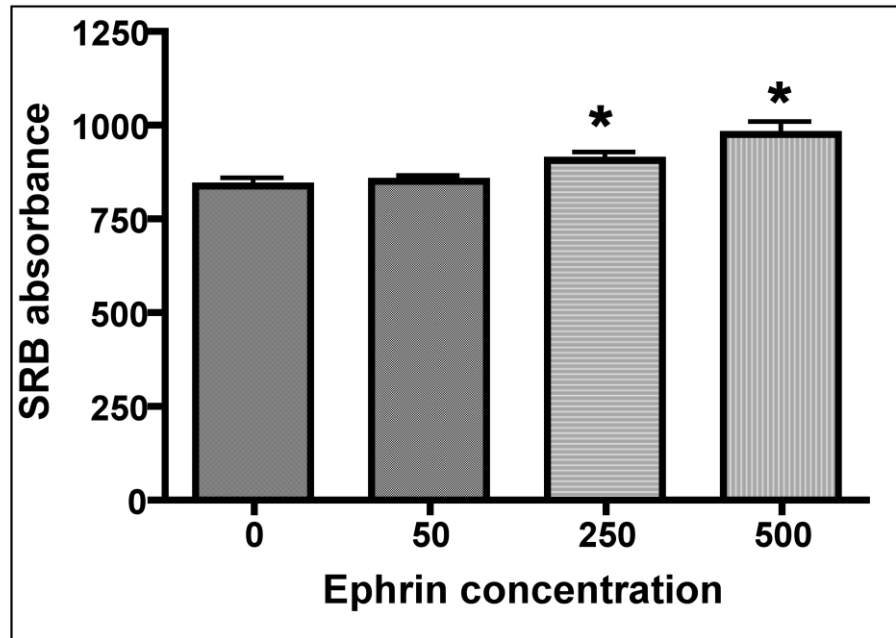


Figure 3B

Figure 4. EphrinB2-Fc stimulated chemotaxis of TMSC towards it. Figure 4A. Experimental layout with plug of collagen gel containing TMSC in the center of the well and CGIPS with

ephrinB2-Fc and CGIPS containing IgG placed at diametrically opposite ends of the well. Well was filled with collagen gel and after 5 days stained with MTT. **Figure 4B.** Removal of central plug was followed by sectioning of the gel in half. Number of cells in each section of the gel can be represented by formazan formation (MTT absorbance). It is shown graphically that significantly greater number of cells had migrated towards ephrinB2-Fc containing CGIPS as compared to CGIPS with IgG. .(Mean and SEM graphed, $n=3$, $p<0.05$)

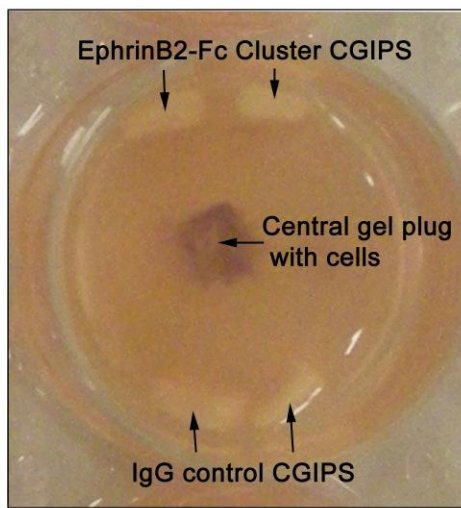


Figure 4A

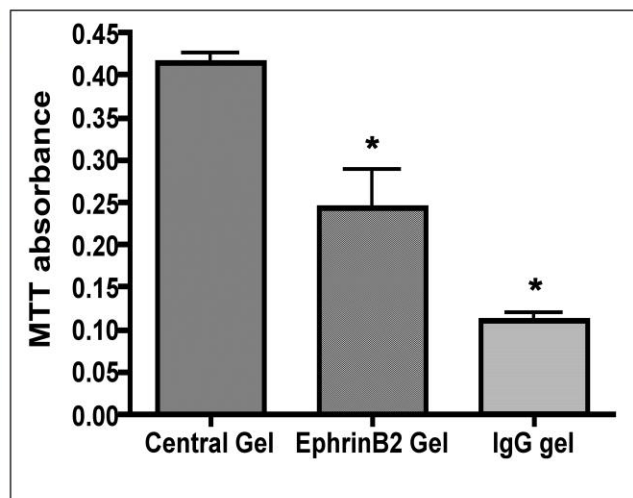


Figure 4B

Figure 5. Release of antibiotic from CGIPS. Figure 5A. Turbidity of bacterial culture medium after 18 hours incubation demonstrated significant turbidity above baseline turbidity occurred at 5 $\mu\text{g/ml}$ when vancomycin was added directly to the culture medium. The corresponding values for vancomycin added to collagen gel set afloat in the medium and vancomycin added to CGIPS placed in the bacterial culture tube were 7.5 and 10 $\mu\text{g/ml}$. These values represent the minimum inhibitory concentration of vancomycin. .(Mean and SEM graphed, $n=3$, $p<0.05$) **Figure 5B.** When aliquots from the bacterial culture tubes were placed on mannitol-salt agar culture plates

growth was observed at concentrations upto 15 $\mu\text{g/ml}$, 15 $\mu\text{g/ml}$ and 25 $\mu\text{g/ml}$ for vancomycin directly added to the culture medium, vancomycin added to collagen gel and vancomycin added to CGIPS. These values represent the minimum bactericidal concentration of vancomycin under these conditions. The numbers in the figures represent the places where the drops from bacterial culture tubes with corresponding antibiotic concentration were placed.

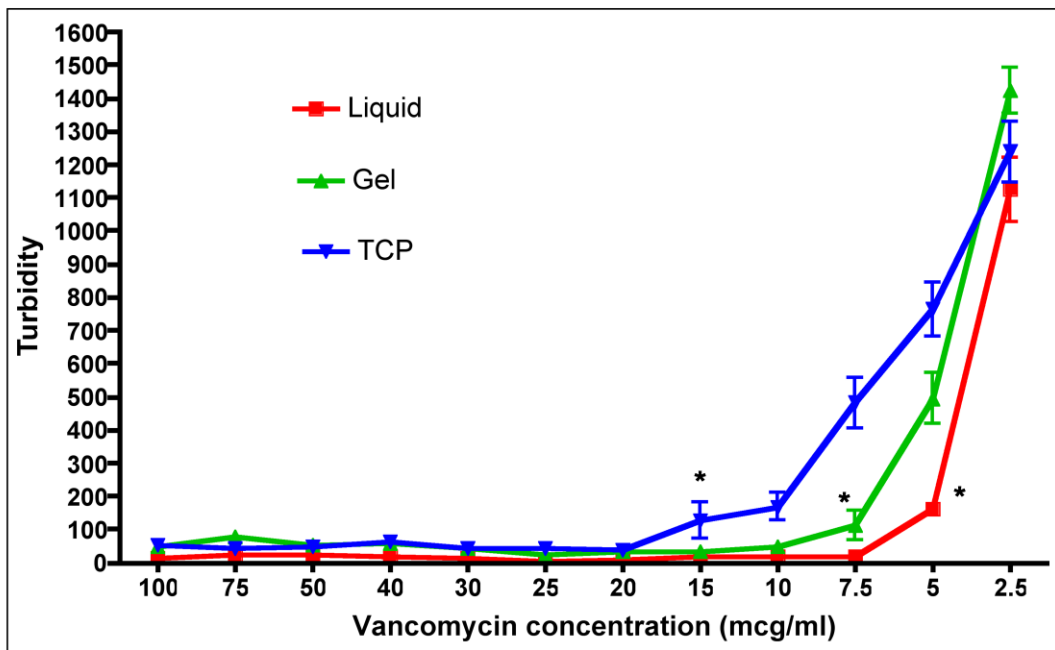


Figure 5A

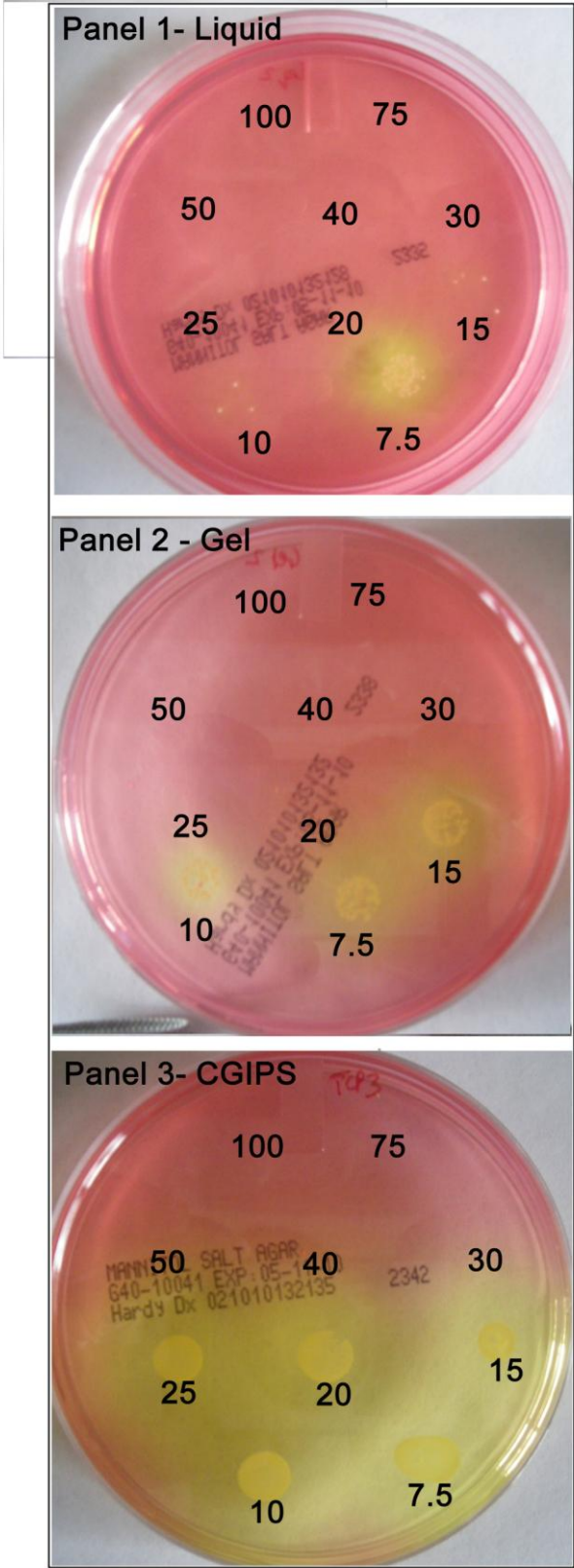
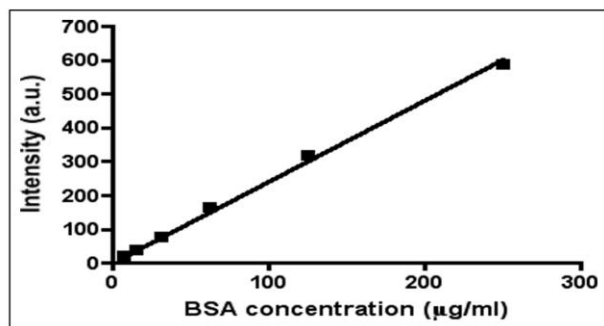
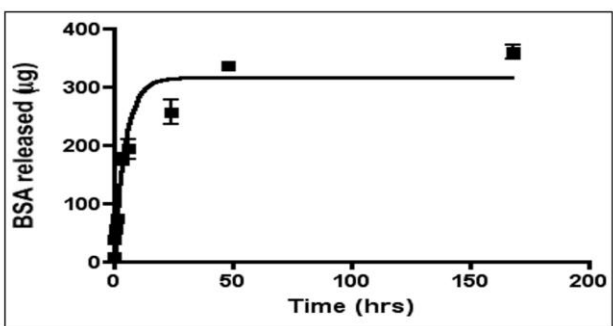


Figure 5B

Supplementary Figure 1A. BSA concentration plotted against intensity of fluorescence emission is a straight line allowing determination of unknown concentrations of BSA from measured fluorescent intensity. **Supplementary figure 1B.** BSA released from collagen gel under static conditions (PBS collected at the experimental time point without replacement with fresh PBS) can be expressed as a smooth curve represented by a one phase exponential equation with y_{\max} of 316 microgram (62% of total BSA incorporated into collagen gel) and half life of 3 hours.



Supp Figure 1A



Supp Figure 1B

Table 1. Comparison of various drug release models. As Higuchi square root model has the highest r^2 value, the drug release is by simple diffusion.

Model	Zero Order Model		First Order Model		Higuchi Square Root Model		Hixson-Crowell Cube-Root Model	
	r^2	$K_0 (h^{-1})$	r^2	$K_I (h^{-1})$	r^2	$K_H (h^{-1/2})$	r^2	$K_{HC} (h^{-1/3})$
Gel	0.7024	3.1271	0.8608	-0.0307	0.9251	17.3419	0.8112	0.0818
CGIPS	0.7356	2.5852	0.8481	-0.0204	0.9424	14.1697	0.8122	0.0590

Discussion

For the purpose of creating any tissue engineered graft the use of a biological matrix which mimics the native tissue ECM would be most suitable for rapid attachment, migration and matrix re-organization by the cells of osteogenic, angiogenic and other lineages (121). The dominant component of bone extracellular matrix is one of the fibrillar collagens-collagen type I (4). Collagen in different forms has been extensively used and is FDA approved for a variety of medical applications including construction of various devices and tissue engineering. Collagen is biocompatible and its already low antigenicity is proposed to be further reduced by enzymatic removal of the telopeptides (121). Recombinant human collagen would be ideal for use but a cost effective production method has not been developed. inFUSE® (collagen sponges with BMP), Collagraft® (mixture of collagen, hydroxyapatite and tricalcium phosphate), Healos® (cross linked collagen fibers coated with hydroxyapatite) are some of the collagen based bone graft substitutes approved by the FDA for clinical use.

Formation of collagen gel when acidic collagen solution was neutralized and warmed to 37°C has been reported (122). Such gels are a product of spontaneous fibrillogenesis with a fibrillar collagen meshwork which makes them visco-elastic in nature (99). Collagen contraction is an undesirable phase of soft tissue wound healing that produces scars. It can pose problems during tissue engineering and multiple strategies have been employed by various groups to minimize the contraction process. Crosslinking collagen is a very common approach but crosslinked collagen is inferior to native collagen with respect to its ability to bind growth factors (119) and is poorly tolerated when compared to native collagen (47). We have developed a dimensionally stable native collagen gel for the purpose of providing 3-D model for engineering various connective tissues (64). We propose that porous scaffolds impregnated with

collagen type I gel would form multiple micro tissue equivalents (one within each pore). This assembly may be used to enhance the cytocompatibility of the scaffolds and make them more amenable to vascularization. In this study we have used porous β -Tricalcium phosphate (β -TCP) as the porous scaffold to contain impregnating collagen gel forming the Collagen Gel Impregnated Porous Scaffold (CGIPS).

The ability to recruit cells to the site of injury is an important requirement for tissue engineered grafts and the accommodation of growth factors is the most commonly used strategy. Since bone homeostasis involves constant bone deposition and resorption an area of research that can provide valuable information about cell recruitment and activity at the site of injury is osteoblast-osteoclast “coupling” (70). When osteoclasts resorb bone, osteoblasts are recruited to start depositing new bone at the time when osteoclasts finish removing the dead or damaged tissue. One of the proposed mechanisms of osteoblast-osteoclast coupling is release of matrix bound growth factors by osteoclasts. A more recent and less well understood mechanism is ephrin-ephrin interaction. Eph receptor stands for Erythropoietin-Producing Hepatocellular Carcinoma receptors, which was the cell type from which Eph receptors were first cloned (94). Eph receptors are members of a family subdivided into classes A (EphA1–EphA9) and B (EphB1 to EphB6, no EphB5). The ligands for Eph receptors are ephrin (Eph Family Receptor Interacting Protein) family of ligands. The ephrinA ligands (ephrinA1–A5) interact with EphA receptors while ephrinB ligands (ephrinB1–B3) interact with EphB receptors. Ephrin-ephrin signaling is bidirectional (70). When cell expressing eph receptor comes in contact with cell expressing ephrin both cells participate in signal transduction. The signal transduction in the cell bearing the Eph receptor constitutes forward signaling and in the cell with ephrin, the signal transduction is considered reverse signaling.

Mesenchymal stem cells and osteoblasts both express ephrinB2 as well as ephB4 (95). Eph-ephrin interactions are involved in bone patterning during development (70) and have also been implicated in osteoarthritis and cancer induced bone pathology (94), (95). EphB4 is constitutively expressed tyrosine kinase receptor on osteoblasts, the stimulation of which leads to osteoblast differentiation possibly via ERK upregulation and suppression of rho activity (96). EphrinB2-ephB4 interaction can occur between osteoblasts as they can express both molecules (94). Parathyroid hormone increases ephrinB2 expression on osteoblasts and increases bone formation. EphrinB2 is induced via RANKL-NFAT signaling cascade and inhibits osteoclastic bone resorption (96). EphrinB2-fc chimeric protein can stimulate ephB4 phosphorylation and osteocalcin expression and calcium deposition by human mesenchymal stem cells (95). EphrinB2-Fc increased angiogenesis at site of injection in mouse bone. Also improved bone parameters BV/TV, Tb.Th, and trabecular number. Thus there is a growing body of evidence to suggest a novel and significant potential for the use of ephrinB2-Fc clusters to accelerate bone healing.

Growth factors can be delivered by systemic, local or gene therapy (9). As targeted local delivery is unlikely to trigger systemic side effects, it is the most commonly attempted delivery technique. Growth factors may have multiple but vastly differing effects dependent on dose, pattern of release, target cells on which they act and the local wound healing status. Adverse effects of locally delivered growth factors have been rarely reported in preclinical and clinical trials. Growth factors can be easily incorporated into our collagen type I gel during its formation (entrapment) or after the gel has formed (passive adsorption). Passive adsorption methods suffer from the drawback of protein denaturation and may cause irreversible binding. Addition of an agent after the gel has formed can lead to rapid release due to convective

washout (99). Yamamoto claimed that alginate gels were superior to collagen gels for the delivery of BMP2 (passively adsorbed) but their process of lyophilizing collagen solution followed by adding an aqueous solution of BMP-2 to the lyophilized collagen would in fact result in the formation of a collagen sponge and not a true “hydrogel” (87). Hydroxyapatite-collagen composite fibers were reported as drug delivery devices by Maehara but the release profile was not reported (123). Furthermore rapid degradation and denaturation of growth factors can take place when growth factors are added to and interact with dry scaffolds.

It has been shown that growth factors can bind to the ECM and form depots in the bone which can regulate local cellular behaviour (9). Binding of growth factors to collagen may be altered by chemical modification of collagen (eg. succinylation or methylation) in attempts to enhance the drug release dynamics (99) but that would be counter productive in terms of biocompatibility and cleavage of linkers. A combination of heparan sulfate and collagen can bind heparin binding growth factors (FGF, TGF, BMP2) and prolong their *in vivo* activity (9). Improved angiogenesis in chorioallantois model with VEGF attached to collagen by covalent linkers was demonstrated (124) Improved activity of TGFβ2 was observed when covalently bound to collagen and compared to injected physical mixture of collagen and TGFβ2 or TGFβ2 alone (125). Alternatively addition of collagen binding domains to growth factors led to uniform and enhanced biological effects (126). Dehydrated collagen can retain growth factors and release an initial burst on day one with sustained release over the next two weeks (120). However, protein degradation and denaturation is likely to occur during the drying process and *in vivo* and *in vitro* efficacy of collagen gel was not compared to dried collagen gel during execution of this experiment. Most of these techniques are applicable to CGIPS to further modify the delivery kinetics of growth factors and enhance the rate of bone regeneration.

Release of molecules from collagen based devices may be affected by binding interactions with collagen and interactions between the polyampholytic and hydrophobic collagen and the molecule of interest (99). Diffusion of molecules larger than 200 to 300 kDa would be hindered during the release from collagen gel whereas smaller molecules would be released by simple diffusion (127). Matrices loaded with lower concentrations of molecule to be delivered, released it at a slower rate as predicted by simple diffusion mode of release which depends on the concentration gradient (99). A slower rate of release of BMP from dried collagen vitrigel (120) was in agreement with previous reports that show the rate of release is proportional to water content (87) Release of growth factors may also be influenced by degradation of the matrix (87).

We chose bovine serum albumin (BSA) as a model for small sized proteins (growth factors) and studied its release from native collagen gel as well as CGIPS. In order to understand the mechanism of drug release kinetics, release constants (K) were calculated and goodness of fit (r^2) was derived from appropriate plots of different kinetic models as shown in table 1. The result of our study showed partial dependence of drug release on concentration (Table 2) and did not conform to zero order drug release which would have yielded a linear relationship between cumulative drug release and time. First order model describes the release which is concentration dependent and played some role in this case. Applicability of the Hixson-Crowell cube root model did not indicate change in surface area or diameter of collagen gel matrix with progressive release of BSA from collagen gel and CGIPS as a function of time which correlated with our experimental observations. However *in vitro* BSA release was best described by Higuchi's equation as the plot showed highest linearity ($r^2 = 0.9251$ for Gel and $r^2 = 0.9424$ for CGIPS) followed by first order kinetics ($r^2 = 0.8608$ for Gel and $r^2 = 0.8481$ for

CGIPS). This data explains why the drug diffuses at comparatively slower rate as the distance of diffusion increases, which is recognized as Higuchi's kinetics (square root kinetics). Higuchi also describes release from an insoluble matrix as square root of time dependent process, which is Fickian diffusion. Fickian diffusion relates the diffusive flux of a drug to its concentration gradient.

Initial portion of the release curve can be ascribed to release of BSA from near the release surface and the slow phase is due to the increased diffusion path length that has to be travelled for BSA to reach the release surface. Similar to a large number of proteins, collagen is a poly-ampholyte, in which charged and hydrophobic amino acid side chains are responsible for weak binding with drugs (99). Thus in addition to diffusion path length, weak interaction of BSA molecule with collagen gel matrix could explain the sustained phase of the release curve. Thus, BSA is released by simple diffusion from gel and CGIPS over 24 hrs period and is appropriate for applications which require a loading dose followed by a slower release. It may be possible to achieve longer release phase by crosslinking collagen or mixing some other polymer with collagen that will retard the release of drug by diffusion. Primary objective of our study was to demonstrate osteoinductive capacity of CGIPS by establishing its ability to function as drug delivery device.

EphrinB2-Fc clusters were released from collagen gel over a period of 120 hours (Figure 2A). The clusters were released without degradation as evident from the position of the electrophoretic band correlating with the band for ephrinB2-Fc cluster that had not been incorporated into collagen gel. A rapid burst of release occurred at 24 to 48 hours and ephrinB2-Fc continued to be released at a slower rate for next 72 hours (Figure 3B).

Treatment of TMSC with ephrinB2-Fc clusters stimulated proliferation of TMSC (Figure 3A). EphrinB2-Fc clusters incorporated into CGIPS could elicit a similar response albeit at higher doses (Figure 3B). This indicated that the ephrinB2-Fc is released from CGIPS in a physiologically active form without degradation or denaturation. More cells migrated into the portion of collagen gel that contained ephrinB2-Fc cluster loaded CGIPS than those with IgG control loaded CGIPS (Figure 4) suggesting a chemotactic activity for ephrinB2-Fc clusters. These data indicate that ephrinB2-Fc clusters could stimulate recruitment, proliferation and differentiation of stem cells to the site of injury and accelerate bone healing. This data also demonstrated the potential of CGIPS as an osteoinductive device when used in combination with ephrinB2-Fc clusters.

In order to optimize repair following surgical intervention local antibiotic therapy has definite advantages over systemic therapy for the treatment of bone infections. Small molecules and drugs can be released rapidly from collagen gels. (99). Vancomycin is an antibiotic with a spectrum of activity against gram positive organisms including MRSA (98) and can be combined with gentamicin when required to broaden the spectrum. Vancomycin suppressed osteoblast cell line proliferation only at doses of 10000 mcg/ml (97). Vancomycin has the advantages of high water solubility, heat stability and low allergy and resistance rates. Vancomycin can be released from CGIPS to inhibit MRSA growth (Figure 3A) as well as kill MRSA (Figure 3B). The doses of vancomycin needed to inhibit bacterial growth and kill bacteria were higher for CGIPS than when the antibiotic was mixed directly with collagen gel, which in turn was higher than when the antibiotic was directly added to the bacterial culture medium. Thus CGIPS can be used to deliver antibiotics to the site of infection in addition to its potential role as a device to accelerate bone healing.

Thus we have shown that CGIPS have the potential to deliver cytokines and drugs to the site of implantation by simple diffusion without degradation of either the CGIPS or drug. The initial loading dose followed by a gradual sustained release over a week would be appropriate for the purpose of tissue engineering to rapidly attract and retain osteogenic cells to the site of implantation. This release profile would also be appropriate to rapidly kill organisms at the site of surgery and prevent infection at the site of surgery over the next few days as the wound heals. Hence CGIPS may serve as osteoinductive bone grafts that may be used at contaminated surgical sites.

CHAPTER VII

CONCLUSION AND FUTURE DIRECTIONS

Collagen gel contraction by MSC

This study established the suitability of MTT conversion to formazan as a simple assay to determine the cell number in collagen gels and other 3-D matrices. Osteogenic differentiation did not affect the ability of MTT assay to determine the cell number establishing MTT assay as a valid technique to track cell proliferation during osteogenic differentiation of human mesenchymal stem cells (MSC) over a range of cell populations from 30,000 to 1 million MSC per ml of collagen type I solution.

The collagen gels were observed to contract by 20% after the first 24 hours regardless of seeding density. A considerably reduced contraction occurred with normal human MSC over a one month culture period in collagen gels prepared in accordance with our patented technology than that previously reported by other groups (55), (57), (102), (103) .

MSC proliferated over 28 days at low (100K/ml) as well as high (400 K/ml) seeding densities when the culture medium was supplemented with 10% FBS. The MSC differentiated to osteoblasts during this time period as seen by expression of osterix and change in cellular morphology to resemble osteoblasts observed on H&E staining. The contraction over one month was significantly higher for high initial seeding density in early as well as late passage cells. We observed that decreasing serum concentration to 4% did not have any effect

on the overall collagen contraction but inhibited proliferation after 14 days in culture. This supports the observation that final collagen contraction is dependent on the initial seeding density as both the gels in which cells proliferated (high serum) and in which the cells could not (low serum) contracted to the same extent. The use of a low cell seeding density to prevent collagen gel contraction during generation of tissue engineered grafts may be a viable option to overcome the problems associated with gel contraction.

Late passage MSC contracted the gel significantly more than early passage MSC over a culture period of 28 days. Late passage MSC did not proliferate during the duration of the experiment i.e. the cell numbers did not change significantly from day one to day 14 or day 28. Lowering the serum concentration to 4% prevented contraction of collagen gels after day one, at all initial seeding densities of MSC. Thus use of late passage cells under low serum conditions may provide an alternative method of preventing collagen gel contraction when a high number of cells is required in the graft.

Telomerase transformed MSC (TMSC) contracted the gel significantly less after 24 hours as well as after 14 days when compared to normal MSC. Osteoblasts contracted the gel significantly more than TMSC during the first 24 hours (10% difference) and over a period of 14 days (8% difference). The cell numbers for hMSC, TMSC and TOST doubled after two weeks of culture in collagen hydrogel under osteogenic differentiation conditions so a difference in cell proliferation would not account for the difference in contraction observed with different cells. Thus it is not only the number of cells but the contractile phenotype of the cells which determines the quantum of gel contraction.

Thus it was demonstrated that high initial cell seeding density, late passage cells, non-transformed cells, differentiated cells all increase collagen gel contraction. A low initial cell seeding density, low serum medium to culture late passage cells, using non-differentiated early passage cells and allowing them to differentiate *in situ* may be some of the strategies employed to prevent collagen gel contraction during the use of collagen hydrogels as 3-D tissue culture models or tissue engineering grafts. A non-contracted matrix will have larger pores with loosely spaced native fibrils. These features would support faster cell invasion, extensive graft remodelling, earlier vascularization and greater survival of implanted grafts leading to better host graft integration and superior graft performance.

Collagen scaffold for 3-D tissue culture models

As another strategy to minimize collagen gel contraction when collagen gel is used as the matrix for tissue engineering the suitability of porous non-denatured commercially available collagen type I foam (Ultrafoam[®]) was examined. This scaffold is stiffer than the collagen gel alone, yet cytocompatible, easy to handle and amenable to physical deformation. Ultrafoam[®] was highly porous and accommodated five times its own weight of collagen type I gel. It was produced from native (non-denatured) collagen type I that was minimally cross-linked as demonstrated by the long wetting time and complete, residue free, degradation after collagenase treatment.

Introduction of cells suspended in a solution of neutralized collagen type I into Ultrafoam[®], and allowing the collagen to gel at 37°C, formed collagen hydrogel containing collagen scaffold (CGCS). This approach ensured that even at low seeding density, cells could penetrate into and be distributed throughout the scaffold. Thus MTT staining, that generates

formazan dark blue color, hematoxylin-eosin staining of paraffin embedded sections of CGCS, and confocal microscopy demonstrated distribution of cells throughout the CGCS, although the cell density was higher at the surface than in the interior of the model. Use of collagen for seeding cells improved the seeding efficacy on Ultrafoam[®] without collagen gel from 85% to more than 92% in the presence of collagen gel.

In my CGCS model MSC proliferated for a period of 8 weeks under differentiation conditions, a much longer survival and viability than has so far been reported. This demonstrates the suitability of our model for long-term studies and four-month viability was also observed but not recorded.

Osteoblasts cultured in Ultrafoam[®] for 4 weeks, migrated to the surface and very few cells were present in the Ultrafoam[®] interior, probably due to a more favorable nutrient supply at the scaffold surface. In contrast, a greater number of osteoblasts were present in CGCS interior due to presence of collagen gel. The collagen gel may have improved the growth factor access and availability, and maintained equally favorable nutritional conditions in the interior of the scaffold as at its surface. Regardless of the cell type (fibroblast, hMSC, osteoblast) the use of collagen gel impregnation facilitated total penetration into the scaffold, a more uniform distribution of cells, higher seeding efficiency and improved cell survival and proliferation. Cells recovered after collagenase digestion of CGCS attached and proliferated when placed in culture.

To produce a seamless interface when serving as a graft, my 3-D model (CGCS) has to allow free migration of cells so that the graft-host interactions are facilitated. The cells (fibroblasts and osteoblasts) were shown to migrate out of CGCS into surrounding acellular collagen gel indicating the potential use of CGCS to deliver cells to the site of injury. Successful

penetration by cells from collagen hydrogel into CGCS indicated its ability to allow invasion by resident host cells during integration of graft with host tissue. When a tensile force was applied to fibroblasts populating our 3-D model - CGCS they realigned parallel to the direction of application of force within 24 hours throughout the specimen, validating the potential use of CGCS for mechanotransduction studies in 3-D.

The exposure of MSC populating CGCS to osteogenic differentiation conditions showed that alkaline phosphatase activity peaked at 14 days and decreased by day 28 similar to that reported to take place during differentiation of hMSC in a monolayer culture (109). Synthesis and pericellular deposition of glycosaminoglycans usually associated with chondrogenesis is also a late event in osteogenesis and was observed sporadically by day 28 in Alcian Blue stained paraffin sections of CGCS. The transcription factor osterix and the extracellular matrix protein osteopontin, were observed after 28 days of differentiation in Ultrafoam[®] without collagen gel as well as in CGCS. These results support our conclusion that osteogenesis takes place in our *in vitro* model. We observed physiological mineralization in cultures of CGCS populated with hMSC under differentiation conditions for 28 days. Quantification of areas rich in calcium deposits showed ten fold increase from day 14 to day 28 corresponding in culture.

Data presented in this study demonstrated several findings critical to ossification. My model is “cytocompatible” and supports the transition of our strategy from successful engineering of 3-D models of living “soft” human tissue to modeling bone morphogenesis. CGCS is not cross-linked, is biodegradable, and has sufficient mechanical integrity to facilitate easy handling and remains intact during prolonged culture periods. It retains its original shape and size without contraction, and supports invasion, proliferation, metabolic homeostasis,

mechanotransduction and osteogenic differentiation of MSC including calcification in a physiological manner. I further demonstrated that the presence of collagen is essential for effective cell delivery and long-term cell viability in the impregnated scaffolds and particularly the importance of collagen in the osteogenic mineralization. I have used several cells types and differentiation along one lineage but the data supports the proposal that CGCS can serve as an excellent *in vitro* 3-D model to study variety of cells in an *in vivo* relevant manner. CGCS is particularly appropriate as an *in vitro* 3-D model for studies of osteogenesis.

β -TCP based 3-D model for bone

One of the key principles of tissue engineering is to develop a scaffold that mimics the tissue of interest biologically as well as physically. Beta-tricalcium phosphate (β -TCP) is a sintered version of hydroxyapatite (hydroxyl deficient calcium phosphate apatite) which has mechanical properties similar to bone, can bond directly with bone (67) and is almost completely resorbed in the human body in 6 to 9 months with no adverse reaction (66).

Porous scaffolds are more advantageous than non-porous scaffolds as pores allow rapid cell migration into the interior of the scaffold, provide space for cell proliferation, allow diffusion of nutrients throughout the scaffold and hence faster and greater quantity of host tissue and vasculature ingrowth, leading to a stronger bond between the graft and bone because of the larger surface area available in porous scaffolds for bonding (1), (7), (71), (72). I demonstrated the presence of large sized pores with big pore interconnections and high pore volume in choroOSTM β -TCP which had the ability to absorb and retain large volume of water and collagen. Native fibrillar collagen gel could be impregnated into the pores to form collagen gel impregnated porous scaffold (CGIPS).

By suspending MSC in collagen solution and then impregnating this cell containing collagen solution into the porous scaffold and allowing the collagen solution to gel *in situ* even cells seeded at a density of 100,000 cells per ml collagen could be introduced into the deep interior of the scaffold. Cells were present in the top (cell seeded surface), bottom (surface opposite to the seeded surface), and the central core. When cells were seeded in CGIPS the cells that penetrated into the scaffold interior were retained in the deeper region while cells seeded directly on TCP migrated to the surface. CGIPS allowed the migration of cells from outside into the porous CGIPS demonstrating potential for invasion of host tissue as well as study of cell migration in 3-D.

MSC could be introduced with 100% efficiency in CGIPS and their number monitored using MTT. MSC proliferated in CGIPS for 8 weeks under proliferation conditions. Even the cells under differentiation conditions proliferated albeit less than those under proliferation conditions. At 100,000 and 200,000 cells per ml collagen, proliferation in CGIPS of the cells at a higher density started earlier. When introduced into CGIPS, the collagen type I gel did not contract as seen by the stable weights of the CGIPS with different seeding densities over a period of four weeks.

Parameters like bone volume density (BV/TV, relative volume of mineralized tissue to total volume), bone surface density (BS/TV, relative volume of bone surface to total volume), trabecular thickness (Tb.Th, average thickness of the individual pillars forming the scaffold wall), trabecular separation (Tb.Sp, distance between trabeculae) and trabecular number (Tb.N, number of trabeculae per unit length) are used to compare morphology of trabecular bone and bone graft specimen. CGIPS had significantly less empty volume than β -TCP. CGIPS had more volume occupied by soft tissue (cells and ECM) than β -TCP at the start

and at the end of eight weeks. CGIPS had significantly more calcium deposition at the end of eight weeks whereas in case of cells cultured on β -TCP a increase in calcium deposition was not observed.

CGIPS was an appropriate model for demonstration and studies of responses of MSC to mechanical forces. While application of 6 kPa pressure for ten minutes every day resulted in increased proliferation of MSC over the first three days, continued application of the same pressure prevented further proliferation. Use of higher pressure (12 kPa) or longer duration of application of pressure (1 hour) led to prevention MSC proliferation.

Thus CGIPS is superior to β -TCP alone with respect to seeding of cells in the deep interior of the scaffold, retention of seeded cells, migration of cells into CGIPS, proliferation of hMSC and mineralization by osteogenically differentiated hMSC. Furthermore we have provided a proof of concept for the use of CGIPS in studies involving mechanotransduction in 3-D.

CGIPS as bone graft

Although bones can heal by formation of new bone tissue, the ability to repair a wound is limited and large bone voids may not heal (1), (2). These critical-sized bone defects can be repaired only by means of grafting. Autologous bone graft is considered the gold standard of treatment against which new therapies are measured (21).

Tissue engineering is a branch of science that attempts to utilize various artificial and natural materials to help repair damaged or dysfunctional tissues and organs in the body (2). For a tissue engineered product to meet FDA approval and be a successful bone graft substitute, it has to be cost effective, sterile, radiographically distinguishable, totally biodegradable with non-

toxic degradation byproducts, mechanically strong, and finally remodelable into native bone tissue (23).

Green fluorescent protein expressing telomerase transfected human MSC implanted within the scaffolds in rat subcutaneous tissue and intramuscularly survived for a period of one month. These transplanted cells differentiated into osteogenic precursors as seen by the expression of osteogenic differentiation markers osterix and osteopontin with the same distribution as the green fluorescence.

An increase in vascular invasion was seen in case of cell containing implants over those not containing cells in case of subcutaneous implantation possibly indicating release of angiogenic factors from the transplanted cells. Presence of MSC alone did not improve the mineralization of implant by the cells or total calcification assessed by X-ray density above that of cell and gel free Empty-TCP. Thus in my experiment subcutaneous and intramuscular xenogenic implants of human cells without collagen gel *in vivo* (rats) did not impact the osteogenesis although it improved angiogenesis.

When β -TCP impregnated with collagen gel containing cells (CGIPS) was compared to β -TCP directly seeded with cells without gel (Cell-TCP) a greater cell density was observed in the pores which corresponds with my *in vitro* observations that collagen gel facilitates migration of cells into porous scaffolds. Cells that invaded the implant adopted an osteogenic lineage as evidenced by expression of markers of differentiation. These observations are supported by the published data proposing osteoinductive nature of native collagen type I and of β -TCP. The presence of gel alone did not improve mineralization of the matrix by the invading cells but the total calcium density of the implant was higher than Cell-TCP. This may have been due to the re-deposition of resorbed calcium and phosphate from the β -TCP scaffold

onto the collagen fibrils near the edge of the pore.

A greater cell density was observed in the pores of CGIPS as compared to Empty-TCP and Cell-TCP confirming the results from my *in vitro* experiments that collagen gel facilitated cell invasion. The expression of differentiation markers osterix and osteopontin, was more prominent in case of CGIPS as compared to Empty-TCP both in subcutaneous and intramuscular sites of implantation. Collagen gel and MSC combination improved the survival of xenogenically transplanted cells. The transplanted cells seemed to preferentially localize at the pore-gel interface and differentiate osteogenically as evidenced by expression of osteopontin, an ECM protein accepted as a marker of osteogenic differentiation, which co-localized with the transplanted cells. CGIPS did not collapse during sectioning and tissue was seen to invade throughout the implant. This supports the conclusion that tissue invaded rapidly into the porous scaffold when collagen gel was present in the pores of the scaffold.

CGIPS had significantly greater mineral deposits within the tissue inside the pores indicating active mineralization of the matrix by the cells within the pores. Rattners observation that collagen gel and a three dimensional morphology are pre-requisites for mineralization (14) and my *in vitro* observation that mineralization is facilitated by and requires the presence of native fibrillar collagen are in agreement. The total calcium density of the CGIPS implants was significantly higher than Empty-TCP and Cell-TCP. This measurement takes into account the mineralization of the matrix by the cells as well as deposition of calcium phosphate on the collagen fibrils near the pore walls.

Thus enhanced mineralization near the pore walls and greater vascular tissue invasion would lead to a bone graft substitute that would rapidly integrate with the host tissue. A high graft tissue interface strength would result due to rapid invasion of surrounding tissue and

mineralization at the surface of β -TCP, bonding it firmly with the native bone. Thus CGIPS has the potential to form a mechanosensitive, completely resorbable, mechanically strong and osteoinductive bone graft substitute that is amenable to remodelling and merits further testing in large animal bone defect models.

Drug delivery with CGIPS

As the role of transplanted cells in graft performance is not well established the ability to recruit cells to the site of injury is an important facet of tissue engineered grafts. Growth factors are the most commonly used chemoattractants. One of the areas of research that can provide valuable information about cell recruitment to the site of injury is osteoblast-osteoclast “coupling”(70). When osteoclasts resorb bone at the site of injury, osteoblasts are recruited to start depositing new bone at the time when osteoclasts finish removing the dead or damaged tissue. One of the proposed mechanisms of osteoblast-clast coupling is release of matrix bound growth factors by osteoclasts. The other is ephrin-eph interaction. We tested the potential for use of ephrinB2-Fc clusters as a mitogen and chemoattractant.

I chose bovine serum albumin (BSA) as a model molecule for small sized proteins (growth factors) and studied its release from native collagen gel and CGIPS. It was found that in-vitro BSA release was best explained by Higuchi's equation for Fickian diffusion. Thus, BSA was released by simple diffusion from gel and CGIPS. Applications which require a loading dose followed by a slower release are appropriate for CGIPS.

EphrinB2-Fc clusters were released from collagen gel over a period of 120 hours without degradation. A rapid burst of release occurred at 24 to 48 hours and ephrinB2-Fc continued to be released at a slower rate for the remaining 72 to 96 hours. Treatment of TMSC

with ephrinB2-Fc clusters stimulated proliferation of TMSC. EphrinB2-Fc clusters incorporated into CGIPS could elicit a similar response albeit at higher doses. This indicated that the ephrinB2-Fc is released from CGIPS in a physiologically active form without degradation or denaturation. I observed a chemotactic activity for ephrinB2-Fc clusters. These data supplement previous work and indicate that ephrinB2-Fc clusters could stimulate recruitment, proliferation and differentiation of stem cells to the site of injury and accelerate bone healing.

Local antibiotic therapy has definite advantages over systemic therapy for the treatment of bone infections. Vancomycin could be released from CGIPS to inhibit MRSA growth as well as kill MRSA. The doses of vancomycin needed to inhibit bacterial growth and kill bacteria were higher for CGIPS than when the antibiotic was mixed directly with collagen gel, which in turn was higher than when the antibiotic was directly added to the bacterial culture medium. Thus CGIPS can be used to deliver antibiotics to the site of infection in addition to its potential role as a device to accelerate bone healing.

Future Directions

CGCS was used as a model for osteogenesis in this study. But the same collagen gel- collagen scaffold combination can be used to develop models for various tissues like cartilage, skin, breast, heart, liver, pancreas, etc.

Bone can remodel according to the forces acting on it for optimum load bearing functionality (1). The ability of cells to sense mechanical forces and respond to the physical stimulus is known as mechanotransduction. The potential of using a 3-D to which compressive forces of high magnitude can be applied would allow biomechanical studies of remodelling and mechanotransduction to be performed in vitro.

When non-biodegradable implants are used (example stems of joint implants) the micro-motion results in formation of sub-micrometer wear particles which may trigger an immune response leading to implant loosening and failure (1). A similar strategy of impregnation of porous metal with collagen gel can be used to obtain stronger bonding between metal implant and bone leading to a decrease in micromotion and subsequent implant failure. I demonstrated the feasibility of the use of this strategy in tantalum metal cylinders.

The first step towards clinical translation is biocompatibility, feasibility, non-toxicity and proof of principle testing in small animals (2). For bone tissue the testing is most often performed in rats. Unfortunately rodent autografts contain a mixture of bone marrow and bone chips so can not be used as clinically relevant controls. Rodent MSC are different from large animal MSC with respect to bone formation. For final testing of a bone graft substitute it has to be tested in a large defect with relatively hypoxic environment eg a segmental bone defect in large animal. The defect has to be larger than 1 cm which is not feasible in rodent long bones. Technique of implantation and cell retrieval should closely mimic the clinical technique possible only in large animals. The efficacy of the bone graft substitute has to be compared to autograft. Thus this work sets the foundation for large animal studies of CGIPS with eventual clinical translation.

Other issues that need to be addressed are the comparison of stem cells obtained from various sources, for example a comparison of autologous stem cells versus allogenic stem cells, comparisons of stem cells obtained from a younger donor to that obtained from an older donor, etc. with respect to their bone forming capacity and posttransplant viability. Similarly the role of pure populations of mesenchymal stem cells needs to be compared to the potential benefit of using a mixture of unrefined bone marrow cells (undifferentiated and partially differentiated

mesenchymal and hematopoietic stem cells). More animal studies need to be conducted to address the potential teratogenicity of implanted stem cells. Various scaffold combinations can be attempted to mimic tissue interfaces like articular surfaces or tendon insertions. The potential for use of recombinant human collagen for the cosmetic and tissue engineering industry is another issue that needs to be addressed.

REFERENCES

1. Hing KA. Bone repair in the twenty-first century: Biology, chemistry or engineering? *Philos Transact A Math Phys Eng Sci.* 2004 Dec 15;362(1825):2821-50.
2. Muschler GF, Raut VP, Patterson TE, Wenke JC, Hollinger JO. The design and use of animal models for translational research in bone tissue engineering and regenerative medicine. *Tissue Eng Part B Rev.* 2010 Feb;16(1):123-45.
3. ROBINSON RA, WATSON ML. Collagen-crystal relationships in bone as seen in the electron microscope. *Anat Rec.* 1952 Nov;114(3):383-409.
4. Kielty CM, Hopkinson I, Grant ME. Collagen- the family: Structure, assembly and organization in the extracellular matrix. In: *Connective Tissue and its Heritable Disorders.* Wiley-Liss; 1993. p. 103--147.
5. Mizuno M, Fujisawa R, Kuboki Y. Type I collagen-induced osteoblastic differentiation of bone-marrow cells mediated by collagen-alpha2beta1 integrin interaction. *J Cell Physiol.* 2000 Aug;184(2):207-13.
6. Mauney JR, Kirker-Head C, Abrahamson L, Gronowicz G, Volloch V, Kaplan DL. Matrix-mediated retention of in vitro osteogenic differentiation potential and in vivo bone-forming capacity by human adult bone marrow-derived mesenchymal stem cells during ex vivo expansion. *J Biomed Mater Res A.* 2006 Dec 1;79(3):464-75.

7. Hing KA, Best SM, Tanner KE, Bonfield W, Revell PA. Mediation of bone ingrowth in porous hydroxyapatite bone graft substitutes. *J Biomed Mater Res A*. 2004 Jan 1;68(1):187-200.
8. Gerstenfeld LC, Cullinane DM, Barnes GL, Graves DT, Einhorn TA. Fracture healing as a post-natal developmental process: Molecular, spatial, and temporal aspects of its regulation. *J Cell Biochem*. 2003 Apr 1;88(5):873-84.
9. Luginbuehl V, Meinel L, Merkle HP, Gander B. Localized delivery of growth factors for bone repair. *Eur J Pharm Biopharm*. 2004 Sep;58(2):197-208.
10. O'Loughlin PF, Morr S, Bogunovic L, Kim AD, Park B, Lane JM. Selection and development of preclinical models in fracture-healing research. *J Bone Joint Surg Am*. 2008 Feb;90 Suppl 1:79-84.
11. Carter DR, Beaupre GS, Giori NJ, Helms JA. Mechanobiology of skeletal regeneration. *Clin Orthop Relat Res*. 1998 Oct;(355 Suppl)(355 Suppl):S41-55.
12. Caplan AI. Mesenchymal stem cells. *J Orthop Res*. 1991 Sep;9(5):641-50.
13. Jaiswal N, Haynesworth SE, Caplan AI, Bruder SP. Osteogenic differentiation of purified, culture-expanded human mesenchymal stem cells in vitro. *J Cell Biochem*. 1997 Feb;64(2):295-312.
14. Rattner A, Sabido O, Le J, Vico L, Massoubre C, Frey J, et al. Mineralization and alkaline phosphatase activity in collagen lattices populated by human osteoblasts. *Calcif Tissue Int*. 2000 Jan;66(1):35-42.

15. Boehrs J, Zaharias RS, Laffoon J, Ko YJ, Schneider GB. Three-dimensional culture environments enhance osteoblast differentiation. *J Prosthodont.* 2008 Oct;17(7):517-21.
16. Kale S, Biermann S, Edwards C, Tarnowski C, Morris M, Long MW. Three-dimensional cellular development is essential for ex vivo formation of human bone. *Nat Biotechnol.* 2000 Sep;18(9):954-8.
17. Niemeyer P, Krause U, Fellenberg J, Kasten P, Seckinger A, Ho AD, et al. Evaluation of mineralized collagen and alpha-tricalcium phosphate as scaffolds for tissue engineering of bone using human mesenchymal stem cells. *Cells Tissues Organs.* 2004;177(2):68-78.
18. Schantz JT, Teoh SH, Lim TC, Endres M, Lam CX, Hutmacher DW. Repair of calvarial defects with customized tissue-engineered bone grafts I. evaluation of osteogenesis in a three-dimensional culture system. *Tissue Eng.* 2003;9 Suppl 1:S113-26.
19. Buxton PG, Bitar M, Gellynck K, Parkar M, Brown RA, Young AM, et al. Dense collagen matrix accelerates osteogenic differentiation and rescues the apoptotic response to MMP inhibition. *Bone.* 2008 Aug;43(2):377-85.
20. Godier AF, Marolt D, Gerecht S, Tajnsek U, Martens TP, Vunjak-Novakovic G. Engineered microenvironments for human stem cells. *Birth Defects Res C Embryo Today.* 2008 Dec;84(4):335-47.
21. Helm GA, Sheehan JM, Sheehan JP, Jane JA, Jr, diPierro CG, Simmons NE, et al. Utilization of type I collagen gel, demineralized bone matrix, and bone morphogenetic protein-2 to enhance autologous bone lumbar spinal fusion. *J Neurosurg.* 1997 Jan;86(1):93-100.

22. Petty W, Spanier S, Shuster JJ. Prevention of infection after total joint replacement. experiments with a canine model. *J Bone Joint Surg Am.* 1988 Apr;70(4):536-9.
23. Dawson JI, Oreffo RO. Bridging the regeneration gap: Stem cells, biomaterials and clinical translation in bone tissue engineering. *Arch Biochem Biophys.* 2008 May 15;473(2):124-31.
24. Hing KA, Best SM, Tanner KE, Bonfield W, Revell PA. Quantification of bone ingrowth within bone-derived porous hydroxyapatite implants of varying density. *J Mater Sci Mater Med.* 1999 Oct-Nov;10(10/11):663-70.
25. Werntz JR, Lane JM, Burstein AH, Justin R, Klein R, Tomin E. Qualitative and quantitative analysis of orthotopic bone regeneration by marrow. *J Orthop Res.* 1996 Jan;14(1):85-93.
26. Schantz JT, Hutmacher DW, Lam CX, Brinkmann M, Wong KM, Lim TC, et al. Repair of calvarial defects with customised tissue-engineered bone grafts II. evaluation of cellular efficiency and efficacy in vivo. *Tissue Eng.* 2003;9 Suppl 1:S127-39.
27. Peters A, Toben D, Lienau J, Schell H, Bail HJ, Matziolis G, et al. Locally applied osteogenic predifferentiated progenitor cells are more effective than undifferentiated mesenchymal stem cells in the treatment of delayed bone healing. *Tissue Eng Part A.* 2009 Oct;15(10):2947-54.
28. Johnson KD, Frierson KE, Keller TS, Cook C, Scheinberg R, Zerwekh J, et al. Porous ceramics as bone graft substitutes in long bone defects: A biomechanical, histological, and radiographic analysis. *J Orthop Res.* 1996 May;14(3):351-69.

29. Grundel RE, Chapman MW, Yee T, Moore DC. Autogeneic bone marrow and porous biphasic calcium phosphate ceramic for segmental bone defects in the canine ulna. *Clin Orthop Relat Res.* 1991 May;(266)(266):244-58.
30. Liu G, Zhao L, Cui L, Liu W, Cao Y. Tissue-engineered bone formation using human bone marrow stromal cells and novel beta-tricalcium phosphate. *Biomed Mater.* 2007 Jun;2(2):78-86.
31. Boo JS, Yamada Y, Okazaki Y, Hibino Y, Okada K, Hata K, et al. Tissue-engineered bone using mesenchymal stem cells and a biodegradable scaffold. *J Craniofac Surg.* 2002 Mar;13(2):231,9; discussion 240-3.
32. Mankani MH, Kuznetsov SA, Wolfe RM, Marshall GW, Robey PG. In vivo bone formation by human bone marrow stromal cells: Reconstruction of the mouse calvarium and mandible. *Stem Cells.* 2006 Sep;24(9):2140-9.
33. Harris CT, Cooper LF. Comparison of bone graft matrices for human mesenchymal stem cell-directed osteogenesis. *J Biomed Mater Res A.* 2004 Mar 15;68(4):747-55.
34. Shayesteh YS, Khojasteh A, Soleimani M, Alikhasi M, Khoshzaban A, Ahmadbeigi N. Sinus augmentation using human mesenchymal stem cells loaded into a beta-tricalcium phosphate/hydroxyapatite scaffold. *Oral Surg Oral Med Oral Pathol Oral Radiol Endod.* 2008 Aug;106(2):203-9.
35. Mihara K, Imai C, Coustan-Smith E, Dome JS, Dominici M, Vanin E, et al. Development and functional characterization of human bone marrow mesenchymal cells immortalized by enforced expression of telomerase. *Br J Haematol.* 2003 Mar;120(5):846-9.

36. Wei A, Tao H, Chung SA, Brisby H, Ma DD, Diwan AD. The fate of transplanted xenogeneic bone marrow-derived stem cells in rat intervertebral discs. *J Orthop Res*. 2009 Mar;27(3):374-9.
37. Niemeyer P, Schonberger TS, Hahn J, Kasten P, Fellenberg J, Suedkamp N, et al. Xenogenic transplantation of human mesenchymal stem cells in a critical size defect of the sheep tibia for bone regeneration. *Tissue Eng Part A*. 2010 Jan;16(1):33-43.
38. Dawson JJ, Wahl DA, Lanham SA, Kanczler JM, Czernuszka JT, Oreffo RO. Development of specific collagen scaffolds to support the osteogenic and chondrogenic differentiation of human bone marrow stromal cells. *Biomaterials*. 2008 Jul;29(21):3105-16.
39. Gelse K, Poschl E, Aigner T. Collagens--structure, function, and biosynthesis. *Adv Drug Deliv Rev*. 2003 Nov 28;55(12):1531-46.
40. Engler AJ, Sen S, Sweeney HL, Discher DE. Matrix elasticity directs stem cell lineage specification. *Cell*. 2006 Aug 25;126(4):677-89.
41. Elsdale T, Bard J. Collagen substrata for studies on cell behavior. *J Cell Biol*. 1972 Sep;54(3):626-37.
42. Hesse E, Hefferan TE, Tarara JE, Haasper C, Meller R, Krettek C, et al. Collagen type I hydrogel allows migration, proliferation, and osteogenic differentiation of rat bone marrow stromal cells. *J Biomed Mater Res A*. 2010 Feb 22.

43. Xu XL, Lou J, Tang T, Ng KW, Zhang J, Yu C, et al. Evaluation of different scaffolds for BMP-2 genetic orthopedic tissue engineering. *J Biomed Mater Res B Appl Biomater*. 2005 Nov;75(2):289-303.
44. Weinand C, Pomerantseva I, Neville CM, Gupta R, Weinberg E, Madisch I, et al. Hydrogel-beta-TCP scaffolds and stem cells for tissue engineering bone. *Bone*. 2006 Apr;38(4):555-63.
45. Sweeney TM, Opperman LA, Persing JA, Ogle RC. Repair of critical size rat calvarial defects using extracellular matrix protein gels. *J Neurosurg*. 1995 Oct;83(4):710-5.
46. Teixeira S, Fernandes H, Leusink A, van Blitterswijk C, Ferraz MP, Monteiro FJ, et al. In vivo evaluation of highly macroporous ceramic scaffolds for bone tissue engineering. *J Biomed Mater Res A*. 2010 May;93(2):567-75.
47. Levy RJ, Schoen FJ, Sherman FS, Nichols J, Hawley MA, Lund SA. Calcification of subcutaneously implanted type I collagen sponges. effects of formaldehyde and glutaraldehyde pretreatments. *Am J Pathol*. 1986 Jan;122(1):71-82.
48. Lutolf MP, Lauer-Fields JL, Schmoekel HG, Metters AT, Weber FE, Fields GB, et al. Synthetic matrix metalloproteinase-sensitive hydrogels for the conduction of tissue regeneration: Engineering cell-invasion characteristics. *Proc Natl Acad Sci U S A*. 2003 Apr 29;100(9):5413-8.
49. Mauney J, Volloch V. Progression of human bone marrow stromal cells into both osteogenic and adipogenic lineages is differentially regulated by structural conformation of collagen I matrix via distinct signaling pathways. *Matrix Biol*. 2009 Jun;28(5):239-50.

50. Taira M, Araki Y, Nakao H, Takahashi J, Hyon SH, Tsutsumi S. Cellular reactions to polylactide-based sponge and collagen gel in subcutaneous tissue. *J Oral Rehabil.* 2003 Jan;30(1):106-9.
51. Hao W, Hu YY, Wei YY, Pang L, Lv R, Bai JP, et al. Collagen I gel can facilitate homogenous bone formation of adipose-derived stem cells in PLGA-beta-TCP scaffold. *Cells Tissues Organs.* 2008;187(2):89-102.
52. Cornell CN. Osteoconductive materials and their role as substitutes for autogenous bone grafts. *Orthop Clin North Am.* 1999 Oct;30(4):591-8.
53. DeLustro F, Dasch J, Keefe J, Ellingsworth L. Immune responses to allogeneic and xenogeneic implants of collagen and collagen derivatives. *Clin Orthop Relat Res.* 1990 Nov;(260)(260):263-79.
54. Bell E, Ivarsson B, Merrill C. Production of a tissue-like structure by contraction of collagen lattices by human fibroblasts of different proliferative potential in vitro. *Proc Natl Acad Sci U S A.* 1979 Mar;76(3):1274-8.
55. Lewus KE, Nauman EA. In vitro characterization of a bone marrow stem cell-seeded collagen gel composite for soft tissue grafts: Effects of fiber number and serum concentration. *Tissue Eng.* 2005 Jul-Aug;11(7-8):1015-22.
56. Kinner B, Zaleskas JM, Spector M. Regulation of smooth muscle actin expression and contraction in adult human mesenchymal stem cells. *Exp Cell Res.* 2002 Aug 1;278(1):72-83.

57. Sumanasinghe RD, Osborne JA, Lobo EG. Mesenchymal stem cell-seeded collagen matrices for bone repair: Effects of cyclic tensile strain, cell density, and media conditions on matrix contraction in vitro. *J Biomed Mater Res A*. 2009 Mar 1;88(3):778-86.
58. Talley-Ronsholdt DJ, Lajiness E, Nagodawithana K. Transforming growth factor-beta inhibition of mineralization by neonatal rat osteoblasts in monolayer and collagen gel culture. *In Vitro Cell Dev Biol Anim*. 1995 Apr;31(4):274-82.
59. Lode A, Bernhardt A, Gelinsky M. Cultivation of human bone marrow stromal cells on three-dimensional scaffolds of mineralized collagen: Influence of seeding density on colonization, proliferation and osteogenic differentiation. *J Tissue Eng Regen Med*. 2008 Oct;2(7):400-7.
60. Holy CE, Shoichet MS, Davies JE. Engineering three-dimensional bone tissue in vitro using biodegradable scaffolds: Investigating initial cell-seeding density and culture period. *J Biomed Mater Res*. 2000 Sep 5;51(3):376-82.
61. Eslaminejad MB, Mirzadeh H, Nickmahzar A, Mohamadi Y, Mivehchi H. Type I collagen gel in seeding medium improves murine mesenchymal stem cell loading onto the scaffold, increases their subsequent proliferation, and enhances culture mineralization. *J Biomed Mater Res B Appl Biomater*. 2009 Aug;90(2):659-67.
62. George J, Kuboki Y, Miyata T. Differentiation of mesenchymal stem cells into osteoblasts on honeycomb collagen scaffolds. *Biotechnol Bioeng*. 2006 Oct 20;95(3):404-11.

63. Grinnell F. Fibroblasts, myofibroblasts, and wound contraction. *J Cell Biol.* 1994 Feb;124(4):401-4.
64. Dimitrijevic SD, Gracy RW, inventors; Non-contracting tissue equivalent. patent 6471958. 2002 10/29/2002.
65. Nishiyama T, Tominaga N, Nakajima K, Hayashi T. Quantitative evaluation of the factors affecting the process of fibroblast-mediated collagen gel contraction by separating the process into three phases. *Coll Relat Res.* 1988 May;8(3):259-73.
66. Hinz P, Wolf E, Schwesinger G, Hartelt E, Ekkernkamp A. A new resorbable bone void filler in trauma: Early clinical experience and histologic evaluation. *Orthopedics.* 2002 May;25(5 Suppl):s597-600.
67. Holtorf HL, Sheffield TL, Ambrose CG, Jansen JA, Mikos AG. Flow perfusion culture of marrow stromal cells seeded on porous biphasic calcium phosphate ceramics. *Ann Biomed Eng.* 2005 Sep;33(9):1238-48.
68. LeGeros RZ. Properties of osteoconductive biomaterials: Calcium phosphates. *Clin Orthop Relat Res.* 2002 Feb;(395)(395):81-98.
69. Chang YL, Stanford CM, Keller JC. Calcium and phosphate supplementation promotes bone cell mineralization: Implications for hydroxyapatite (HA)-enhanced bone formation. *J Biomed Mater Res.* 2000 Nov;52(2):270-8.
70. Mundy GR, Eleftheriou F. Boning up on ephrin signaling. *Cell.* 2006 Aug 11;126(3):441-3.

71. Yang ZJ, Yuan H, Zou P, Tong W, Qu S, Zhang XD. Osteogenic responses to extraskeletally implanted synthetic porous calcium phosphate ceramics: An early stage histomorphological study in dogs. *J Mater Sci Mater Med*. 1997 Nov;8(11):697-701.
72. Karageorgiou V, Kaplan D. Porosity of 3D biomaterial scaffolds and osteogenesis. *Biomaterials*. 2005 Sep;26(27):5474-91.
73. Kuboki Y, Jin Q, Kikuchi M, Mamood J, Takita H. Geometry of artificial ECM: Sizes of pores controlling phenotype expression in BMP-induced osteogenesis and chondrogenesis. *Connect Tissue Res*. 2002;43(2-3):529-34.
74. Boo JS, Yamada Y, Okazaki Y, Hibino Y, Okada K, Hata K, et al. Tissue-engineered bone using mesenchymal stem cells and a biodegradable scaffold. *J Craniofac Surg*. 2002 Mar;13(2):231,9; discussion 240-3.
75. Sun H, Ye F, Wang J, Shi Y, Tu Z, Bao J, et al. The upregulation of osteoblast marker genes in mesenchymal stem cells prove the osteoinductivity of hydroxyapatite/tricalcium phosphate biomaterial. *Transplant Proc*. 2008 Oct;40(8):2645-8.
76. Sanchez-Salcedo S, Izquierdo-Barba I, Arcos D, Vallet-Regi M. In vitro evaluation of potential calcium phosphate scaffolds for tissue engineering. *Tissue Eng*. 2006 Feb;12(2):279-90.
77. Lim JY, Donahue HJ. Biomaterial characteristics important to skeletal tissue engineering. *J Musculoskelet Neuronal Interact*. 2004 Dec;4(4):396-8.

78. Kasten P, Luginbuhl R, van Griensven M, Barkhausen T, Krettek C, Böhner M, et al. Comparison of human bone marrow stromal cells seeded on calcium-deficient hydroxyapatite, beta-tricalcium phosphate and demineralized bone matrix. *Biomaterials*. 2003 Jul;24(15):2593-603.
79. Zou C, Weng W, Cheng K, Du P, Shen G, Han G, et al. Porous beta-tricalcium phosphate/collagen composites prepared in an alkaline condition. *J Biomed Mater Res A*. 2008 Oct;87(1):38-44.
80. Weinand C, Gupta R, Weinberg E, Madisch I, Jupiter JB, Vacanti JP. Human shaped thumb bone tissue engineered by hydrogel-beta-tricalciumphosphate/poly-epsilon-caprolactone scaffolds and magnetically sorted stem cells. *Ann Plast Surg*. 2007 Jul;59(1):46,52; discussion 52.
81. Weinand C, Gupta R, Huang AY, Weinberg E, Madisch I, Qudsi RA, et al. Comparison of hydrogels in the in vivo formation of tissue-engineered bone using mesenchymal stem cells and beta-tricalcium phosphate. *Tissue Eng*. 2007 Apr;13(4):757-65.
82. Hao W, Pang L, Jiang M, Lv R, Xiong Z, Hu YY. Skeletal repair in rabbits using a novel biomimetic composite based on adipose-derived stem cells encapsulated in collagen I gel with PLGA-beta-TCP scaffold. *J Orthop Res*. 2010 Feb;28(2):252-7.
83. Canalis E. The fate of circulating osteoblasts. *N Engl J Med*. 2005 May 12;352(19):2014-6.

84. Deckers MM, Karperien M, van der Bent C, Yamashita T, Papapoulos SE, Lowik CW. Expression of vascular endothelial growth factors and their receptors during osteoblast differentiation. *Endocrinology*. 2000 May;141(5):1667-74.
85. Harper J, Klagsbrun M. Cartilage to bone--angiogenesis leads the way. *Nat Med*. 1999 Jun;5(6):617-8.
86. Gerber HP, Vu TH, Ryan AM, Kowalski J, Werb Z, Ferrara N. VEGF couples hypertrophic cartilage remodeling, ossification and angiogenesis during endochondral bone formation. *Nat Med*. 1999 Jun;5(6):623-8.
87. Yamamoto M, Takahashi Y, Tabata Y. Controlled release by biodegradable hydrogels enhances the ectopic bone formation of bone morphogenetic protein. *Biomaterials*. 2003 Nov;24(24):4375-83.
88. Wang DS, Miura M, Demura H, Sato K. Anabolic effects of 1,25-dihydroxyvitamin D3 on osteoblasts are enhanced by vascular endothelial growth factor produced by osteoblasts and by growth factors produced by endothelial cells. *Endocrinology*. 1997 Jul;138(7):2953-62.
89. Lind M, Eriksen EF, Bunger C. Bone morphogenetic protein-2 but not bone morphogenetic protein-4 and -6 stimulates chemotactic migration of human osteoblasts, human marrow osteoblasts, and U2-OS cells. *Bone*. 1996 Jan;18(1):53-7.
90. Fiedler J, Roderer G, Gunther KP, Brenner RE. BMP-2, BMP-4, and PDGF-bb stimulate chemotactic migration of primary human mesenchymal progenitor cells. *J Cell Biochem*. 2002;87(3):305-12.

91. Fiedler J, Etzel N, Brenner RE. To go or not to go: Migration of human mesenchymal progenitor cells stimulated by isoforms of PDGF. *J Cell Biochem.* 2004 Nov 15;93(5):990-8.
92. Fiedler J, Brill C, Blum WF, Brenner RE. IGF-I and IGF-II stimulate directed cell migration of bone-marrow-derived human mesenchymal progenitor cells. *Biochem Biophys Res Commun.* 2006 Jul 7;345(3):1177-83.
93. Nakasaki M, Yoshioka K, Miyamoto Y, Sasaki T, Yoshikawa H, Itoh K. IGF-I secreted by osteoblasts acts as a potent chemotactic factor for osteoblasts. *Bone.* 2008 Nov;43(5):869-79.
94. Matsuo K. Eph and ephrin interactions in bone. *Adv Exp Med Biol.* 2010;658:95-103.
95. Pennisi A, Ling W, Li X, Khan S, Shaughnessy JD, Jr, Barlogie B, et al. The ephrinB2/EphB4 axis is dysregulated in osteoprogenitors from myeloma patients and its activation affects myeloma bone disease and tumor growth. *Blood.* 2009 Aug 27;114(9):1803-12.
96. Zhao C, Irie N, Takada Y, Shimoda K, Miyamoto T, Nishiwaki T, et al. Bidirectional ephrinB2-EphB4 signaling controls bone homeostasis. *Cell Metab.* 2006 Aug;4(2):111-21.
97. Edin ML, Miclau T, Lester GE, Lindsey RW, Dahners LE. Effect of cefazolin and vancomycin on osteoblasts in vitro. *Clin Orthop Relat Res.* 1996 Dec;(333)(333):245-51.
98. Hsieh PH, Tai CL, Lee PC, Chang YH. Liquid gentamicin and vancomycin in bone cement: A potentially more cost-effective regimen. *J Arthroplasty.* 2009 Jan;24(1):125-30.

99. Wallace DG, Rosenblatt J. Collagen gel systems for sustained delivery and tissue engineering. *Adv Drug Deliv Rev.* 2003 Nov 28;55(12):1631-49.
100. Brooks PM. The burden of musculoskeletal disease--a global perspective. *Clin Rheumatol.* 2006 Nov;25(6):778-81.
101. Lidgren L. The bone and joint decade 2000-2010. *Bull World Health Organ.* 2003;81(9):629.
102. Awad HA, Butler DL, Harris MT, Ibrahim RE, Wu Y, Young RG, et al. In vitro characterization of mesenchymal stem cell-seeded collagen scaffolds for tendon repair: Effects of initial seeding density on contraction kinetics. *J Biomed Mater Res.* 2000 Aug;51(2):233-40.
103. Nirmalanandhan VS, Levy MS, Huth AJ, Butler DL. Effects of cell seeding density and collagen concentration on contraction kinetics of mesenchymal stem cell-seeded collagen constructs. *Tissue Eng.* 2006 Jul;12(7):1865-72.
104. Steinberg BM, Smith K, Colozzo M, Pollack R. Establishment and transformation diminish the ability of fibroblasts to contract a native collagen gel. *J Cell Biol.* 1980 Oct;87(1):304-8.
105. Dimitrijevic SD, inventor; The University of North Texas Health Science Center at Fort Worth (Fort Worth, TX), assignee. Pericardial anti-adhesion patch. patent United States Patent 6599526. 2003 .

106. Bodnar AG, Ouellette M, Frolkis M, Holt SE, Chiu CP, Morin GB, et al. Extension of life-span by introduction of telomerase into normal human cells. *Science*. 1998 Jan 16;279(5349):349-52.
107. Cornell CN. Osteoconductive materials and their role as substitutes for autogenous bone grafts. *Orthop Clin North Am*. 1999 Oct;30(4):591-8.
108. Morgan DML. Tetrazolium (MTT) assay for cellular viability and activity. In: *Polyamine Protocols*. Humana Press; 1998. p. 179,180, 181, 182, 183, 184.
109. Gentleman E, Swain RJ, Evans ND, Boonrungsiman S, Jell G, Ball MD, et al. Comparative materials differences revealed in engineered bone as a function of cell-specific differentiation. *Nat Mater*. 2009 Jul 26.
110. Kasten P, Luginbuhl R, van Griensven M, Barkhausen T, Krettek C, Böhner M, et al. Comparison of human bone marrow stromal cells seeded on calcium-deficient hydroxyapatite, beta-tricalcium phosphate and demineralized bone matrix. *Biomaterials*. 2003 Jul;24(15):2593-603.
111. Lutolf MP, Lauer-Fields JL, Schmoekel HG, Metters AT, Weber FE, Fields GB, et al. Synthetic matrix metalloproteinase-sensitive hydrogels for the conduction of tissue regeneration: Engineering cell-invasion characteristics. *Proc Natl Acad Sci U S A*. 2003 Apr 29;100(9):5413-8.
112. Jones JR, Atwood RC, Poologasundarampillai G, Yue S, Lee PD. Quantifying the 3D macrostructure of tissue scaffolds. *J Mater Sci Mater Med*. 2009 Feb;20(2):463-71.

113. Muller R. Hierarchical microimaging of bone structure and function. *Nat Rev Rheumatol*. 2009 Jul;5(7):373-81.
114. Ng AM, Tan KK, Phang MY, Aziyati O, Tan GH, Isa MR, et al. Differential osteogenic activity of osteoprogenitor cells on HA and TCP/HA scaffold of tissue engineered bone. *J Biomed Mater Res A*. 2008 May;85(2):301-12.
115. Brighton CT, Hunt RM. Early histological and ultrastructural changes in medullary fracture callus. *J Bone Joint Surg Am*. 1991 Jul;73(6):832-47.
116. Parfitt AM. Osteonal and hemi-osteonal remodeling: The spatial and temporal framework for signal traffic in adult human bone. *J Cell Biochem*. 1994 Jul;55(3):273-86.
117. Dai J, Rabie AB. VEGF: An essential mediator of both angiogenesis and endochondral ossification. *J Dent Res*. 2007 Oct;86(10):937-50.
118. Hennessy KM, Pollot BE, Clem WC, Phipps MC, Sawyer AA, Culpepper BK, et al. The effect of collagen I mimetic peptides on mesenchymal stem cell adhesion and differentiation, and on bone formation at hydroxyapatite surfaces. *Biomaterials*. 2009 Apr;30(10):1898-909.
119. Friess W, Uludag H, Foskett S, Biron R, Sargeant C. Characterization of absorbable collagen sponges as rhBMP-2 carriers. *Int J Pharm*. 1999 Sep 30;187(1):91-9.
120. Zhao J, Shinkai M, Takezawa T, Ohba S, Chung UI, Nagamune T. Bone regeneration using collagen type I vitrigel with bone morphogenetic protein-2. *J Biosci Bioeng*. 2009 Mar;107(3):318-23.

121. Malafaya PB, Silva GA, Reis RL. Natural-origin polymers as carriers and scaffolds for biomolecules and cell delivery in tissue engineering applications. *Adv Drug Deliv Rev.* 2007 May 30;59(4-5):207-33.
122. GROSS J, KIRK D. The heat precipitation of collagen from neutral salt solutions: Some rate-regulating factors. *J Biol Chem.* 1958 Aug;233(2):355-60.
123. Maehara H, Sotome S, Yoshii T, Torigoe I, Kawasaki Y, Sugata Y, et al. Repair of large osteochondral defects in rabbits using porous hydroxyapatite/collagen (HAp/Col) and fibroblast growth factor-2 (FGF-2). *J Orthop Res.* 2010 May;28(5):677-86.
124. Koch S, Yao C, Grieb G, Prevel P, Noah EM, Steffens GC. Enhancing angiogenesis in collagen matrices by covalent incorporation of VEGF. *J Mater Sci Mater Med.* 2006 Aug;17(8):735-41.
125. Bentz H, Schroeder JA, Estridge TD. Improved local delivery of TGF-beta2 by binding to injectable fibrillar collagen via difunctional polyethylene glycol. *J Biomed Mater Res.* 1998 Mar 15;39(4):539-48.
126. Pang Y, Wang X, Ucuzian AA, Brey EM, Burgess WH, Jones KJ, et al. Local delivery of a collagen-binding FGF-1 chimera to smooth muscle cells in collagen scaffolds for vascular tissue engineering. *Biomaterials.* 2010 Feb;31(5):878-85.
127. Rosenblatt J, Rhee W, Wallace D. The effect of collagen fiber size distribution on the release rate of proteins from collagen matrices by diffusion. *J Controlled Release.* 1989 8;9(3):195-203.